

PACIFIC EARTHQUAKE ENGINEERING
RESEARCH CENTER

Experimental Study on the Cyclic Behavior of Welded Steel Tee Joints and Elbows

A Report for the "Performance-based Earthquake Engineering Assessment Tool for Natural Gas Storage and Pipeline Systems" Project

Elide Pantoli
Tara Hutchinson

Department of Structural Engineering
University of California, San Diego
La Jolla, California

PEER Report 2025/16
Pacific Earthquake Engineering Research Center
Headquarters at the University of California, Berkeley
December 2025

PEER 2025/16
December 2025

Disclaimer

The opinions, findings, and conclusions or recommendations expressed in this publication are those of the author(s) and do not necessarily reflect the views of the study sponsor(s), the Pacific Earthquake Engineering Research Center, or the Regents of the University of California.

Experimental Study on the Cyclic Behavior of Welded Steel Tee Joints and Elbows

A Report for the "Performance-based Earthquake Engineering Assessment Tool for Natural Gas Storage and Pipeline Systems" Project

Elide Pantoli

Tara C. Hutchinson

Department of Structural Engineering
University of California, San Diego
La Jolla, California

PEER Report 2025/16
Pacific Earthquake Engineering Research Center
Headquarters at the University of California, Berkeley
May 2025

ABSTRACT

This report is one of a series of reports documenting the methods and findings of a multi-year, multi-disciplinary project conducted by the Pacific Earthquake Engineering Research Center (PEER) with the Lawrence Berkeley National Laboratory (LBNL), and funded by the California Energy Commission (CEC). The overall project is titled "*Performance-based Earthquake Engineering Assessment Tool for Natural Gas Storage and Pipeline Systems*" henceforth referred to as the "*OpenSRA* Project." The overall goal of the *OpenSRA* project is to create an open-source research-based seismic risk assessment tool for natural gas infrastructure that can be used by utility stakeholders to better understand state-wide risks, prioritize mitigation, plan new gas infrastructure, and help focus on post-earthquake repair work.

The project team includes researchers from LBNL, UC Berkeley, UC San Diego, University of Nevada Reno, the NHERI SimCenter at UC Berkeley, and Slate Geotechnical Consultants and its subcontractors Lettis Consultants International (LCI) and Thomas O'Rourke. Focused research to advance the seismic risk assessment tool was conducted by Task Groups, each addressing a particular area of study and expertise, and collaborating with the other Task Groups.

This report is the product of Task Group D: *Performance of gas storage and pipeline system surface infrastructure*. The scope of this report is to describe in detail an experimental program on piping components performed at UC San Diego. This experimental study included displacement-controlled cyclic tests, loading specimens both in-plane and out-of-plane, on four tee and four elbow specimens. Two combinations of pipe diameter and Schedule (thickness) were considered, namely: 4 in. diameter Schedule 80 and 8 in. diameter Schedule 40. These two geometries were selected as they are typically used in natural gas storage facilities and in the natural gas distribution network, respectively.

Keywords: quasi-static, testing, limit states, experiments, steel elbows, steel tees, welded pipes

ACKNOWLEDGMENTS AND DISCLAIMER

The Performance-Based Earthquake Engineering Assessment Tool for Natural Gas Storage and Pipeline Systems project is led by Professor Jonathan Bray at the University of California Berkeley, with partners at the University of California (UC) Berkeley, University of Nevada Reno (UNR), Lawrence Berkeley National Laboratories (LBNL), University of California San Diego, NHERI SimCenter at UC Berkeley, and Slate Geotechnical Consultants and its subcontractors Lettis Consultants International (LCI) and Professor Thomas O'Rourke. The authors are grateful for the technical input and advice from all members of the project team, and especially Professor Thomas O'Rourke of Cornell University. The authors are also grateful for the support of the staff at the UC San Diego and UNR Laboratories; donations of materials by University Mechanical and Engineering Contractors (UMEC) of El Cajon, California and SoCalGas; and fabrication and delivery of the component specimens tested at UC San Diego by UMEC.

This research study was funded by the California Energy Commission, under Contract No. PIR 18-003. The opinions, findings, conclusions, and recommendations expressed in this publication are those of the author(s) and do not necessarily reflect the view of California Energy Commission and its employees, the State of California, the Pacific Earthquake Engineering Research (PEER) Center, and the Regents of the University of California.

TABLE OF CONTENTS

ACKNOWLEDGMENTS and disclaimer ..... **v**

TABLE OF CONTENTS ..... **vii**

LIST OF TABLES ..... **ix**

LIST OF FIGURES ..... **xi**

EXECUTIVE SUMMARY ..... **xxi**

1 Introduction **1**

1.1 Prior Research **4**

2 Project Approach **7**

2.1 Description of the Test Specimens **7**

2.1.1 Geometry 7

2.1.2 Material Properties 13

2.2 Test Setup **13**

2.2.1 Specimen 4T-IP 14

2.2.2 Specimen 8T-IP 15

2.2.3 Specimen 4T-OP 17

2.2.4 Specimen 8T-OP 18

2.2.5 Specimen 4E-90 19

2.2.6 Specimen 4E-45 20

2.2.7 Specimen 8E-90 21

2.2.8 Specimen 8E-45 22

2.3 Instrumentation Plans **23**

2.3.1 Specimen 4T-IP 24

2.3.2 Specimen 4T-OP 26

2.3.3 Specimen 8T-IP 28

2.3.4 Specimen 8T-OP 30
2.3.5 Specimen 4E-90 32
2.3.6 Specimen 4E-45 34
2.3.7 Specimen 8E-90 36
2.3.8 Specimen 8E-45 37
2.3.9 Camera Plan 39
2.4 Description of the Test Protocol 47

3 Project Results 51
3.1 Force-Displacement Response 52
3.2 Moment-Rotation Response 54
3.2.1 Calculation of Rotation and Moment for Tee Joints 54
3.2.2 Calculation of Rotation and Moment for Elbows 57
3.2.3 Presentation of Moment-Rotation Response Results 58
3.3 Physical Observations 61
3.3.1 Tee Joints 61
3.3.2 Elbows 69
3.4 Strain Measurements 78

4 Conclusions and Recommendations 81

GLOSSARY AND LIST OF ACRONYMS 83

REFERENCES 87

Appendix A: Weld Properties and Procedure 91

Appendix B: Mill Certificates 97

Appendix C: Loading Protocol Details 103

Appendix D: Measurements obtained by strain gauges 111

LIST OF TABLES

Table 1.1 Test matrix of component specimens 3

Table 2.1 Main geometric features of the tested specimens 12

Table 2.2 Additional geometric features of the tested specimens 13

Table 2.4 Summary of views from cameras 39

Table 2.5 Load protocol details for specimens 4T-IP and 4T-OP 49

Table 3.1 Limit states observed for specimen 4T-IP 62

Table 3.2 Limit states observed for specimen 4T-OP 64

Table 3.3 Limit states observed for specimen 8T-IP 66

Table 3.4 Limit states observed for specimen 8T-OP 67

Table 3.5 Limit states observed for specimen 4E-90 69

Table 3.6 Limit states observed for specimen 4E-45 71

Table 3.7 Limit states observed for specimen 8E-90 72

Table 3.8 Limit states observed for specimen 8E-45 76

Table C.1 Load protocol details for specimens 8T-IP 103

Table C.2 Load protocol details for specimens 8T-IP and 8T-OP 104

Table C.3 Load protocol details for specimen 4E-90 105

Table C.4 Load protocol details for specimen 4E-45 106

Table C.5 Load protocol details for specimen 8E-90 107

Table C.6 Load protocol details for specimen 8E-45..... 108

LIST OF FIGURES

Figure 1.1 Examples of tee joints and elbows used in the field within the natural gas surface infrastructure: (a) M&R station (Rongere and Eimon, 2019), (b) wellhead in a gas storage facility (SoCalGas 2016)..... 4

Figure 1.2 Examples of previous tests on steel elbows performed by (a) Yoshizaki et al. 2000, (b) Varelis et al. 2013, (c) Nakamura and Kasahara 2017..... 5

Figure 1.3 Examples of previous tests on tee joints performed by (a) Papatheocharis et al. (2013), (b) Di Filippo et al. 2019, (c) Watakabe et al. 2014..... 5

Figure 2.1 Construction drawings for each of the tested specimens 8

Figure 2.1 Construction drawings for each of the tested specimens (continued)..... 9

Figure 2.2 Details of the plate-to-pipe and stiffeners connection (a) for the 4 in. specimens, (b) for the 8 in. tee specimens and (c) for the 8 in. elbow specimens..... 10

Figure 2.3 Corbel details (a)Photograph of the corbel, (b) main view of the corbel, (c) elevation A-A', (d) elevation B-B', (e) elevation C-C', (f) elevation D-D' 11

Figure 2.4 Photographs of select specimens: (a), (b) 4T-OP specimen and relevant nomenclature for tees, (c) and 8E-90 and 8E-45 specimens (d) 4E-90 and relevant nomenclature for elbows..... 12

Table 2.3 Properties of the tested component specimens14

Figure 2.5 Photographs of the test setup for specimen 4T-IP: (a) view from above, (b) view from North-East 15

Figure 2.6 Specimen 4T-IP setup construction drawings: (a) plan view, (b) elevation, section C-C' and (c) elevation, section D-D' 15

Figure 2.7 Photographs of the test setup for specimen 8T-IP: (a)View from North-East, (b) from South-East 16

Figure 2.8 Specimen 8T-IP setup construction drawings: (a)plan view, (b) elevation view of the specimen and (c) elevation view of the actuator, corbel and steel block 16

Figure 2.9 Test setup for specimen 4T-OP: (a) View from South-West, (b) from North-East 17

Figure 2.10 Specimen 4T-OP setup construction drawings: (a) plan view, (b) elevation view of the specimen and (c) elevation view of the actuator, corbel and steel block 18

Figure 2.11 Test setup for specimen 8T-OP: (a) View from South-East, (b) from North-West 18

Figure 2.12 Specimen 8T-OP setup construction drawings: (a) plan view, (b) elevation view of the specimen (A-A) and (c) elevation view of the actuator, corbel and steel block (B-B) 19

Figure 2.13 Test setup for specimen 4E-90: (a) View from East, (b) from South-West 20

Figure 2.14 Specimen 4E-90 setup construction drawings: (a) elevation and (b) plan view 20

Figure 2.15 Test setup for specimen 4E-45: (a) view from East, (b) from South-East 21

Figure 2.16 Specimen 4E-45 setup construction drawings (elevation view) 21

Figure 2.17 Test setup for specimen 8E-90 (a) view from East, (b) from North-East 22

Figure 2.18 Specimen 8E-90 setup construction drawings (elevation view) 22

Figure 2.19 Test setup for specimen 8E-45 (a) view from East, (b) from South-East 23

Figure 2.20 Specimen 8E-45 setup construction drawings (elevation view) 23

Figure 2.21 Instrumentation plan for specimen 4T-IP: displacement potentiometers (EW=east west; NS= north south; V=vertical) 24

Figure 2.22 Instrumentation plan for specimen 4T-IP: (a) uniaxial strain gauges and (b) rosettes (T=top; B=bottom) 25

Figure 2.23 Photographs of select sensors of Specimen 4T-IP: (a) Linear potentiometers L02, L03, L04 (b) linear potentiometer L08 (with L05 and L06 in the background), (c) rosette R03, (d) attachment points of L12 and L13. 26

Figure 2.24 Instrumentation plan for specimen 4T-OP, string potentiometers (a) horizontal and (b) vertical direction (EW=east west; NS= north south; V=vertical) 27

Figure 2.25 Instrumentation plan for specimen 4T-OP, uniaxial strain gauges and rosettes: (a) north side and (b) south side 27

Figure 2.26 Photographs of select sensors of Specimen 4T-OP: (a) String potentiometers L02, L03, L04, (b) details of point of attachment between strings and pipe (c) strain gauges on the north side of the specimen (d) string potentiometers L06 (front) and L01 (back) 28

Figure 2.27 Instrumentation plan for specimen 8T-IP, string potentiometers: (a) horizontal and (b) vertical direction (EW=east west; NS= north south; V=vertical) 29

Figure 2.28 Instrumentation plan for specimen 8T-IP: uniaxial strain gauges and rosettes 30

Figure 2.29 Photographs of selected sensors for specimen 8T-IP: (a) string potentiometers monitoring the specimen and (b) R02 30

Figure 2.30 Instrumentation plan for specimen 8T-IP, string potentiometers: (a) plan and (b) elevation views (EW=east west; NS= north south; V=vertical) 31

Figure 2.31 Instrumentation plan for specimen 8T-OP: (a) uniaxial strain gauges and (b) rosettes (T=top; B=bottom) 32

Figure 2.32 Photographs of selected sensors for specimen 8T-OP: (a) R01 and SG02 and (b) string potentiometers L06, L02 and L03 32

Figure 2.33 Instrumentation plan for specimen 4E-90: (a) uniaxial strain gauges and rosettes in the east and (b) west side of the specimen, (c) displacement

potentiometers and (d) inclinometers (EW=east west; NS= north south; V=vertical; IP= in plane; OP=out of plane) 33

Figure 2.34 Photographs of selected sensors for specimen 4E-90 34

Figure 2.35 Instrumentation plan for specimen 4E-45: (a) uniaxial strain gauges and rosettes in the east and (b) west side of the specimen 34

Figure 2.36 Instrumentation plan for specimen 4E-45: (a) displacement potentiometers (east side) and (b) inclinometers (west side) (EW=east west; NS= north south V=vertical; IP= in plane; OP=out of plane) 35

Figure 2.37 Photographs of selected sensors for specimen 4E-45 (west side) 35

Figure 2.38 Instrumentation plan for specimen 8E-90: uniaxial strain gauges and rosettes in the (a) west and (b) east side of the specimen 36

Figure 2.39 Instrumentation plan for specimen 8E-90: displacement potentiometers and inclinometers (EW=east west; NS= north south; V=vertical; IP= in plane; OP=out of plane). Note that the inclinometers are installed in the east side of the specimen 36

Figure 2.40 Photographs of select sensors for specimen 8E-90: (a) east side and (b) west side 37

Figure 2.41 Instrumentation plan for specimen 8E-45: (a) uniaxial strain gauges and rosettes in the west and (b) east side of the specimen 37

Figure 2.42 Instrumentation plan for specimen 8E-45: displacement potentiometers and inclinometers (EW=east west; NS= north south; V=vertical; IP= in plane; OP=out of plane). Note that the inclinometers are installed in the east side of the specimen 38

Figure 2.43 Photographs of selected sensors for specimen 8E-45: (a) east side and (b) west side 38

Figure 2.44 Views from the six cameras for specimen 4T-IP: (a) C1; (b) C2; (c) C3; (d) C4; (e) C5; (f) C6 40

Figure 2.45 Views from the six cameras for specimen 4T-OP: (a) C1; (b) C2; (c) C3; (d) C4; (e) C5; (f) C6 41

Figure 2.46 Views from the six cameras for specimen 8T-IP: (a) C1; (b) C2; (c) C3; (d) C4; (e) C5; (f) C6 42

Figure 2.47 Views from the six cameras for specimen 8T-OP: (a) C1; (b) C2; (c) C3; (d) C4; (e) C5; (f) C643

Figure 2.48 Views from the six cameras for specimen 4E-90: (a) C1; (b) C2; (c) C3; (d) C4; (e) C5; (f) C6 44

Figure 2.49 Views from the six cameras for specimen 4E-45: (a) C1; (b) C2; (c) C3; (d) C4; (e) C5; (f) C6 45

Figure 2.50 Views from the six cameras for specimen 8E-90: (a) C1; (b) C2; (c) C3; (d) C4; (e) C5; (f) C6 46

Figure 2.51 Views from the six cameras for specimen 8E-45: (a) C1; (b) C2; (c) C3; (d) C4; (e) C5; (f) C6 47

Figure 2.52 Typical load protocol (numerical values relative to the test on specimen 4T-IP) 48

Figure 3.1 Internal pressure measured within specimen 4T-OP during testing 52

Figure 3.2 Force-displacement response of tee joint specimens 53

Figure 3.3 Force-displacement response of elbow specimens 54

Figure 3.4 Plan view of the setup for test 4T-IP 55

Figure 3.5 Key parameters used to calculate the moment for the tee joint specimens ... 55

Figure 3.6 Geometry of the specimen as it moves in the northward direction 56

Figure 3.7 Geometry of the specimen as it moves in the southward direction 56

Figure 3.8 Side view of the setup for test 4E-90 57

Figure 3.9 Relevant geometry for the elbow specimens: (a) undeformed and (b) deformed 58

Figure 3.10 Moment-rotation hysteresis and limit states for tee joint specimens 60

Figure 3.11 Moment-rotation hysteresis and limit states for the elbow specimens 61

Figure 3.12 Photographs of representative limit states for 4T-IP: (a) flaking of the tee joint during cycle set 14, (b) shallow cracks in the neck of the tee after the first positive peak of cycle set 17, (c) deformation of the tee joint at the first northward (negative) peak of cycle set 17, (d) cracks in the tee joint during the second southward cycle of cycle set 17 (e) cracks on the south side of the neck during the second northward cycles of cycle set 17 (f) deformed shape during the first southward cycles of cycle set 18 (g) deformed shape at the moment of failure (h) final through crack 64

Figure 3.13 Photographs of representative limit states for 4T-OP: (a) Bulging of the tee at cycle 15, (b) cracking on the north side of the tee after the first positive peak of cycle 17, (c) necking on the south side of the tee after the first positive peak of cycle 17, (d) cracks following the second positive peak of cycle 17 (north side), (e) cracks after the first positive peak of cycle 18 (north side), and (f) through crack at cycle 18 (at the end of the cycle) 65

Figure 3.14 Photographs of representative limit states for 8T-IP 66

Figure 3.14 Photographs of representative limit states for 8T-IP…continued: (a) Deformation of the tee at cycle 12, (b) Bulging of the tee at cycle 13 (c), (d) Crack formed at cycle 15 67

Figure 3.15 Photographs of representative limit states for 8T-OP: (a) Incipient ovalization at Cycle 10 (b) Necking of the specimen during the first southward push of cycle 15 (c) Cracks of the specimen during the first northward push of cycle 15 (d) Through cracks in the specimen after the final cycle. 68

Figure 3.16 Photographs of representative limit states for 4E-90: (a) Flattening of the top of the elbow during closing direction of cycle 11 (b) flattening of the sides during opening direction of cycle 12 (c) microcracks after the first opening

cycle of set 17 first (d) ovalization of the specimen during first cycle of set 17 (e) flattening of the elbow during cycle 17 (f) Through crack developed on cycle 17..... 70

Figure 3.17 Photographs of representative limit states for 4E-45: (a) closing cycle 10 (b) open cycle 10 (c) cracks during first opening cycle of set 13 (d) overall picture during the closing of the second cycle of set 13 (e) overall picture during the second opening cycle of set 13 (f) final through crack (view from bottom)... 72

Figure 3.18 Photographs of representative limit states for 8E-90..... 74

Figure 3.18 Photographs of representative limit states for 8E-90: (a) First flaking observed in the closing direction during cycle 14 (1st cycles) (b) flaking after the second closing of cycle 14 (c) flaking outside the elbow observed after the first opening cycle of cycle set 15 (d) "bump" at the midline of the elbow during the second opening cycle of cycle set 15 (e) shape of the elbow during the first closing cycle of cycle set 16 (f) deformation of the specimen during the first opening cycle of cycles set 16 (g) hardening of the side of the specimen after the second opening cycle of cycle set 16 (h) shallow crack observed during monotonic push at 13.2 inch (i) cracks during the first push at 17 inch (j) final through crack after the removal of the mastic..... 75

Figure 3.19 Photographs of representative limit states for 8E-45..... 77

Figure 3.19 Photographs of representative limit states for 8E-45…continued: (a) first flaking after the first southward cycle of cycle set 15 (b) deformed shape during the first southward cycle of cycle set 17 (c) deformed shape during the first southward cycle of cycle set 18 (d) deformed shape during the first southward cycle of cycle set 19 (e),(f) shallow crack observed upon unloading of the second cycle of cycle set 19 from the side and from below (g) deformed shape during the first southward cycle of cycle set 20 (h) through crack as when it was first observed..... 78

Figure 3.20 Strain measured by uniaxial strain gauges i specimen 4T-IP 79

Figure 3.21 Strain measured by rosettes in specimen 4T-IP .... Error! Bookmark not defined.

Figure A.1 UMEC Weld Procedure (page 1) 91

Figure A.2 UMEC Weld Procedure (page 2) 92

Figure A.3 UMEC Weld Procedure (page 3) 93

Figure A.4 UMEC Weld Procedure (page 4) 94

Figure A.5 UMEC Weld Procedure (page 5) 95

Figure B.1 Mill certificate for the 4 in. Schedule 80 tee 97

Figure B.2 Mill certificate for the 4 in. Schedule 80 90-degrees elbow 98

Figure B.3 Mill certificate for the 4 in. Schedule 80 90-degrees elbow 99

Figure B.4 Mill certificate for the 8 in. Schedule 40 tee 100

Figure B.5 Mill certificate for the 8 in. Schedule 40 90-degrees elbow 101

Figure B.6 Mill certificate for the 8 in. Schedule 40 45-degrees elbow 102

Figure D.1 Strain measured by strain gauges in specimen 4T-OP 111

Figure D.2 Strain measured by rosettes in specimen 4T-OP.....112

Figure D.3 Strain measured by strain gauges in specimen 8T-IP.....112

Figure D.4 Strain measured by rosettes in specimen 8T-IP 113

Figure D.5 Strain measured by strain gauges in specimen 8T-OP 113

Figure D.6 Strain measured by rosettes in specimen 8T-OP.....114

Figure D.7 Strain measured by strain gauges in specimen 4E-90 114

Figure D.8 Strain measured by rosettes in specimen 4E-90.....115

Figure D.9 Strain measured by strain gauges in specimen 4E-45 115

Figure D.10 Strain measured by rosettes in specimen 4E-45.....116

Figure D.11 Strain measured by strain gauges in specimen 8E-90 116

Figure D.12 Strain measured by rosettes in specimen 8E-90.....117

Figure D.13 Strain measured by strain gauges in specimen 8E-45 117

Figure D.14 Strain measured by rosettes in specimen 8E-45.....118

EXECUTIVE SUMMARY

Introduction and Background

Welded steel pipelines are used extensively in a variety of industrial facilities and in the energy sector to transport hazardous materials such as oil and natural gas. Earthquake-induced damage to such pipelines could have devastating consequences in terms of pollution, life safety, and disruption of important supply chains. For example, seismic damage to a natural gas pipeline could lead to the release of methane, which is a hazardous pollutant and a greenhouse gas, could cause explosions, and leave millions without electricity.

The network of welded steel pipelines used in the industrial and energy sectors consists of a variety of components, such as straight pipe segments, fittings, valves, and bolted flange joints. These components may run either above or below ground. Amongst the most common components within the natural gas network are the fittings used to redirect or redistribute flow, namely, elbows and tee joints. These fittings may be of varying diameter, Schedule (thickness), and material properties. In addition, the nature of the network can lead to a wide variety of geometries (e.g., elbows can have different angles and tee joints may be equal or reducing). Understanding the seismic behavior of these fittings is essential to ensure the continuous operation of industrial and energy facilities after a strong earthquake. However, the large variety noted above as well as the multi-directional loading induced during an earthquake can lead to complexities with regard to defining the behavior of these components and their limit states. Experimental investigations can play an important role towards characterizing these essential components.

Project Purpose and Approach

To enrich the existing understanding of the seismic behavior of the welded steel elbow and tee joints commonly used in the natural gas infrastructure, a suite of eight pseudo-static displacement-controlled experiments of these components was performed at the Powell Laboratories at the University of California, San Diego. Specimens were loaded with a constant nominal internal gas (air) pressure targeted at between 25-35 psi while subjected to a simulated seismic displacement protocol. Specifically, 4-in. diameter Schedule 80 and 8-in diameter Schedule 40 tee joints and elbows were tested following the reversed cyclic load protocol proposed by FEMA-461 (FEMA 2007). The two combinations of diameter and Schedule were selected because they are readily used in the natural gas infrastructure in California. It is noted however that 4-in. Schedule 80 components are typical of high-pressure facilities (e.g. natural gas storage fields), while Schedule 40 pipes are commonly used in the distribution network, which operates at lower pressures. The tee joint specimens were tested both in-plane and out-of-plane, while the 90 degree and 45 degree elbows were tested only in-plane.

Project Results

The component experiments showed that these fittings are generally very ductile. Notably, the development of a through crack was almost always preceded by ample visible plastic deformation and a reasonably distributed network of shallow cracks. In addition, the specimens displayed a large rotational capacity, ranging from approximately 7 degrees to greater than 20 degrees. However, tests did reveal that certain tee joint geometries may be problematic and lead to an early brittle failure. Namely, in this program, the 8 in. tee joint specimen tested in-plane failed abruptly with little warning when a diagonal crack formed unexpectedly along the body of the tee. For these larger diameter pipes, the body region at the fitting is almost completely flat to accommodate the large transition required of a tee joint, thus a high stress compression strut developed and resulted in an abrupt through crack, resulting in failure of the fitting and consequential loss of internal gas pressure.

1 Introduction

This report is one of a series of reports documenting the methods and findings of a multi-year, multi-disciplinary project conducted by the Pacific Earthquake Engineering Research Center (PEER) with the Lawrence Berkeley National Laboratory (LBNL) and funded by the California Energy Commission (CEC). The overall project is titled "Performance-based Earthquake Engineering Assessment Tool for Natural Gas Storage and Pipeline Systems" henceforth referred to as the "*OpenSRA* Project."

The overall goal of the *OpenSRA* project is to create an open-source research-based seismic risk assessment tool for natural gas infrastructure that can be used by utility stakeholders to better understand state-wide risks, prioritize mitigation, plan new gas infrastructure, and help focus post-earthquake repair work. The probabilistic seismic risk tool developed in this project follows the widely accepted risk methodology of Dr. A. Cornell (Cornell 1968). A seismic source characterization is used to develop a suite of earthquake scenarios with associated rates of occurrence to represent the seismic hazard. Fault ruptures and the resulting ground deformation are generated for each earthquake scenario to represent the seismic loading, which includes a map of ground motion parameters. This scenario-based seismic parameter map is overlaid on the infrastructure system and the seismic loading combined with the capacities of the infrastructure to calculate the seismic performance of the natural gas system for the scenario. By repeating the process for all the scenarios in the suite, the tool can evaluate the seismic risk to the system.

A user-driven research approach was adopted to develop *OpenSRA* to facilitate and encourage its ready use by regulators and utilities, and to allow inclusion of updated models and methods for the seismic demands and capacities that control the seismic risk for natural gas systems. The project includes several innovative approaches that improve the basic methodology and distinguish this project's approach from standard approaches currently used. Current risk studies developed by the utilities use risk scoring approaches that are highly subjective and qualitative. They do not properly incorporate the uncertainties in the seismic demand and in the fragility of the system and its components. Targeted research was conducted in this project to improve the characterization of uncertainty of key inputs to the seismic risk assessment tool. The seismic risk methodology employed in this project provides quantitative estimates of the probabilistic seismic risk. For risk-informed decision-making processes, the reliability of the risk estimates needs to be considered because this can be significant, particularly for large, rare earthquakes.

The project team includes researchers from LBNL, UC Berkeley, UC San Diego, University of Nevada Reno, the NHERI SimCenter at UC Berkeley, and Slate Geotechnical Consultants and its subcontractors Lettis Consultants International (LCI) and Thomas O'Rourke. Focused research to advance the seismic risk assessment tool was conducted by Task Groups, each addressing a particular area of study and expertise, and collaborating with the other Task Groups. The Task Groups are as follows:

- Task A: Fault Displacement
- Task B: Liquefaction-induced deformation and seismically induced slope displacement
- Task C: Performance of natural gas storage well casings and caprock
- **Task D: Performance of gas storage and pipeline system surface infrastructure**
- Task E: Smart gas infrastructure sensing of wells and pipeline connections performance
- Task F: Synthesis of component fragilities into a system performance model

This report is the product of the Task Group denoted in **bold** text above. The report aims to describe and present results of a unique experimental program focused on characterizing the seismic behavior of steel piping components performed at the University of California, San Diego (UCSD). The work of Task D is also documented within reports of Elfass et al. (2025) and Pantoli and Hutchinson (2025).

The experimental campaign described in this report includes tests on different types of elbows and tee joints, as summarized in Table 1.1. These components were selected as they are amongst the most heavily loaded regions within the surface infrastructure gas storage and pipeline inventory, thus may behave nonlinearly during an earthquake. As a result, they may serve as a point of failure within select subsystems of the natural gas network. Two combinations of diameter and Schedule were tested, namely 8-in. diameter Schedule 40 pipe and 4-in. diameter Schedule 80 pipe. These were selected because they are readily used within the surface infrastructure. The latter has a larger wall thickness, and it is more typical of the high-pressure section of the infrastructure, while the former is often used in lower pressure applications, e.g., in the natural gas distribution network. Table 1.1 presents a summary of the specimens tested and their associated short names.

Table 1.1 Test matrix of component specimens

Component Type	Diameter (Schedule)	Direction of Loading	Shortname	Test date
Tee Joint	4 inch (80)	In-plane	4T-IP	February 22, 2021
	4 inch (80)	Out-of-plane	4T-OP	March 29, 2021
	8 inch (40)	In-plane	8T-IP	April 23, 2021
	8 inch (40)	Out-of-plane	8T-OP	May 10, 2021
90 degree elbow	4 inch (80)	In-plane	4E-90	July 22, 2021
	8 inch (40)	In-plane	8E-90	August 3, 2021
45 degree elbow	4 inch (80)	In-plane	4E-45	October 6, 10, 2022
	8 inch (40)	In-plane	8E-45	October 25, 2022

For all specimens, the connections between the elbows/tee joints and the straight pipe segments were welded, as this is typical of such applications. Examples of tees and elbows used in metering and regulating (M&R) stations and storage facilities are shown in Figure 1.1. Threaded connections in the surface natural gas infrastructure are also observed, though generally only in low pressure applications and thus not a focus of the present study. Such connections are common for example in smaller diameter applications, such as service risers.

The specific tests goals of this program were as follows:

- Develop a database of information on critical components specific to the material and technologies used in California. This included data from an array of analog sensors as well as from cameras monitoring the tests.
- Understand the damage development and limit states of the components. This included not only understanding crack formation, but also tracking the deformation at which the component develops important limit states.
- Obtain the global behavior of the components, namely the joint's moment, and rotation.
- Measure local behavior of the components, in particular local strains.



(a) (b)

Figure 1.1 Examples of tee joints and elbows used in the field within the natural gas surface infrastructure: (a) M&R station (Rongere and Eimon, 2019), (b) wellhead in a gas storage facility (SoCalGas 2016)

1.1 Prior Research

Research specific to the seismic behavior of the surface components of the natural gas infrastructure is limited. However, general research on steel pipes, which are widely utilized within a variety of industrial facilities, can be extended to understand the behavior of the natural gas surface infrastructure. As such, an overview of this research is presented in this section.

Prior research on the critical components of industrial systems have been both analytical and experimental in nature. One component extensively studied is the steel elbow, as this serves an essential service facilitating a pipelines transition in direction. Experimental campaigns on elbows have included monotonic tests in the in-plane and out-of-plane directions (e.g. Yoshizaki et al. 2000, see Figure 1.2a, Karamanos et al. 2003, Karamanos et al. 2006), in-plane cyclic tests (e.g. Varelis et al. 2013, see Figure 1.2b, Kim et al. 2020), and pseudo-static and shake table tests on elbow-pipe subsystems (e.g. Karvelas et al. 2021, Nakamura and Kasahara 2017 see Figure 1.2c, Kiran et al. 2019), to name select investigations. A summary of past experimental studies on elbows is presented by Karamanos (2016).

Research on the behavior of steel tee joints however is more limited, though select investigations are available. Relevant studies have included monotonic and cyclic tests of tees with loading imposed in the out-of-plane and in-plane directions (e.g. Papatheocharis et al. 2013 see Figure 1.3a, Di Filippo et al. in 2019 Figure 1.3b, Kim et al. 2020b) as well as shake table tests (e.g. Watakabe et al. 2014 Figure 1.3c, Kiran et al. 2018). Data from these and other experimental studies have been subsequently complemented and expanded with numerical investigations on both tee joints and elbows by many researchers (e.g., Chatzopoulou and Karamanos 2020; Varelis et al. 2022; Nakamura, 2019).

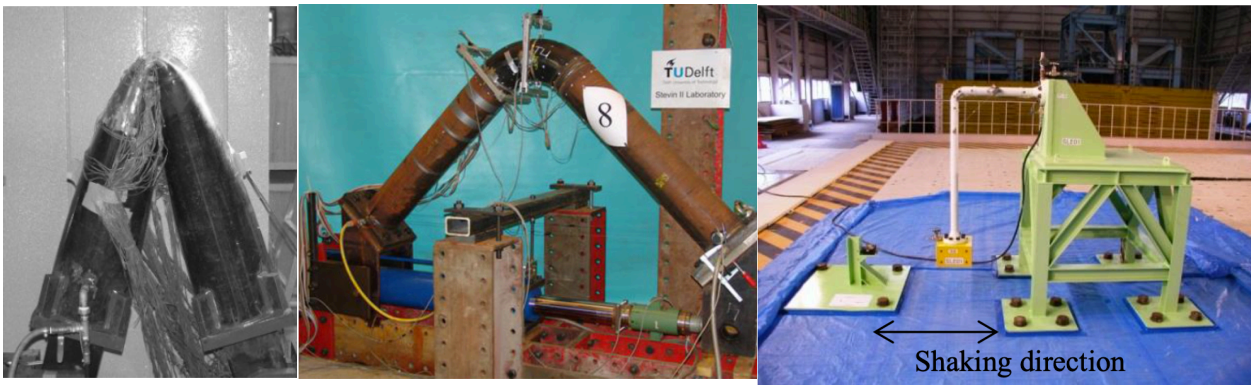

(a) (b) (c)

Figure 1.2 Examples of previous tests on steel elbows performed by (a) Yoshizaki et al. 2000, (b) Varelis et al. 2013, (c) Nakamura and Kasahara 2017



(a) (b) (c)

Figure 1.3 Examples of previous tests on tee joints performed by (a) Papatheocharis et al. (2013), (b) Di Filippo et al. 2019, (c) Watakabe et al. 2014

While these and related studies provide a wealth of information to understand the behavior of critical pipeline fittings, several limitations are noted particularly regarding characterizing the seismic behavior of components. Importantly, most prior studies have involved imposition of either an increasing amplitude monotonic or a constant amplitude cyclic loading regime, the later with the aim of determining the fatigue life. In addition, many studies focus on either thin-walled components (up to Schedule 40) or small diameters. Finally, most prior studies have focused on one fitting and geometry at a time, making direct comparison between components difficult.

2 Project Approach

2.1 Description of the Test Specimens

2.1.1 Geometry

To recreate field conditions, each specimen was fabricated by welding the critical component under consideration to segments of straight pipes. In this regard, the specimens most important region dominating the behavior is isolated. The length of the straight pipe segments was selected between 3-5 times the specimen's diameter. This extension was in part to emulate boundary conditions realized in the field, where longer straight length segments interconnect portions of the piping assembly, and thus nonlinear behavior and ensuing damage concentrate within the fitting. As a result, the straight pipe region remains essentially elastic. This approach is similar to that adopted by previous researchers (e.g., Di Filippo et al. 2019). The ends of the straight pipes not connected to the critical component were welded to 1-¼ inch thick steel plates connecting the specimen to the test frame or actuator. Stiffeners were added at the end of the pipe far from the critical component region to provide ample overstrength at the specimen boundaries and limit the potential for failure at these locations. Three olets were inserted in each specimen to allow for the continuous pressurization and pressure monitoring of the specimens, see Figure 2.2. The olets were located at the end of the straight pipe far from the critical components. The fittings were welded to the pipe segments using arc welding and a combination of ER70S-6 and E71T-1 filler material. Documentation regarding the weld procedure can be found in Appendix A. Select dimensions of each specimen are presented in Figure 2.1. Figure 2.2 shows the details of the connection of the pipe specimens to the end plates and stiffeners, while Figure 2.3 presents a photograph and the construction drawings of the corbel used to connect the specimens to the actuator.

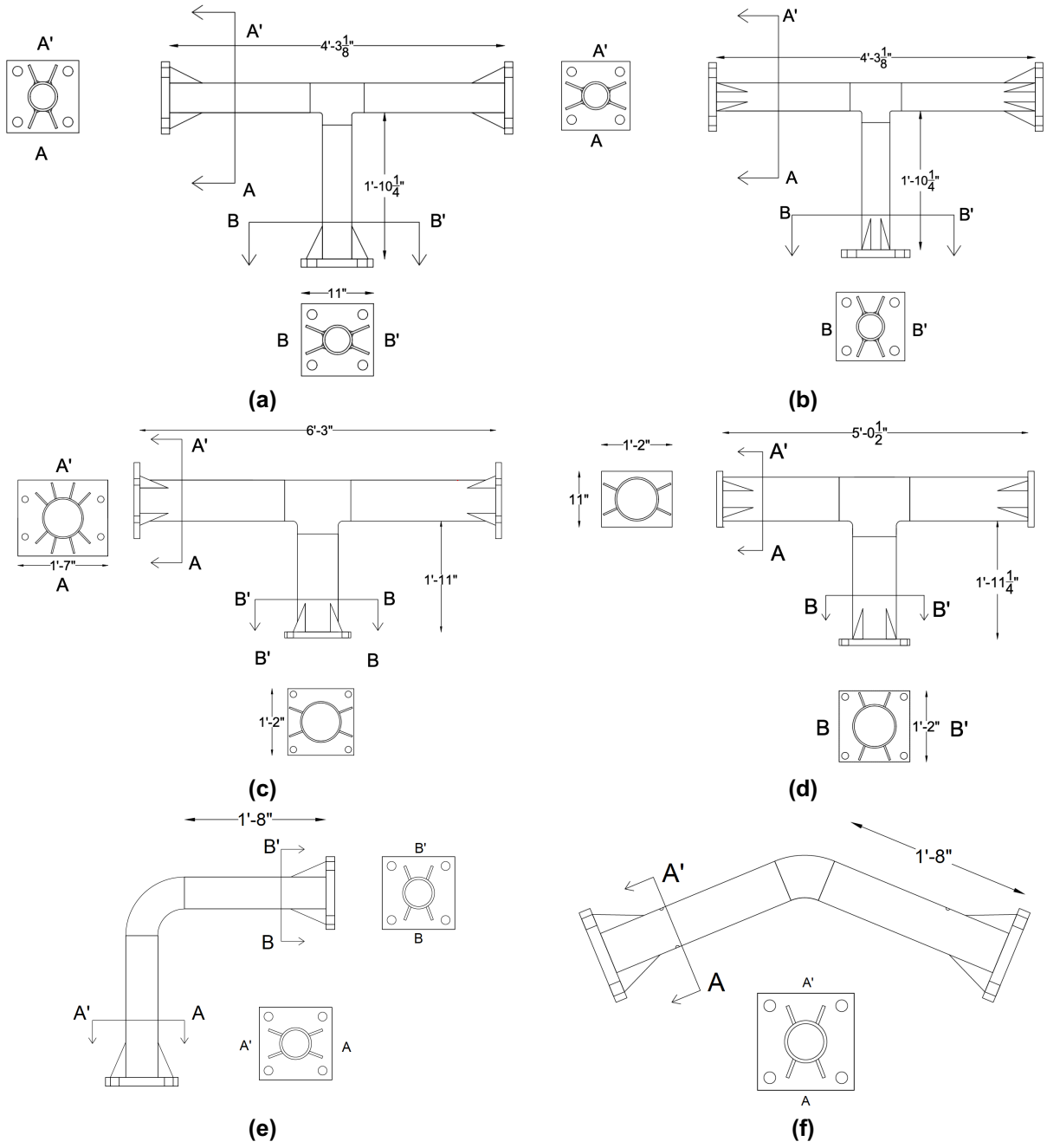

Figure 2.1 Construction drawings for each of the tested specimens

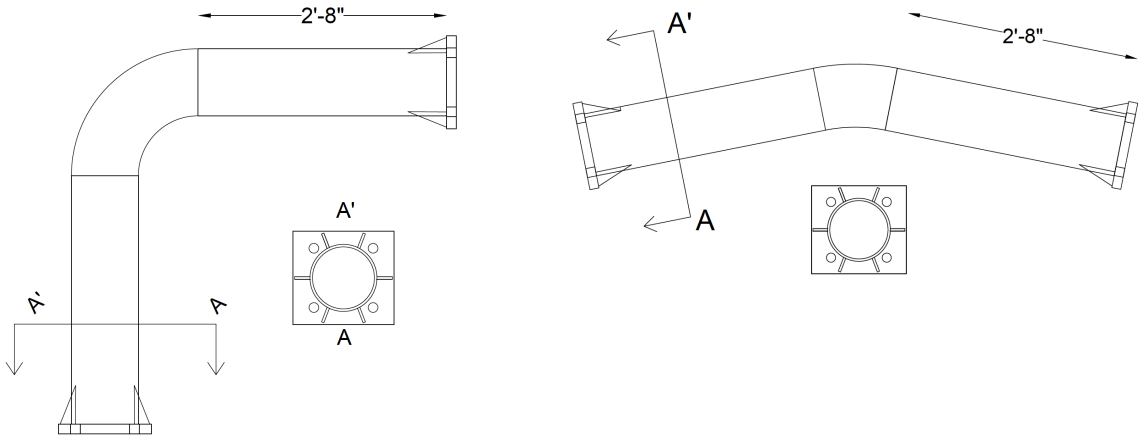

(g) (h)

(a) 4T-IP (b) 4T-OP (c) 8T-IP (d) 8T-OP (e) 4E-90 (f) 4E-45 (g) 8E-90 (h) 8E-45

Figure 2.1 Construction drawings for each of the tested specimens (continued)

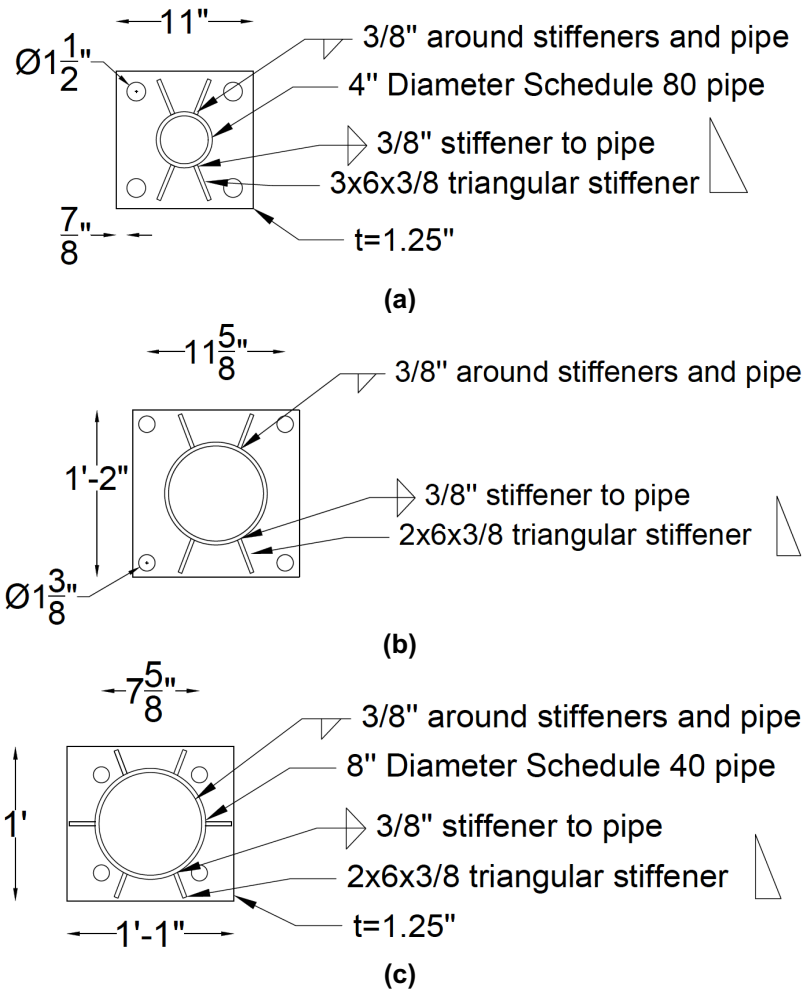

Figure 2.2 Details of the plate-to-pipe and stiffeners connection (a) for the 4 in. specimens, (b) for the 8 in. tee specimens and (c) for the 8 in. elbow specimens

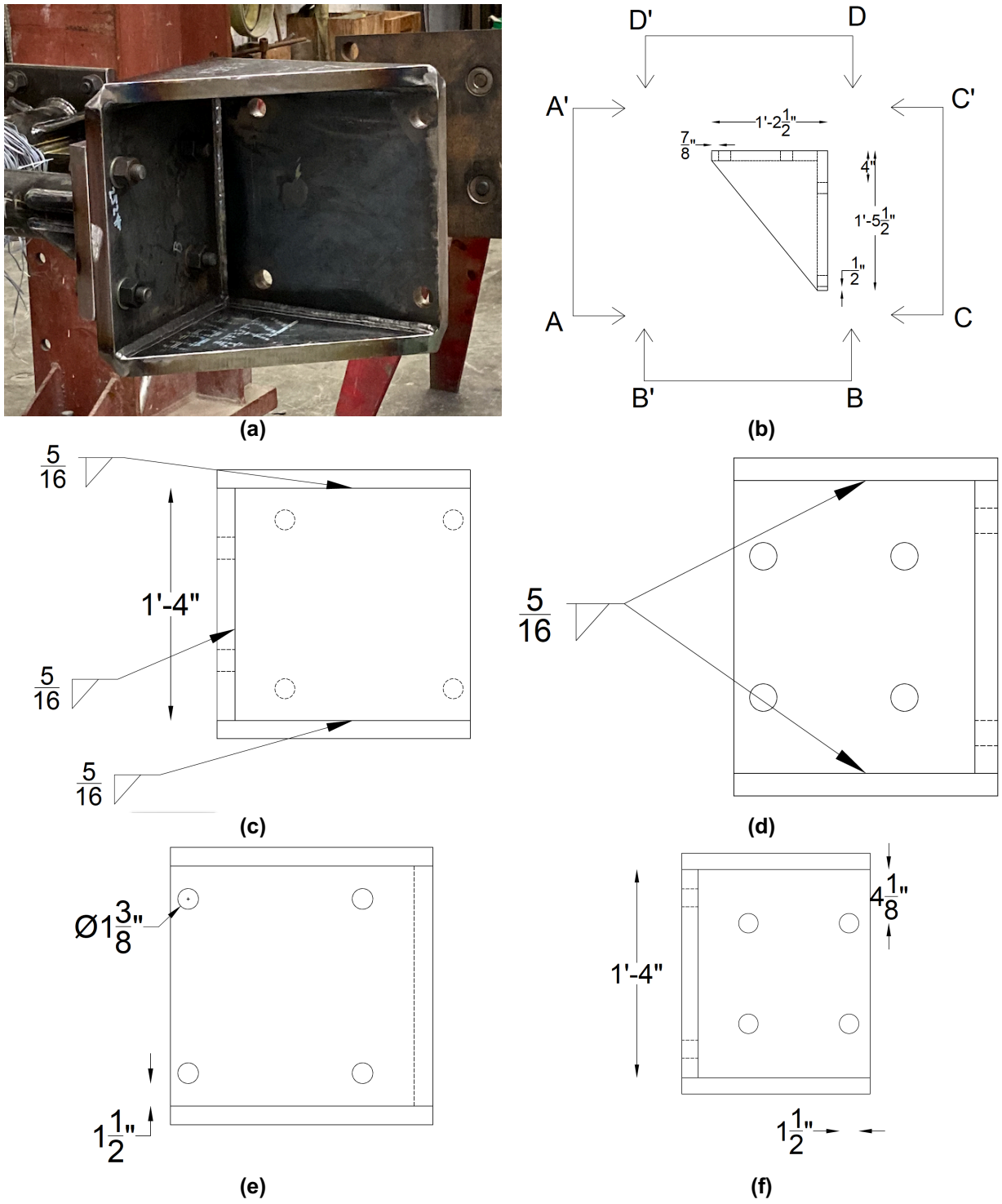

Figure 2.3 Corbel details (a)Photograph of the corbel, (b) main view of the corbel, (c) elevation A-A', (d) elevation B-B', (e) elevation C-C', (f) elevation D-D'

Photographs of select specimens showing the relevant nomenclature used herein is presented in Figure 2.4. The main geometrical features of the two types of pipes used is presented in Table 2.1. The fittings were manufactured per ASME 16.9-2018, which prescribes the additional features "c",

"m" and "a" shown in Figure 2.4 and Table 2.2. The thickness of the components was measured in an array of locations, and the main outcomes in terms of minimum measured thickness, maximum measured thickness and average thickness are presented in Table 2.2. This is consistent with data reported by previous researchers (Yahiaoui et al. 2000, Xuan et al. 2005).

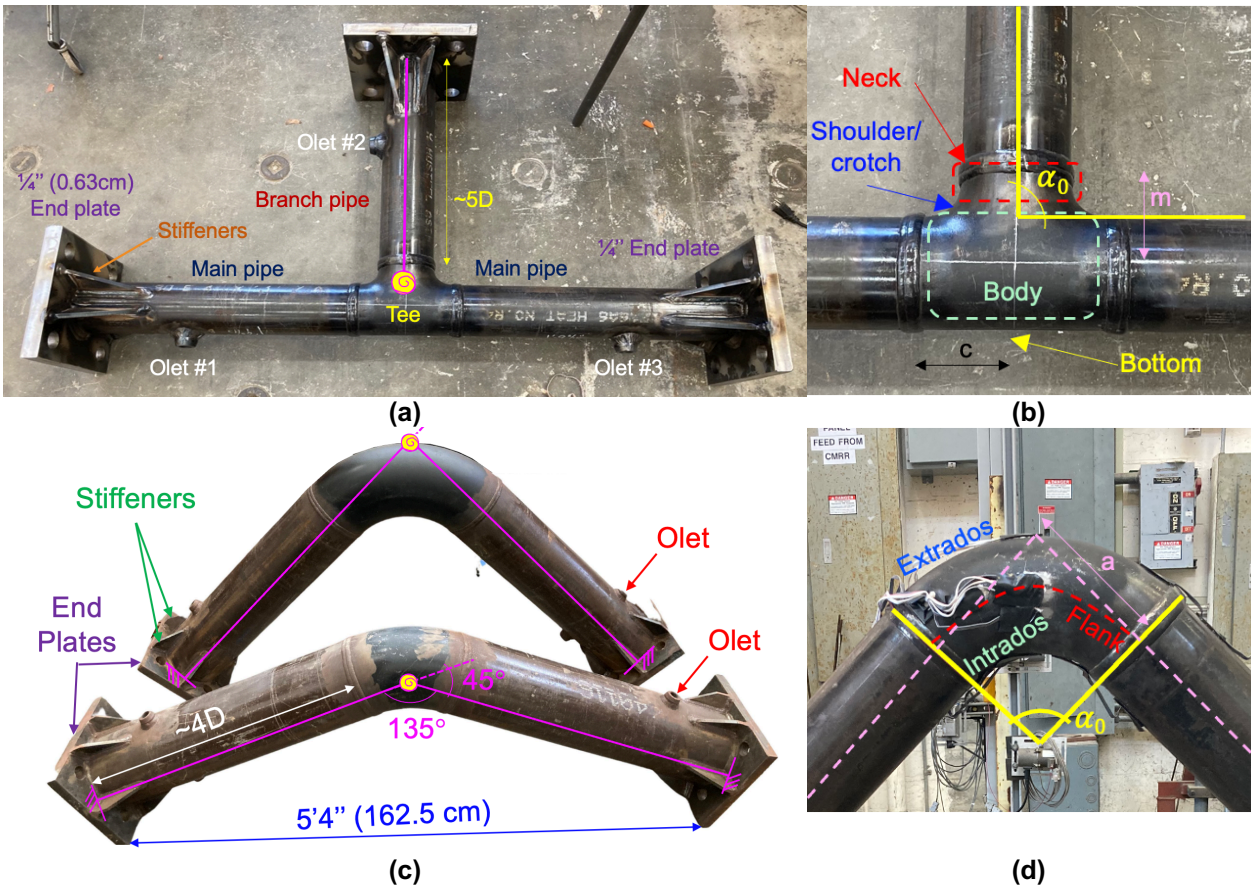

Figure 2.4 Photographs of select specimens: (a), (b) 4T-OP specimen and relevant nomenclature for tees, (c) and 8E-90 and 8E-45 specimens (d) 4E-90 and relevant nomenclature for elbows

Table 2.1 Main geometric features of the tested specimens

Pipe Type	Outside diameter [OD] (inch)	Inside diameter [ID] (inch)	Thickness [t] (inch)	OD/t
4 inch Schedule 80	4.5	3.826	0.337	13.3
8 inch Schedule 40	8.625	7.981	0.322	26.8

Table 2.2 Additional geometric features of the tested specimens

Specimen	c (inch)	m (inch)	a (inch)	t_{mean} (inch)	t_{min} (inch)	t_{max} (inch)
4T	4.12	4.12	-	0.45	0.35	0.54
8T	7.00	7.00	-	0.38	0.29	0.48
4E-90	-	-	6	0.33	0.29	0.37
4E-45	-	-	2.5	0.34	0.31	0.35
8E-90	-	-	12	0.33	0.30	0.36
8E-45	-	-	5	0.33	0.32	0.35

2.1.2 Material Properties

The specimen and fabrication were donated by local manufacturers, who procured the material locally and welded the components according to standards common in practice. Two types of straight pipes were utilized: electric resistance welded (ERW) pipes and seamless pipes. Seamless pipes were donated by SoCalGas. The ERW pipes and seamless pipes were used for the 4-in. and the 8-in. specimens, respectively.

Table 2.3 summarizes the type of raw material and steel grade, yield strength (f_y), tensile strength (f_u), tensile strain (ε_u) obtained from the mill certificates as well as the yield strain (ε_y) calculated from f_y and assuming an elastic modulus E of 29000 ksi. The mill certificates are presented in Appendix B.

2.2 Test Setup

Photographs and descriptions of each of the component specimen test setups are presented in this section. In what follows, the individual specimen setup is documented, including nuances particular to achieving the intended loading and boundary conditions, as well as specific construction details.

Table 2.3 Properties of the tested component specimens

Component	Raw material type and grade	f_y (ksi)	f_u (ksi)	ε_y (%)*	ε_u (%)
Fittings					
4T	A106 Gr. B	42.0	72.6	0.14	42.0
8T	CSA Z245.11 Gr. 241	47.1	66.8	0.16	30.7
4E-90	A106 Gr. B	37.8	61.6	0.13	44.0
4E-45	A106 Gr. B	38.6	61.9	0.13	44.0
8E-90	A106 Gr. B	47.8	68.3	0.16	40.0
8E-45	CSA Z245.11 Gr. 241	45.1	68.7	0.15	43.0
Straight Pipe Segments					
4 in (ERW)	ASTM A53B	68.6	72.4	0.23	31.0**
8 in (Seamless)	API 5L X42/B	47.2	72.1	0.16	43.1

***Calculated assuming an elastic modulus of 29000 ksi**
****Two different mill certificates were provided for the 4-in ERW pipe. As their properties were very similar, the average is reported herein.**

2.2.1 Specimen 4T-IP

Figure 2.5 shows the test setup for specimen 4T-IP. In this setup, the ends of the main straight legs of the pipe, i.e. to the left and right of the tee-joint fitting, were bolted to reaction columns, while the end of the branch pipe was bolted to a corbel, which was in turn attached to a +/- 50 kip (+/- 24 inch) capacity hydraulic actuator. When the load was applied, the head of the actuator and the corbel slid on a concrete block which was covered in Teflon (TR) to reduce friction. Figure 2.6 provides a schematic drawing documenting the complete test setup.

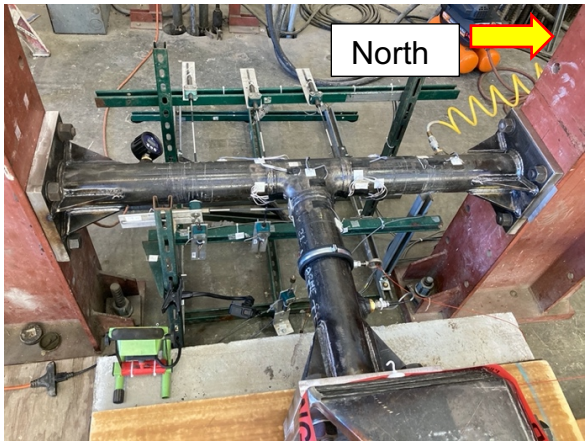

(a)

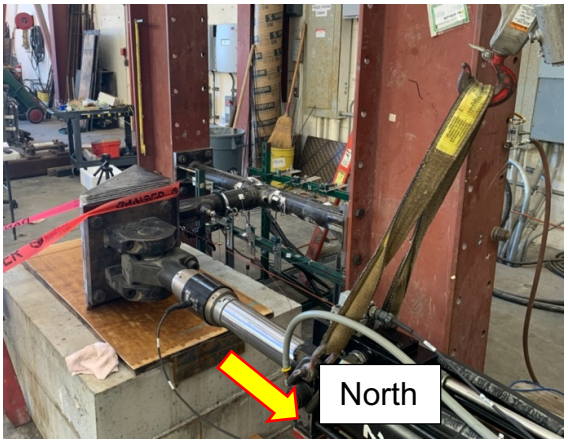

(b)

Figure 2.5 Photographs of the test setup for specimen 4T-IP: (a) view from above, (b) view from North-East

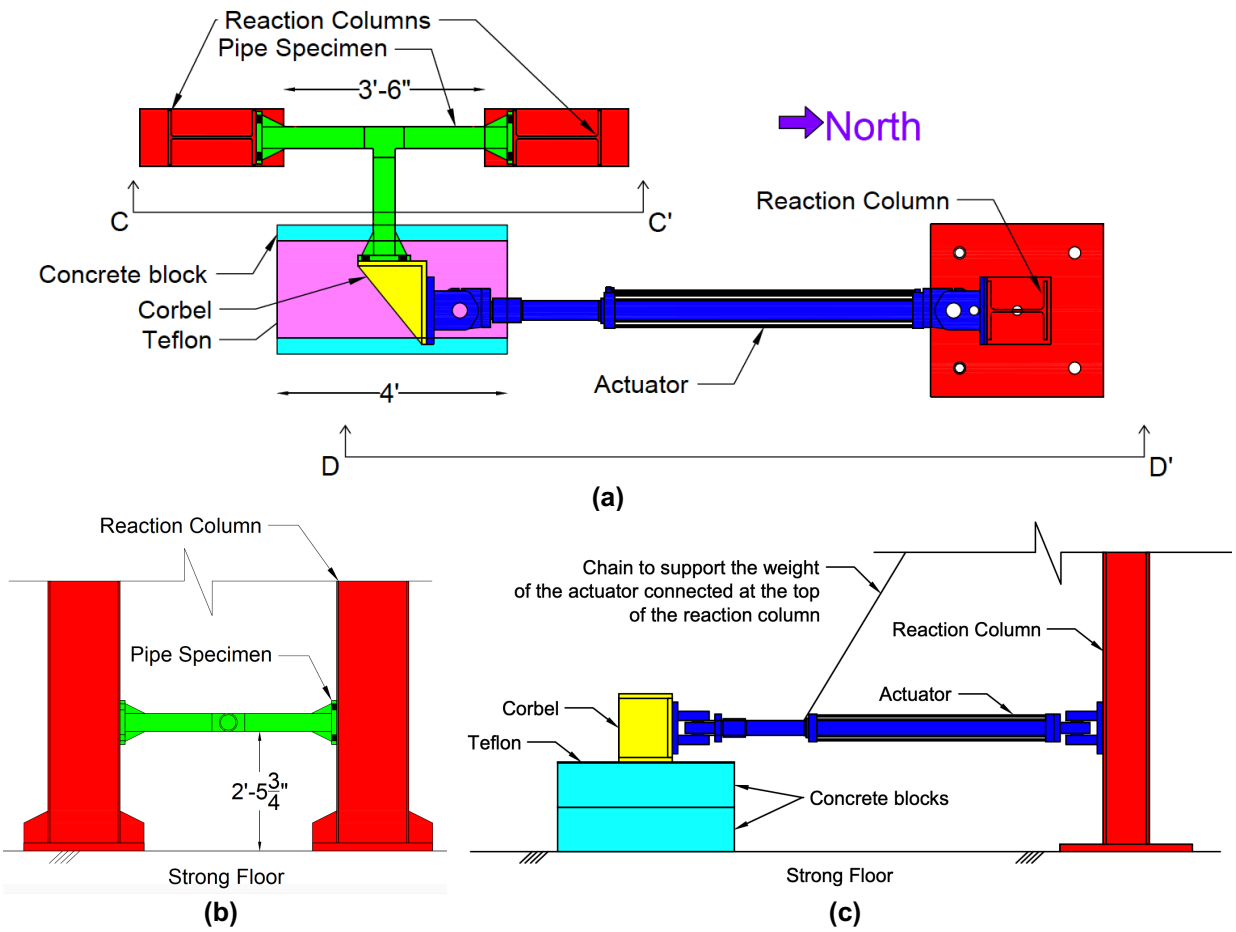

Figure 2.6 Specimen 4T-IP setup construction drawings: (a) plan view, (b) elevation, section C-C' and (c) elevation, section D-D'

2.2.2 Specimen 8T-IP

The setup for this specimen was similar to that utilized for specimen 4T-IP, with the exception that the reaction columns were moved further apart to accommodate the longer length of the 8-in. specimen. Figure 2.7 andFigure 2.8 show two photographs and construction drawings of this specimen, respectively.



Figure 2.7 Photographs of the test setup for specimen 8T-IP: (a)View from North-East, (b) from South-East

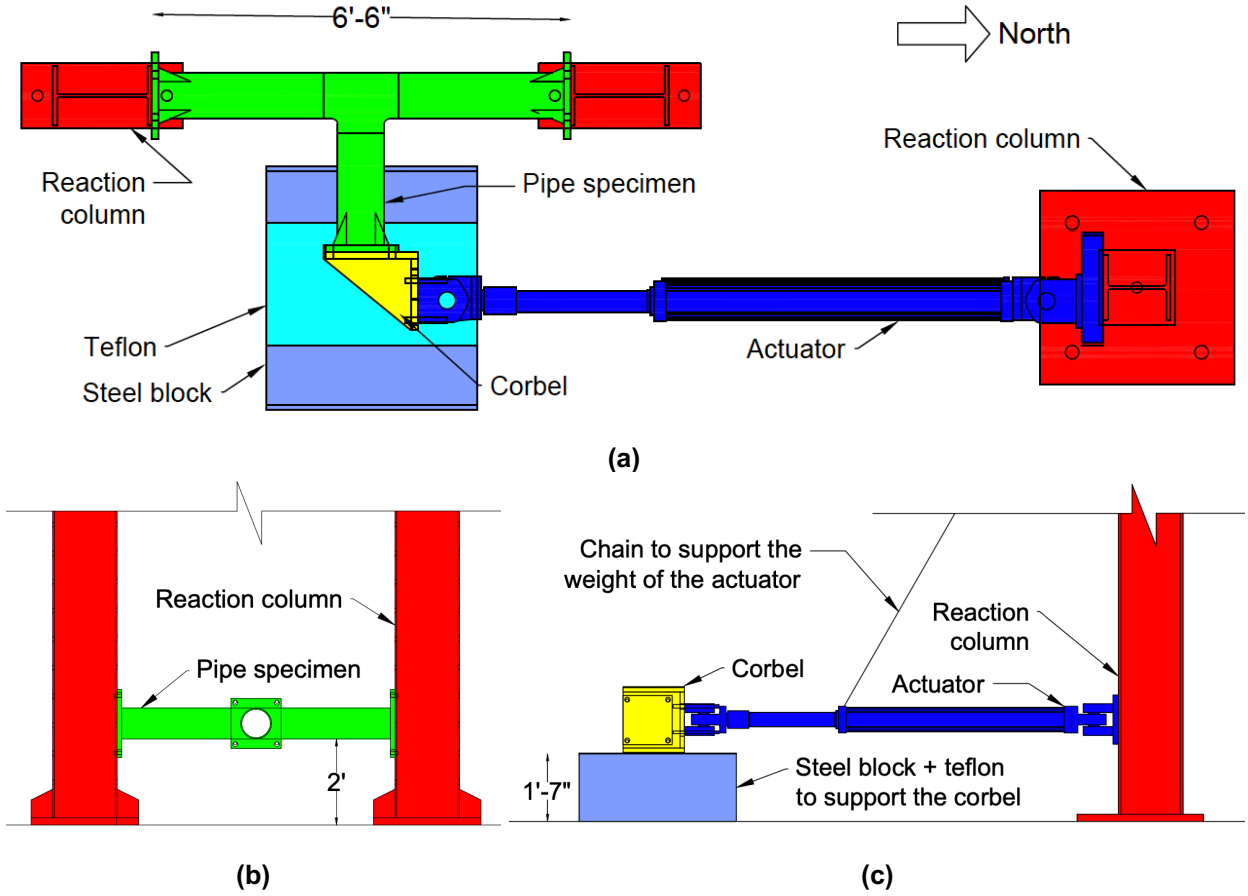

Figure 2.8 Specimen 8T-IP setup construction drawings: (a)plan view, (b) elevation view of the specimen and (c) elevation view of the actuator, corbel and steel block

2.2.3 Specimen 4T-OP

Figure 2.9 shows photographs of the test setup for specimen 4T-OP. The setup for this specimen was similar to that used for the in-plane tests, with the exception that the specimen was rotated 90 degrees and welded at its top to a reaction frame and at its bottom to a steel plate post-tensioned to the strong floor of the laboratory. A cross-bar was lowered and spanned between the reaction columns to capture the boundary reaction at the top of the specimen. Construction drawings of the setup are presented in Figure 2.10.

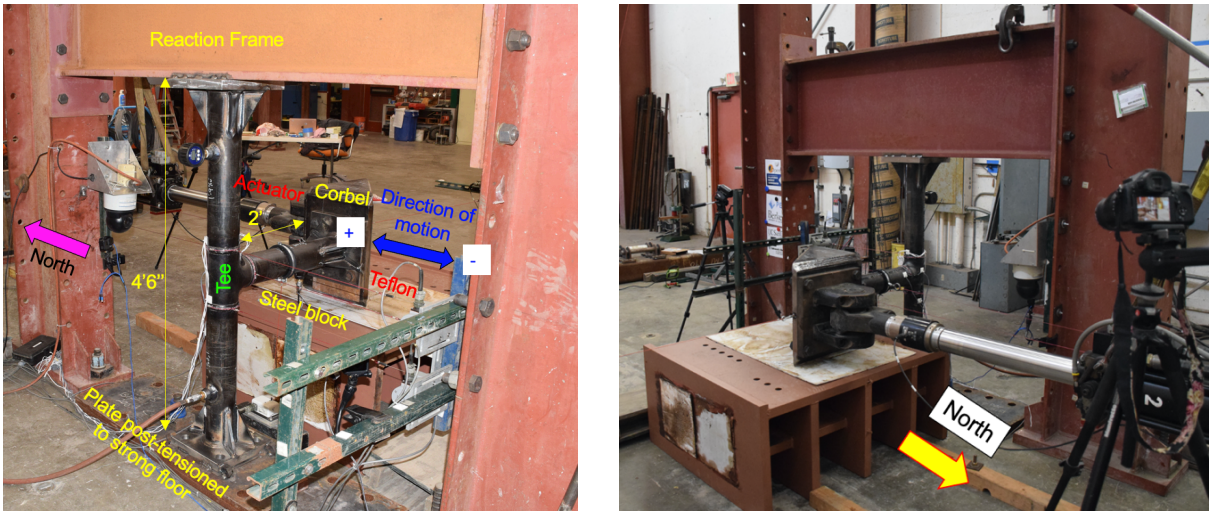

(a) (b)

Figure 2.9 Test setup for specimen 4T-OP: (a) View from South-West, (b) from North-East

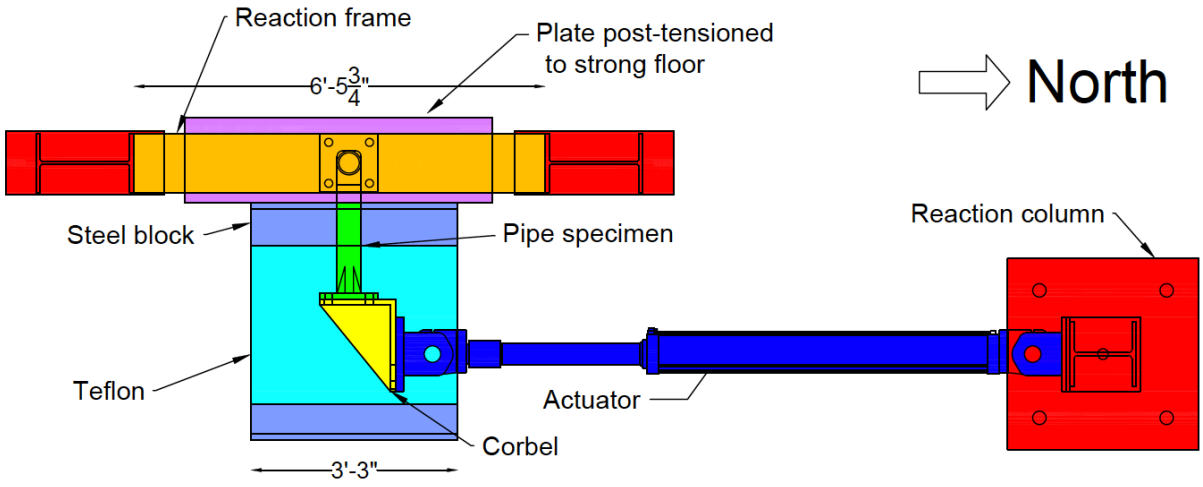

(a)

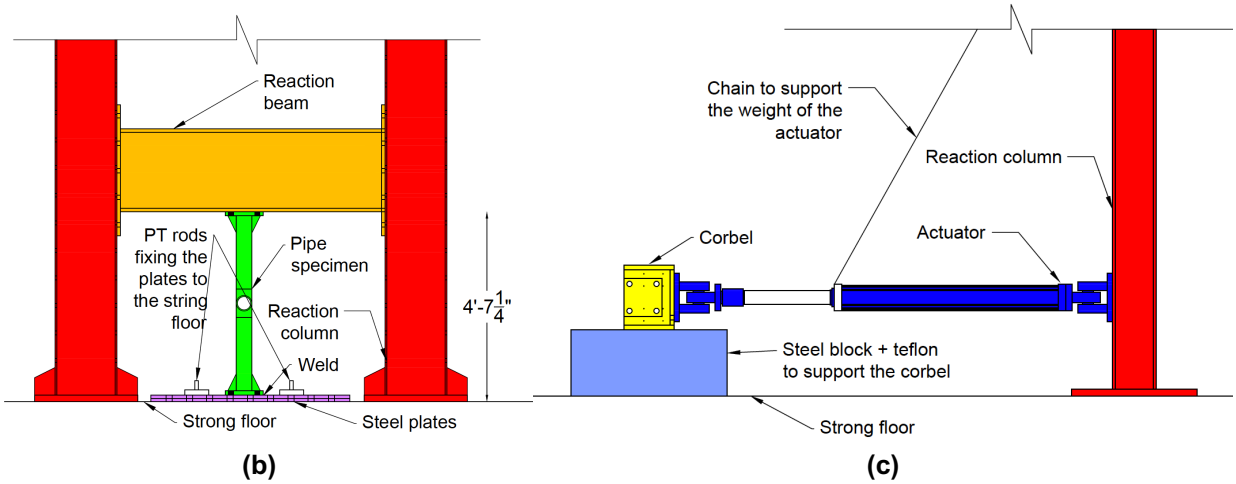

Figure 2.10 Specimen 4T-OP setup construction drawings: (a) plan view, (b) elevation view of the specimen and (c) elevation view of the actuator, corbel and steel block

2.2.4 Specimen 8T-OP

The setup for specimen 8T-OP was similar to that of specimen 4T-OP except that the reaction beam was installed further from the floor to accommodate the longer dimensions of the 8-in specimen, as shown in Figure 2.11 and Figure 2.12. In addition, a taller concrete block was used to elevate the location of the corbel support. Note that a steel block was used for the 4-in OP specimen.

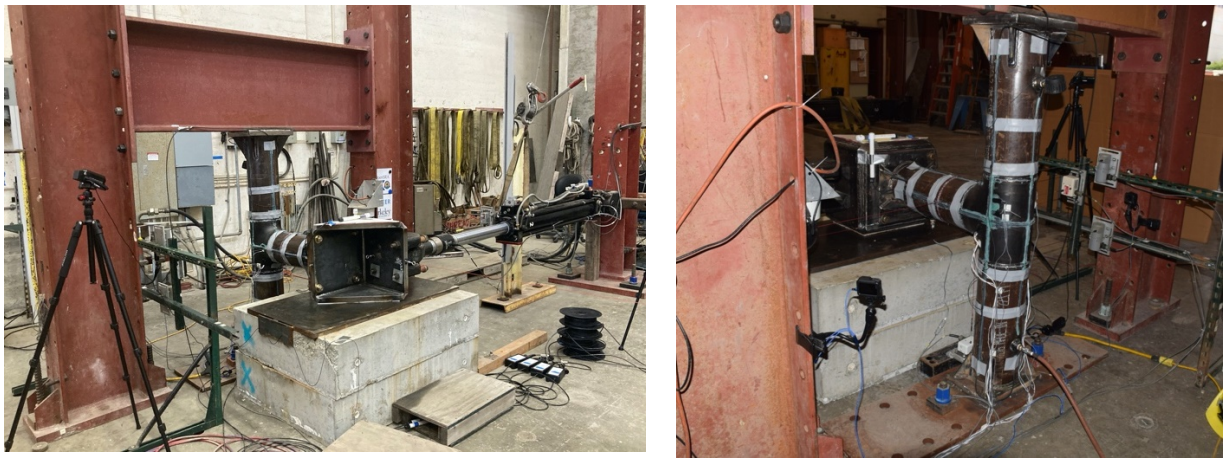

Figure 2.11 Test setup for specimen 8T-OP: (a) View from South-East, (b) from North-West

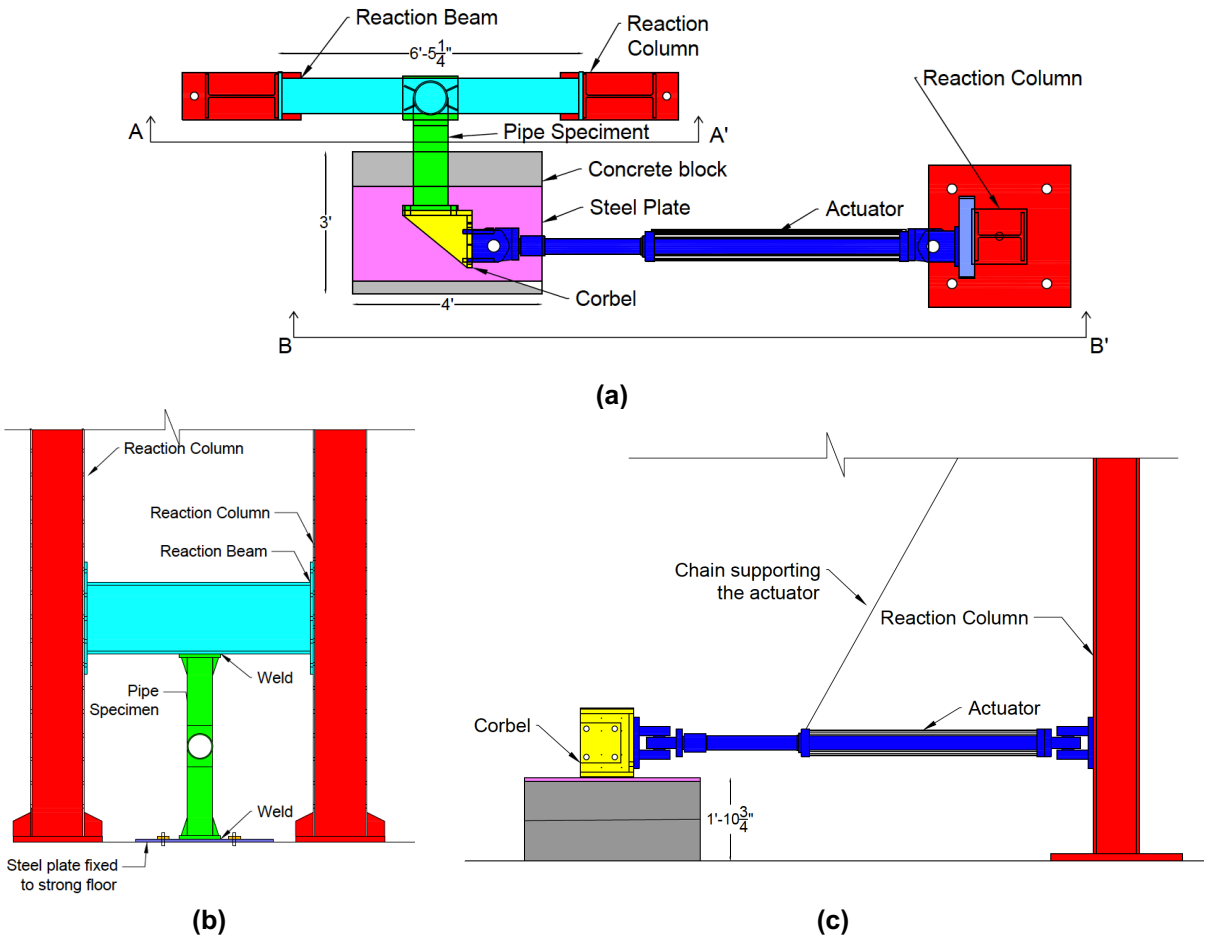

Figure 2.12 Specimen 8T-OP setup construction drawings: (a) plan view, (b) elevation view of the specimen (A-A) and (c) elevation view of the actuator, corbel and steel block (B-B)

2.2.5 Specimen 4E-90

Figure 2.13 shows the test setup for specimen 4E-90. This specimen was supported in between pins allowing rotation of the straight pipe segments. While the southern hinge was bolted to a reaction column, the northern hinge was connected to the actuator through a corbel. The bottom of the corbel was connected to a railing system designed to ensure that the movement remained in the plane of the specimen and that out-of-plane movement was avoided. The rail system was fabricated using two rectangular sliders connected to the corbel and moving along smooth steel rods. These steel rods were then fixed to a hollow structural steel (HSS) beam, which was post-tensioned to the strong floor of the laboratory. Figure 2.13 and Figure 2.14 present photographs and drawings of this specimens' test setup, respectively.

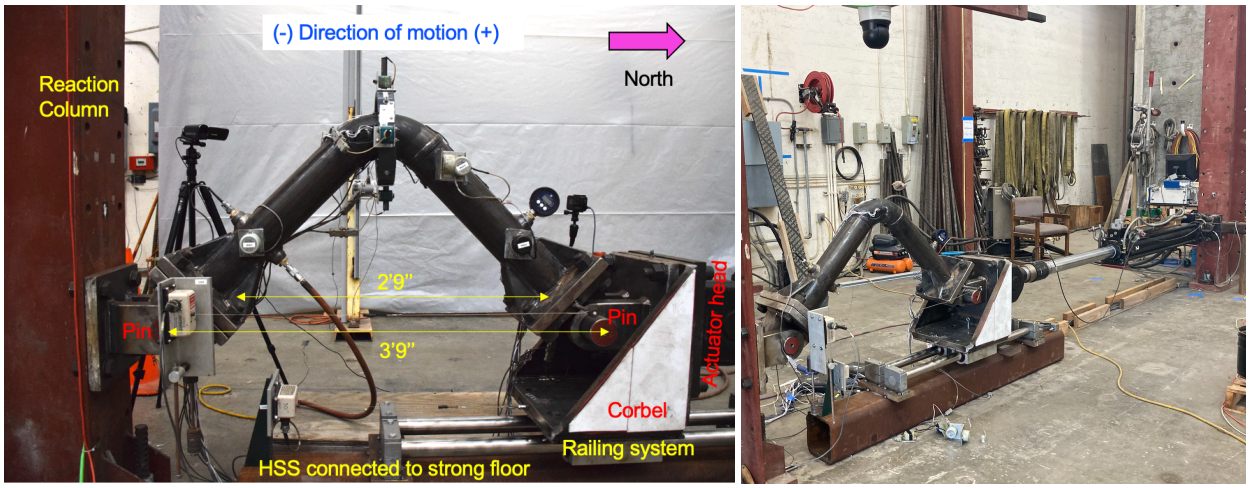

Figure 2.13 Test setup for specimen 4E-90: (a) View from East, (b) from South-West

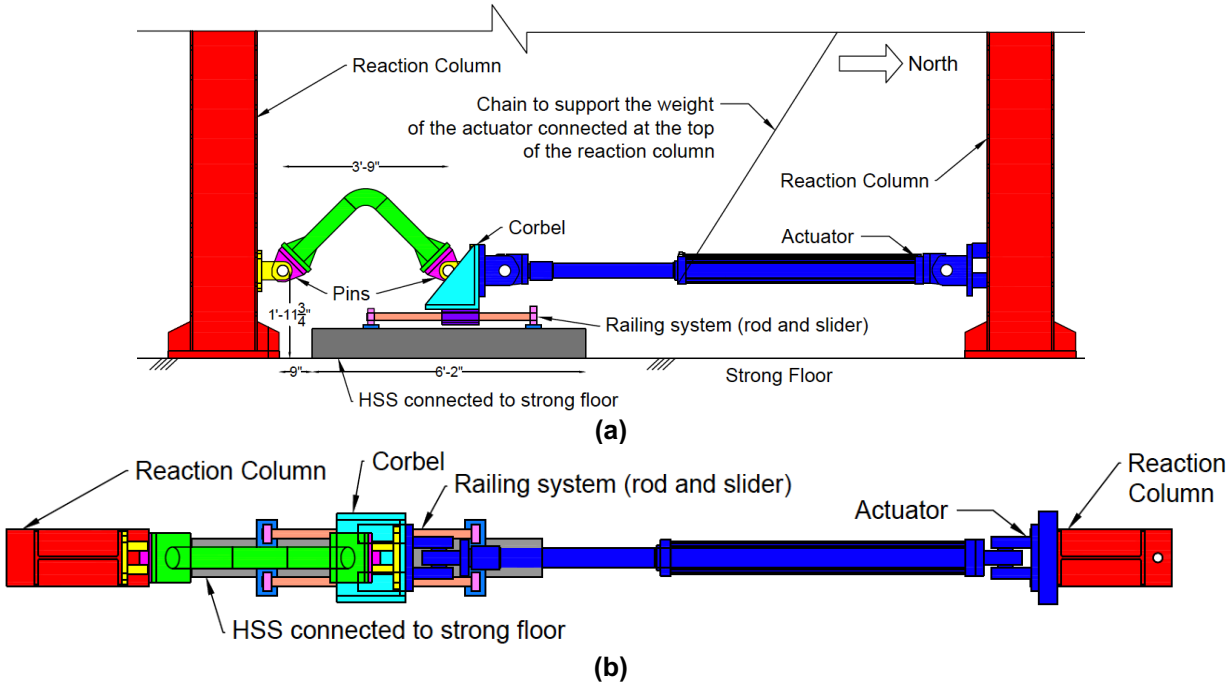

Figure 2.14 Specimen 4E-90 setup construction drawings: (a) elevation and (b) plan view

2.2.6 Specimen 4E-45

The test setup for specimen 4E-45 was similar to that of specimen 4E-90 with the exception that the actuator was retracted further to accommodate the revised geometry of this specimen. Figure 2.15 and Figure 2.16 present photographs and construction setup drawings for this specimen.

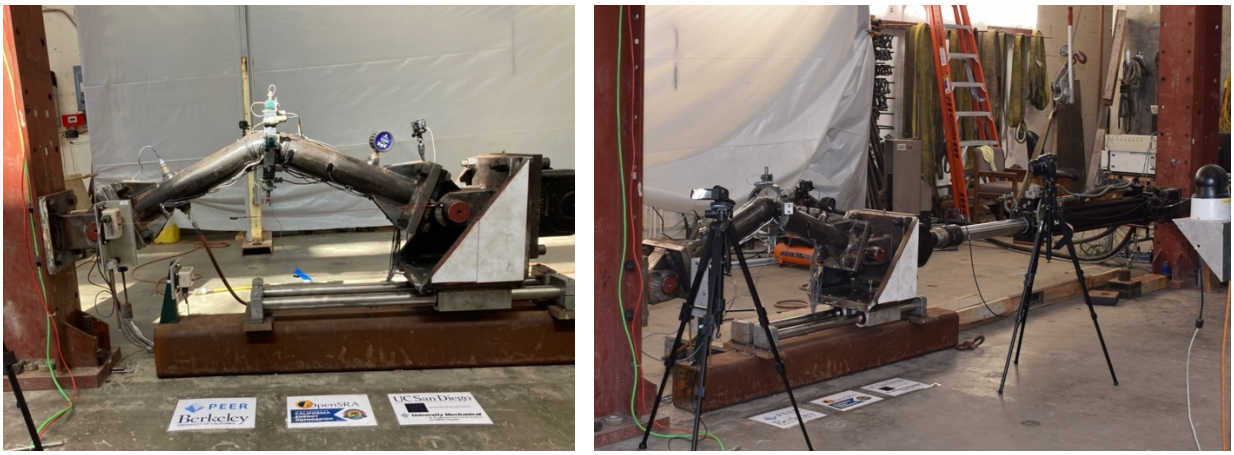

(a) (b)

Figure 2.15 Test setup for specimen 4E-45: (a) view from East, (b) from South-East

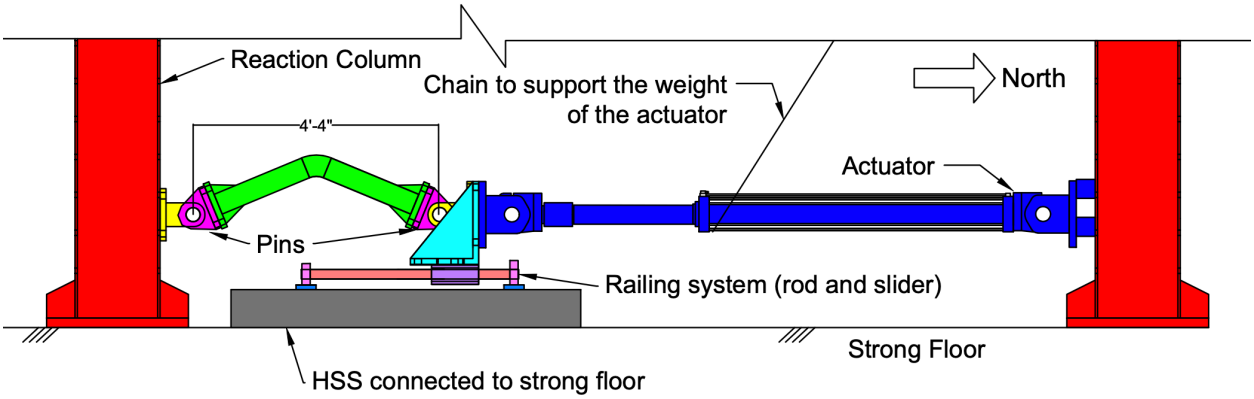

Figure 2.16 Specimen 4E-45 setup construction drawings (elevation view)

2.2.7 Specimen 8E-90

The test setup for specimen 8E-90 was similar to that of specimen 4E-90 with the exception that the Southern column was moved further southward to accommodate the larger diameter (and hence length) specimen, as shown in Figure 2.17 and Figure 2.18.



(a) (b)

Figure 2.17 Test setup for specimen 8E-90 (a) view from East, (b) from North-East

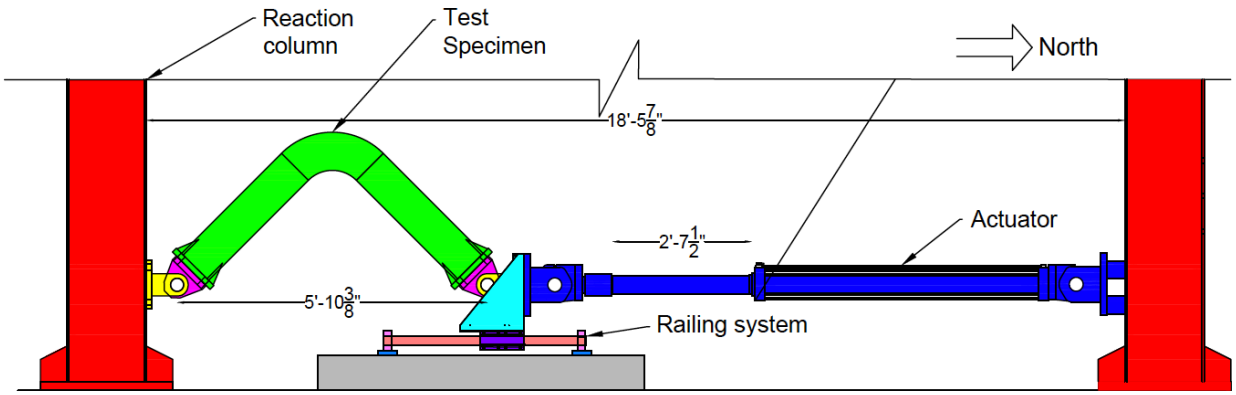

Figure 2.18 Specimen 8E-90 setup construction drawings (elevation view)

2.2.8 Specimen 8E-45

The test setup for specimen 8E-45 was similar to that of specimen 8E-90 with the exception that the actuator was more retracted in its initial position, as show in the photographs of the setup and in the construction drawings (Figure 2.19 and Figure 2.20, respectively). The accommodation of the 45-degree specimen, from the 90-degree specimen for the 8-in diameter models, adopted a similar strategy to that adopted for the 4-in elbows, that is absorbing the geometric differences courtesy of the long stroke available with the hydraulic actuator.

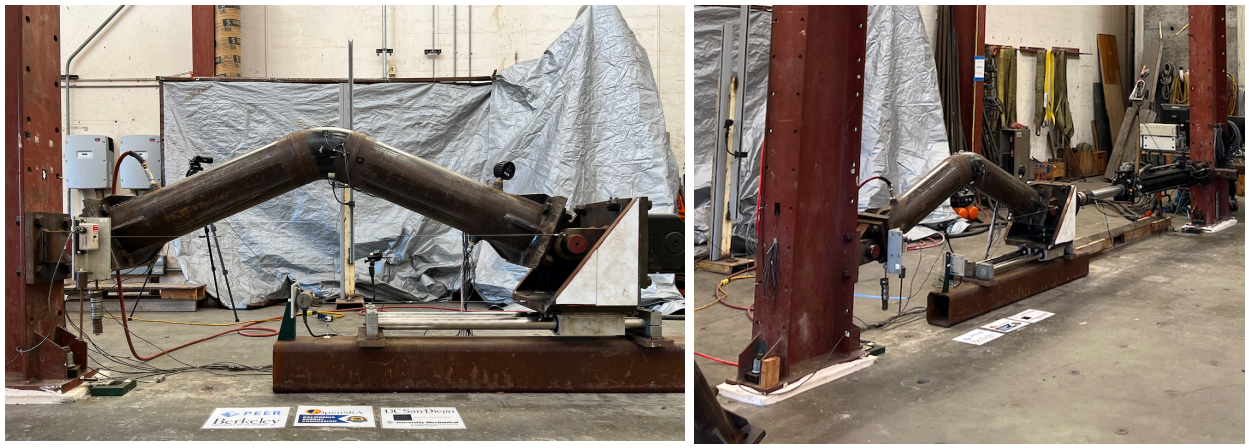

(a) (b)

Figure 2.19 Test setup for specimen 8E-45 (a) view from East, (b) from South-East

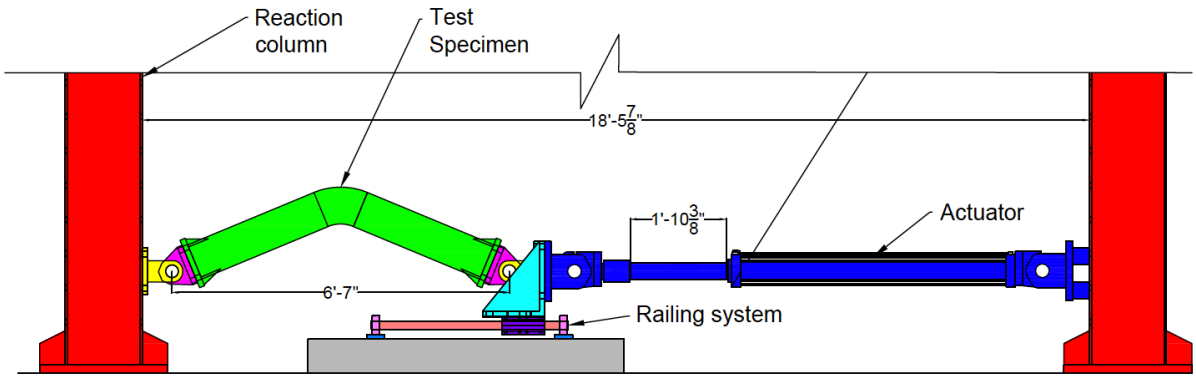

Figure 2.20 Specimen 8E-45 setup construction drawings (elevation view)

2.3 Instrumentation Plans

The specimens were instrumented with an array of displacement potentiometers, uniaxial and rosette strain gauges, and only for elbows, inclinometers. An analog and a digital pressure sensor were also used to monitor the internal gas pressure in the specimens during each test. These sensors were installed in two of the olets of the specimens, while the third olet was connected to a compressor that held the internal gas (air) pressure constant during testing. In addition to these sensors, the displacement and load applied by the actuator were measured with a load cell and tempo sonic displacement sensor internal to the actuator itself. In total, between 13 and 36 analog sensor channels were used for each specimen. In addition, an array of digital high-resolution video

cameras surrounding the specimen was used to document physical damage during each experiment. Test 8T-OP was also instrumented with fiber optics installed by the project team from the University of California, Berkeley (Wang et al. 2025). The location of the analog sensors was selected strategically to obtain the displacement at relevant locations and strains at the location of strain concentrations predicted by the Abaqus model (Smith 2009).

2.3.1 Specimen 4T-IP

The test setup for Specimen 4T-IP was instrumented with 36 channels of analog sensors, whose location is shown in the instrumentation plans provided in Figure 2.21Figure 2.22. Select photographs of the instrumentation are presented in Figure 2.23. The specific distribution of sensors was as follows:

- 13 displacement potentiometers (Figure 2.21). For this test, L02 through L09 were linear potentiometers, while L01, and L09 through L13 were string potentiometers.
- 11 strain gauges (Figure 2.22a).
- 4 rosettes (Figure 2.22b). Each rosette has 3 channels that can be used to find the principal strains and their direction. These three strain gauges contained in a rosette are marked by color: blue, yellow or red. The direction of these three channels is relevant to computing the principal strains and it is shown in the instrumentation plan. In total this test specimen was outfitted with 12 sensor channels for the 4 rosettes.

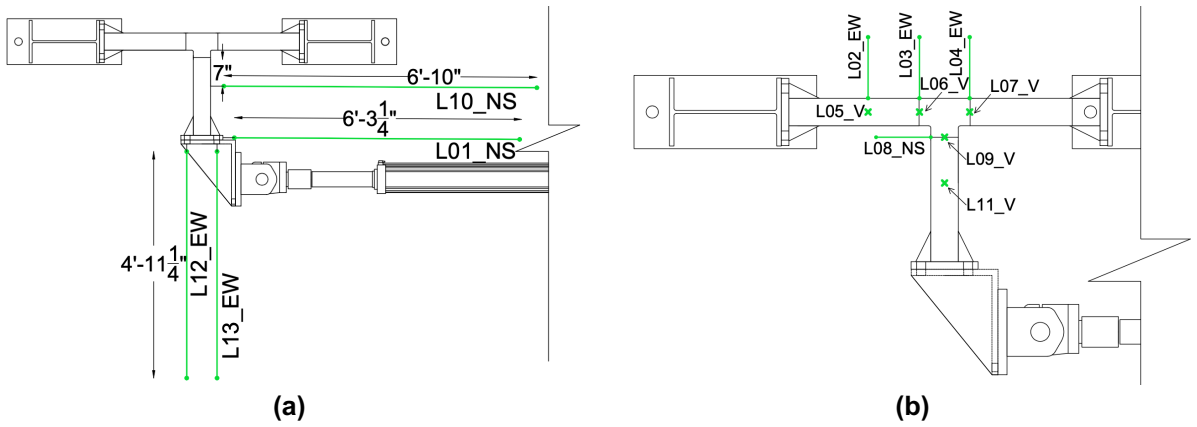

Figure 2.21 Instrumentation plan for specimen 4T-IP: displacement potentiometers (EW=east west; NS= north south; V=vertical)

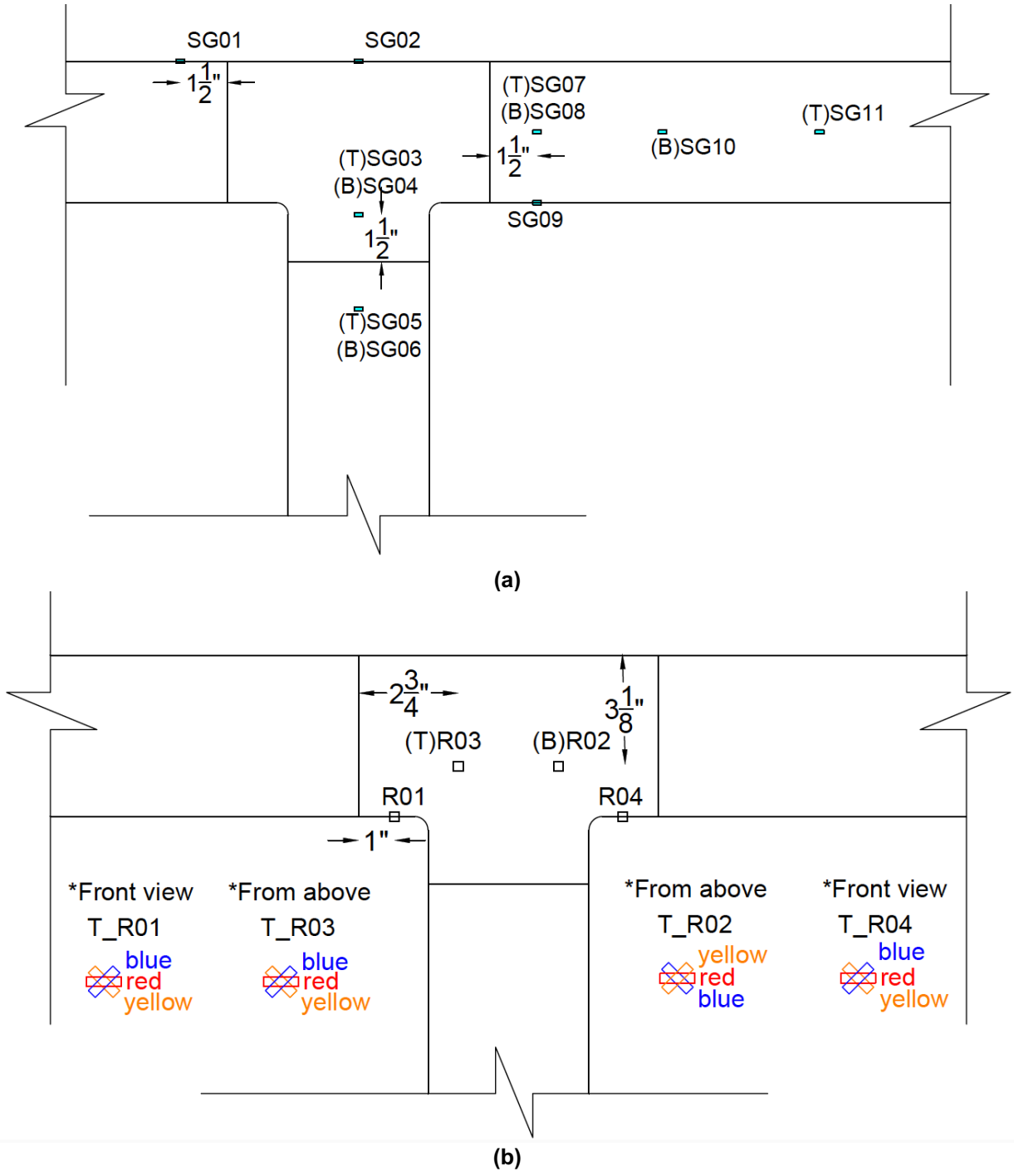

Figure 2.22 Instrumentation plan for specimen 4T-IP: (a) uniaxial strain gauges and (b) rosettes (T=top; B=bottom)

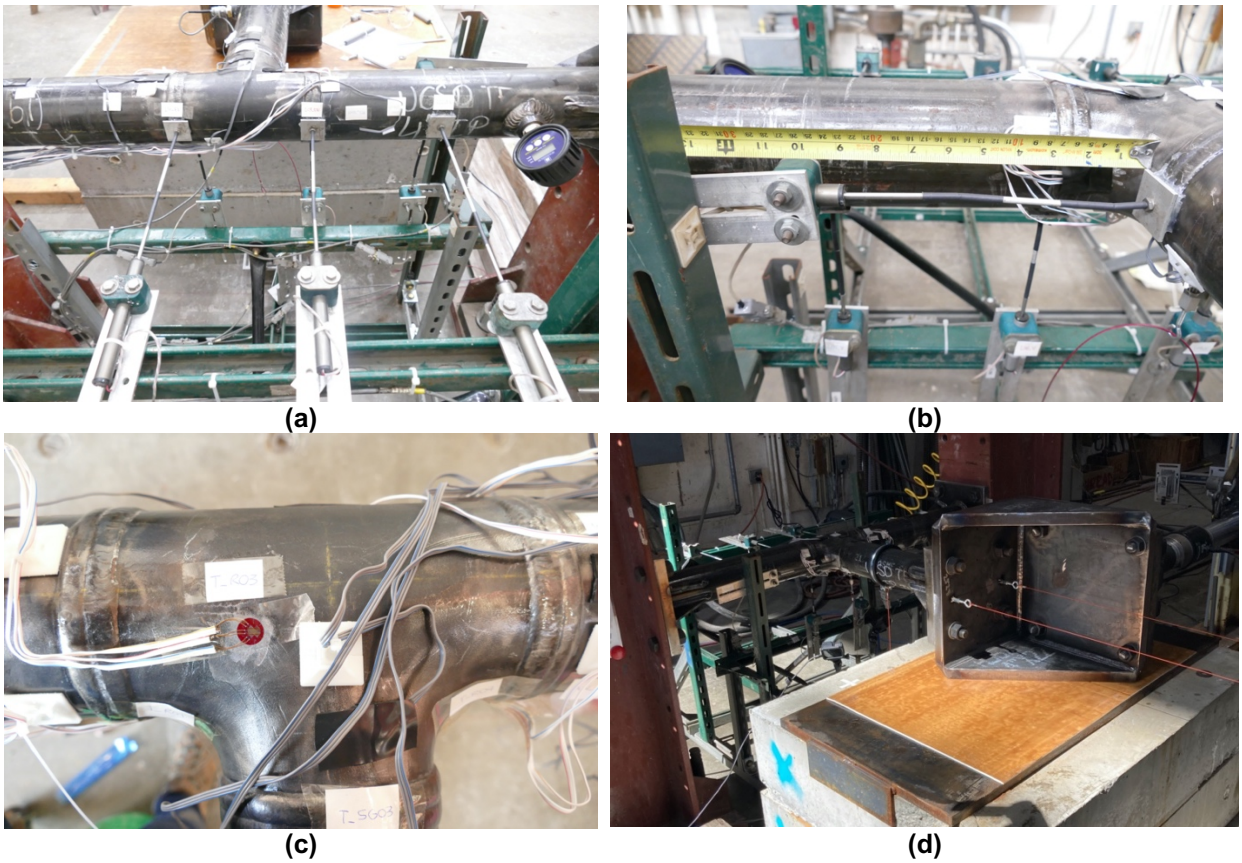

Figure 2.23 Photographs of select sensors of Specimen 4T-IP: (a) Linear potentiometers L02, L03, L04 (b) linear potentiometer L08 (with L05 and L06 in the background), (c) rosette R03, (d) attachment points of L12 and L13.

2.3.2 Specimen 4T-OP

Specimen 4T-OP was instrumented with 7 displacement potentiometers (Figure 2.24), 3 uniaxial strain gauges and 1 rosette (Figure 2.25), for a total of 13 channels of analog sensors. The linear potentiometers were varied compared with Specimen 4T-IP to capture the out-of-plane specimen displacement. Specifically, string potentiometers were utilized in this case, attached to the specimen with a string wrapped around the pipe and held in place firmly with hot glue (Figure 2.26a). Select photographs of strain gauges and string potentiometers as distributed on this specimen are shown in Figure 2.26.

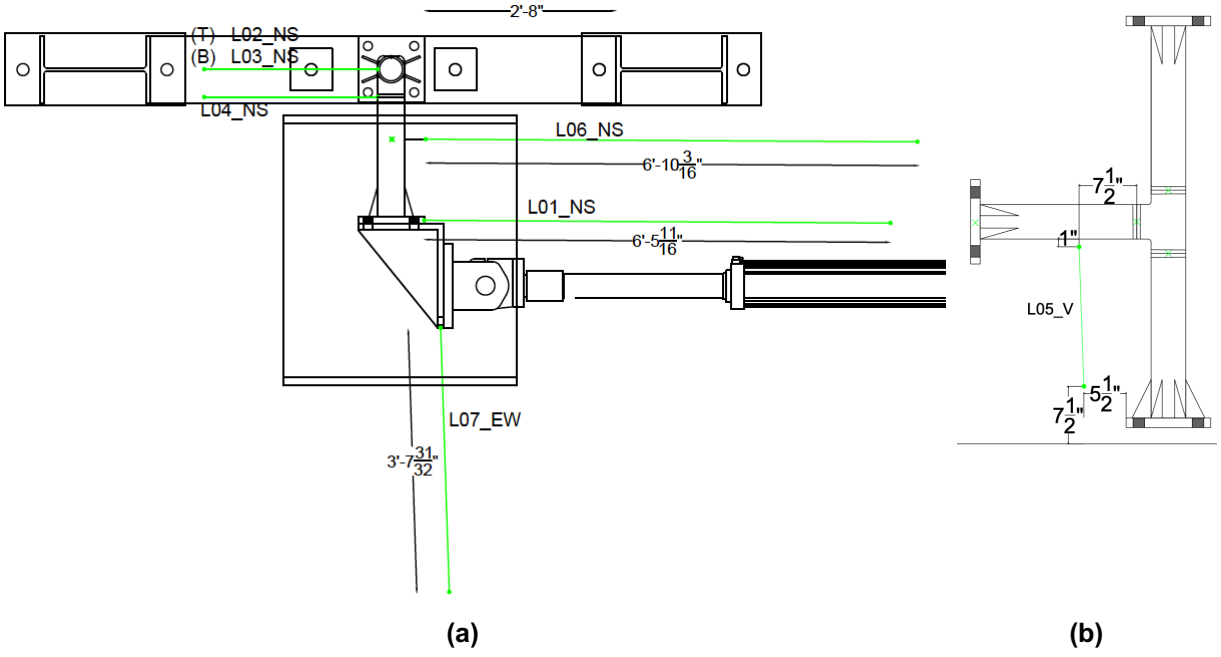

Figure 2.24 Instrumentation plan for specimen 4T-OP, string potentiometers (a) horizontal and (b) vertical direction (EW=east west; NS= north south; V=vertical)

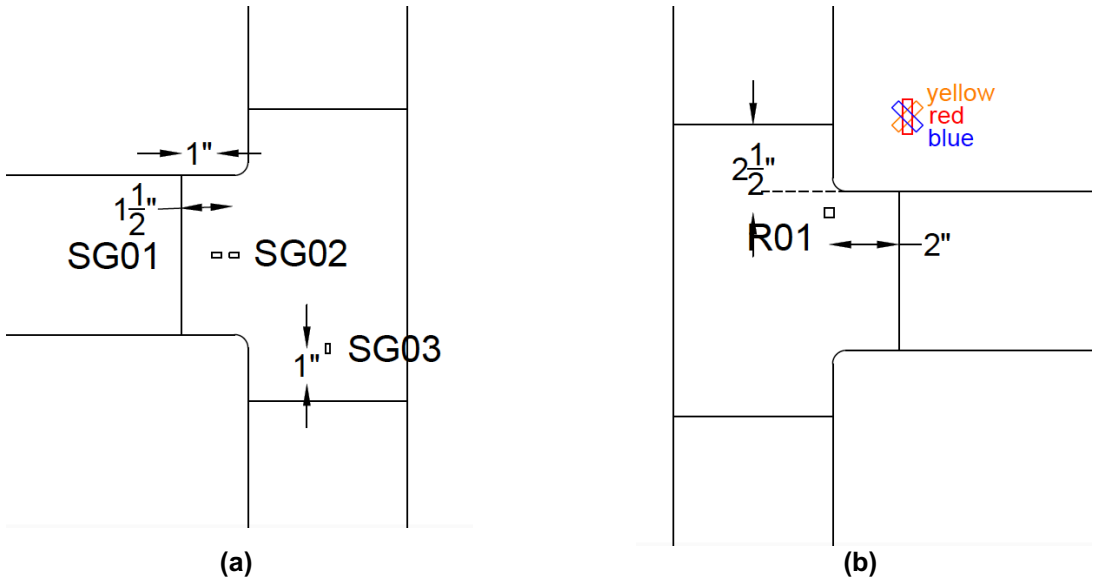

Figure 2.25 Instrumentation plan for specimen 4T-OP, uniaxial strain gauges and rosettes: (a) north side and (b) south side



Figure 2.26 Photographs of select sensors of Specimen 4T-OP: (a) String potentiometers L02, L03, L04, (b) details of point of attachment between strings and pipe (c) strain gauges on the north side of the specimen (d) string potentiometers L06 (front) and L01 (back)

2.3.3 Specimen 8T-IP

This specimen was instrumented with seven string potentiometers (Figure 2.27), five strain gauges and two rosettes (Figure 2.28) for a total of 18 channels of sensors. Photographs of representative string potentiometers, strain gauges and rosettes are shown in Figure 2.29.

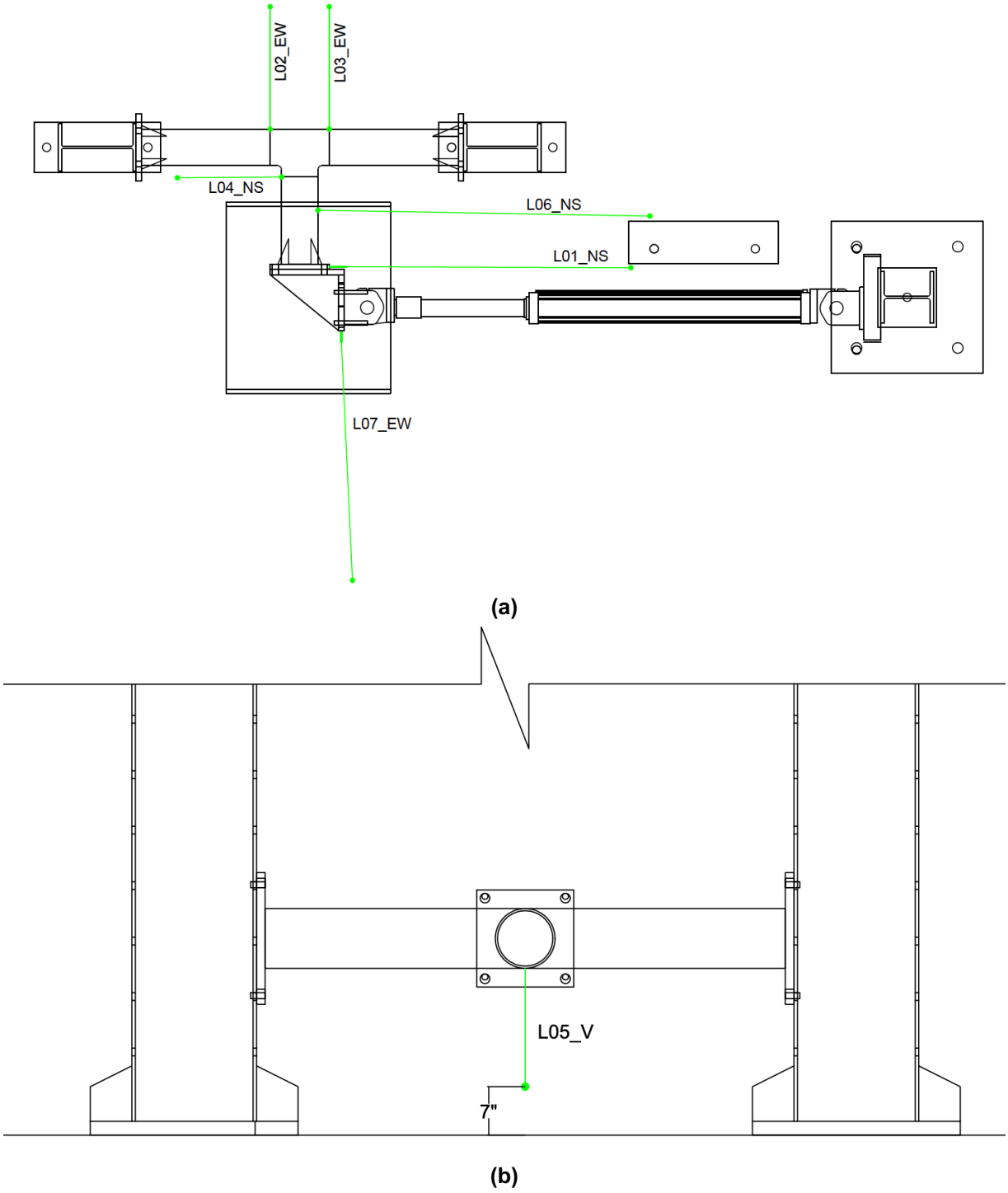

Figure 2.27 Instrumentation plan for specimen 8T-IP, string potentiometers: (a) horizontal and (b) vertical direction (EW=east west; NS= north south; V=vertical)

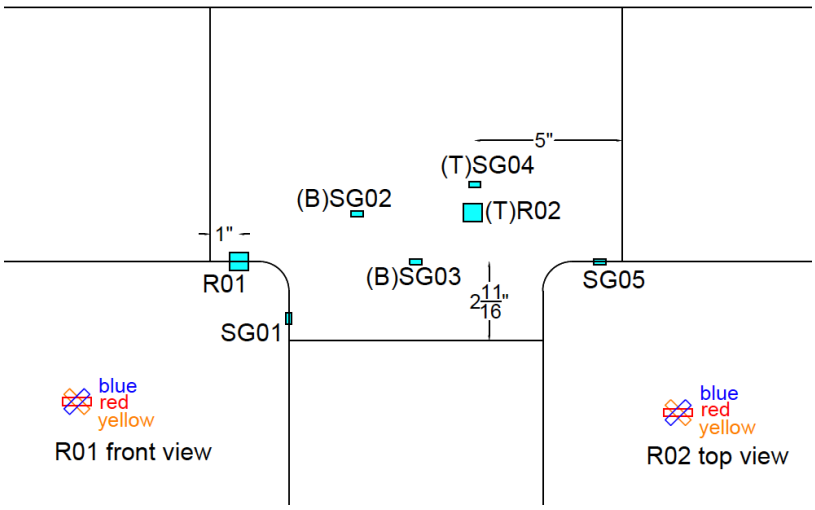

Figure 2.28 Instrumentation plan for specimen 8T-IP: uniaxial strain gauges and rosettes

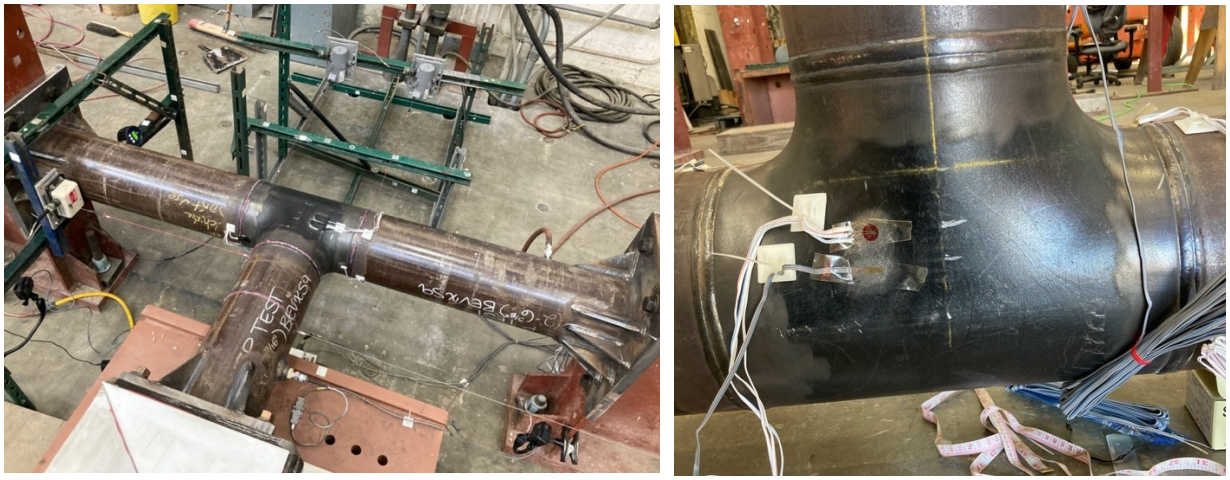

(a) (b)

Figure 2.29 Photographs of selected sensors for specimen 8T-IP: (a) string potentiometers monitoring the specimen and (b) R02

2.3.4 Specimen 8T-OP

Specimen 8T-OP was instrumented with seven string potentiometers (Figure 2.30), four strain gauges and two rosettes (Figure 2.31), for a total of 17 channels of sensors. Photographs of select sensors are presented in Figure 2.32.

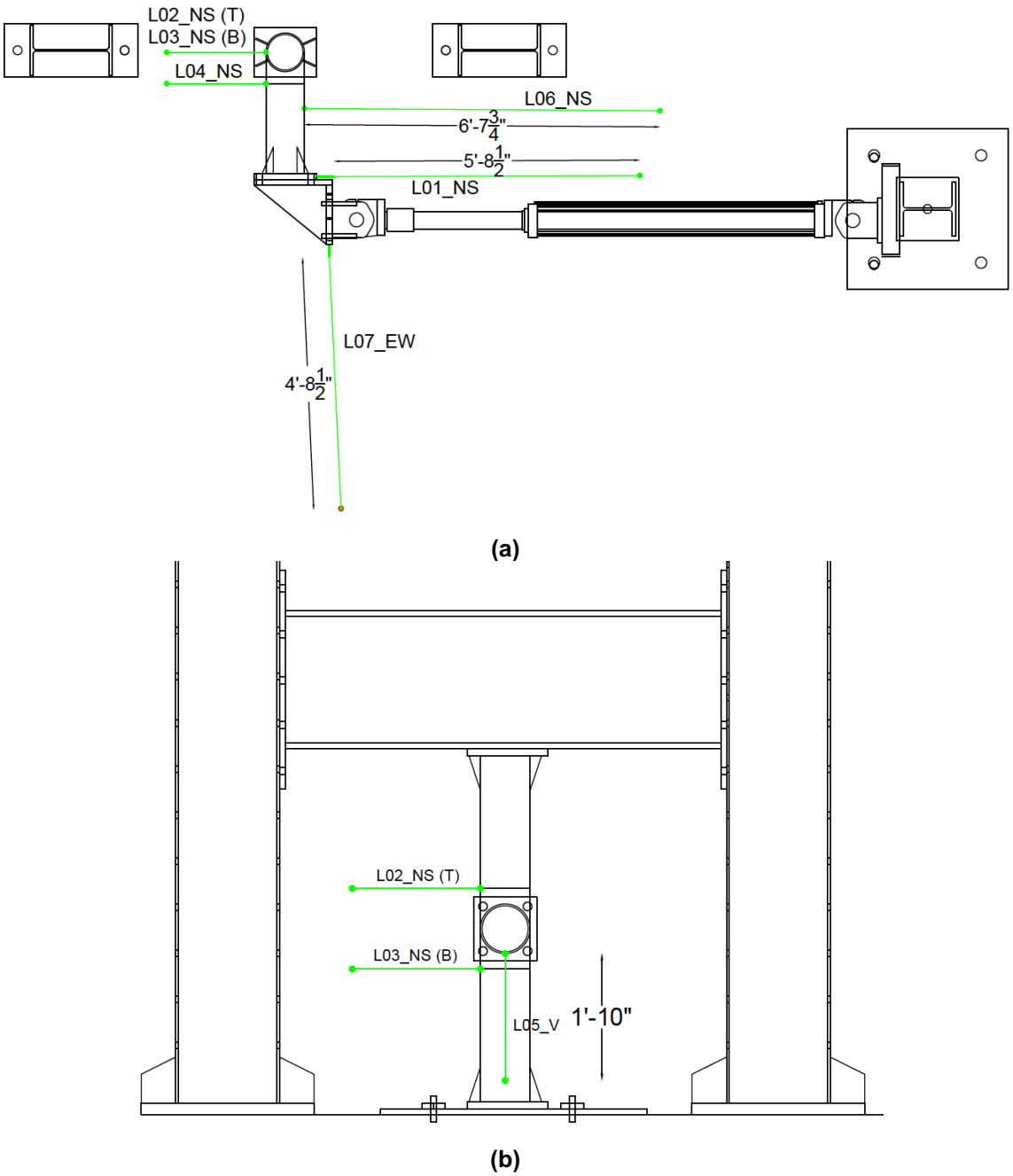

Figure 2.30 Instrumentation plan for specimen 8T-IP, string potentiometers: (a) plan and (b) elevation views (EW=east west; NS= north south; V=vertical)

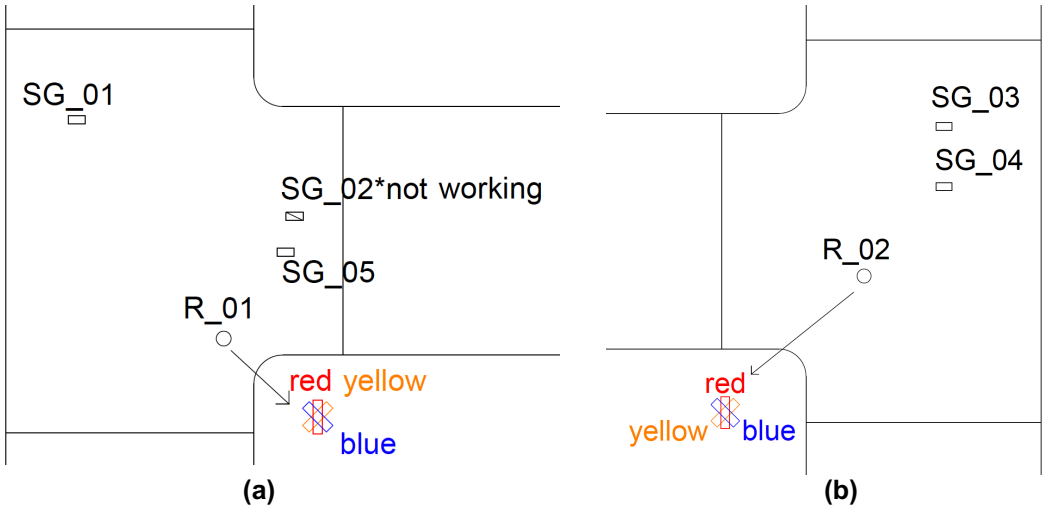

Figure 2.31 Instrumentation plan for specimen 8T-OP: (a) uniaxial strain gauges and (b) rosettes (T=top; B=bottom)

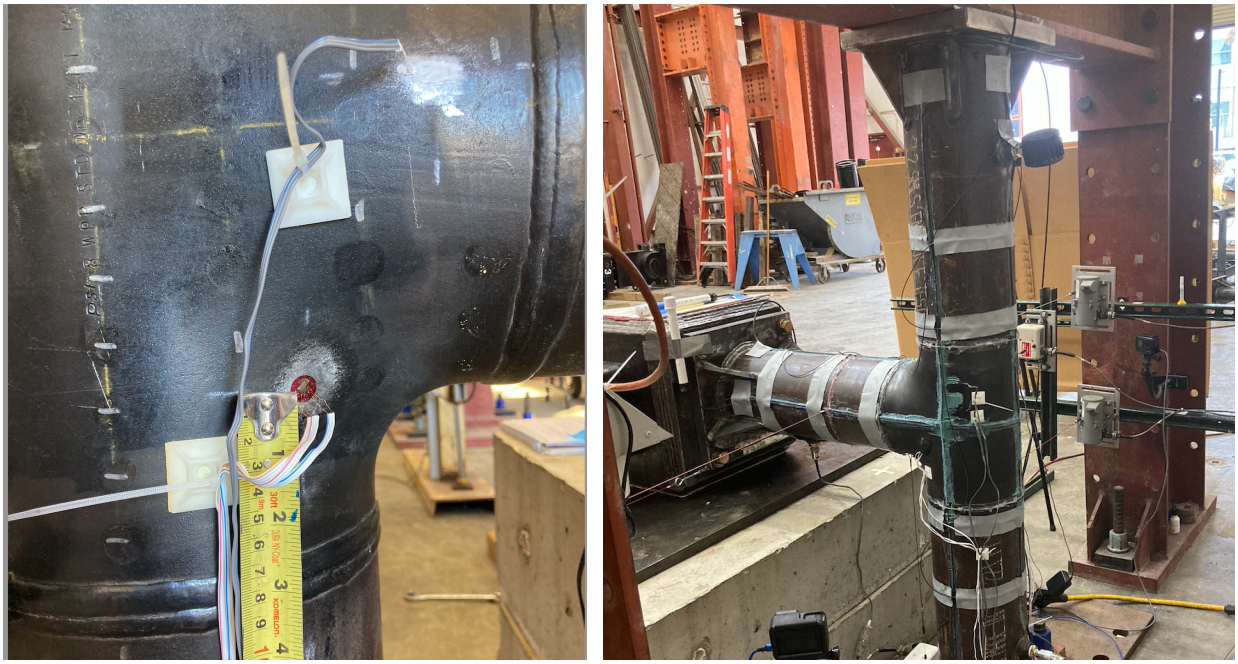

Figure 2.32 Photographs of selected sensors for specimen 8T-OP: (a) R01 and SG02 and (b) string potentiometers L06, L02 and L03

2.3.5 Specimen 4E-90

This specimen was instrumented with eleven uniaxial strain gauges, three rosettes (Figure 2.33a and b), eight displacement potentiometers (Figure 2.33c) and four inclinometers (Figure 2.33d), for a total of 32 sensor channels. Sensors L07 and L08 were not monitoring the specimen itself but

the bottom of the northern and southern columns, respectively. A photograph of the setup documenting the location of select sensors is presented in Figure 2.34.

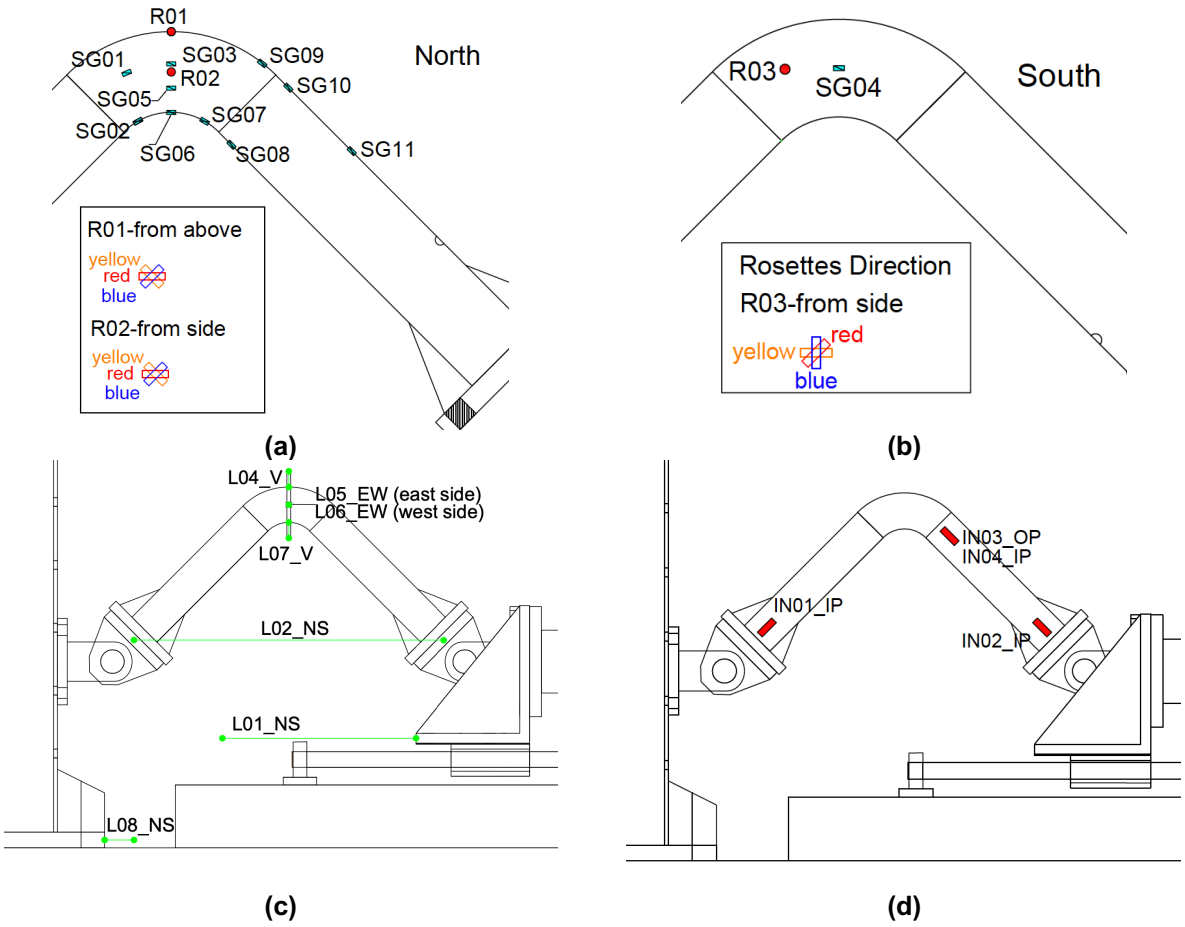

Figure 2.33 Instrumentation plan for specimen 4E-90: (a) uniaxial strain gauges and rosettes in the east and (b) west side of the specimen, (c) displacement potentiometers and (d) inclinometers (EW=east west; NS= north south; V=vertical; IP= in plane; OP=out of plane)

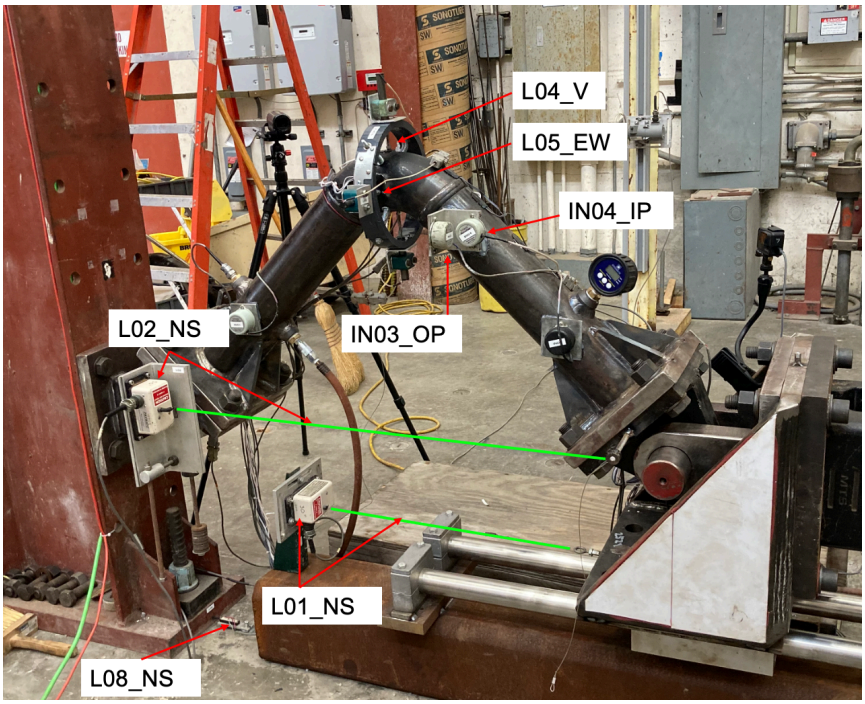

Figure 2.34 Photographs of selected sensors for specimen 4E-90

2.3.6 Specimen 4E-45

This specimen was instrumented with thirteen strain gauges, two rosettes (Figure 2.35), eight displacement potentiometers (Figure 2.36a) and four inclinometers (Figure 2.36b), for a total of 31 sensor channels. The sensor selected to control the test was L01. A photograph of the setup showing the location of select sensors is presented in Figure 2.37.

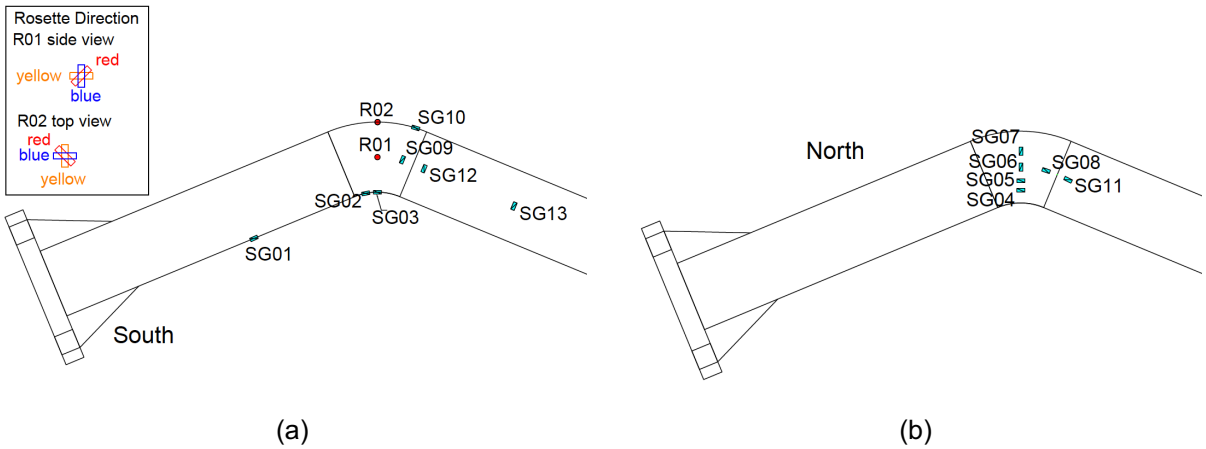

Figure 2.35 Instrumentation plan for specimen 4E-45: (a) uniaxial strain gauges and rosettes in the east and (b) west side of the specimen

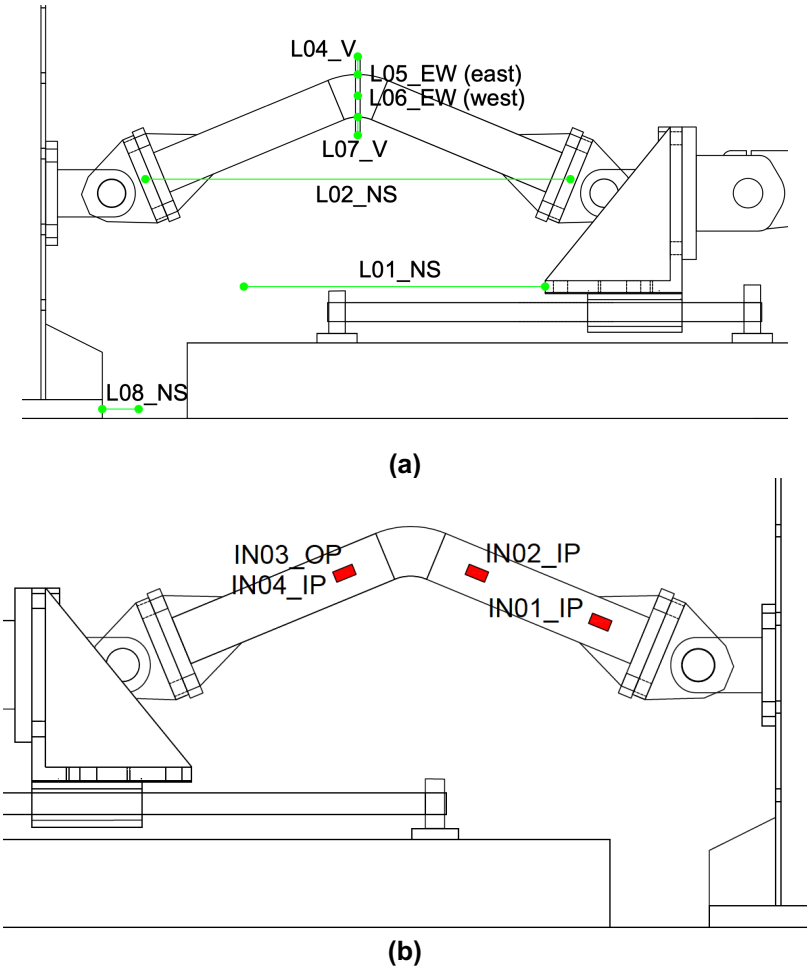

Figure 2.36 Instrumentation plan for specimen 4E-45: (a) displacement potentiometers (east side) and (b) inclinometers (west side) (EW=east west; NS= north south V=vertical; IP= in plane; OP=out of plane)

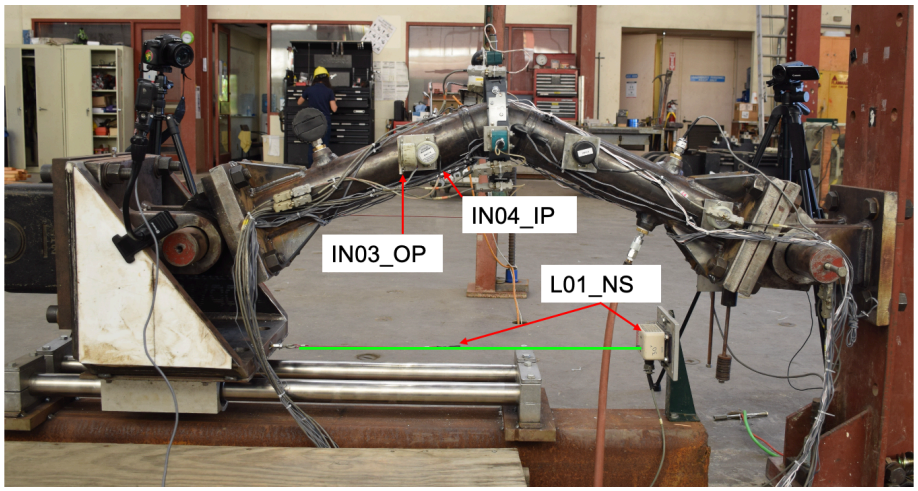

Figure 2.37 Photographs of selected sensors for specimen 4E-45 (west side)

2.3.7 Specimen 8E-90

Specimen 8E-90 was instrumented with fourteen uniaxial strain gauges, four rosettes, four displacement potentiometers and four inclinometers, similarly to 4E-90. The total number of sensor channels in this test setup was 34. Most of the strain gauges were installed in the back (west side) of the specimen, as shown in Figure 2.38. Figure 2.39 shows the location of displacement potentiometers and inclinometers, it is noted that inclinometers are installed in the back (east side) of the specimen. Figure 2.40 shows photographs of selected analog sensors.

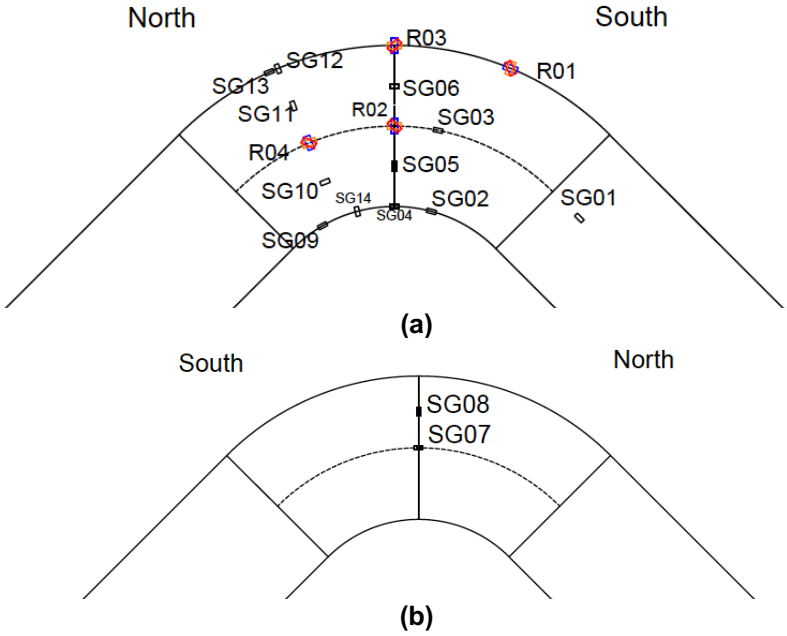

Figure 2.38 Instrumentation plan for specimen 8E-90: uniaxial strain gauges and rosettes in the (a) west and (b) east side of the specimen

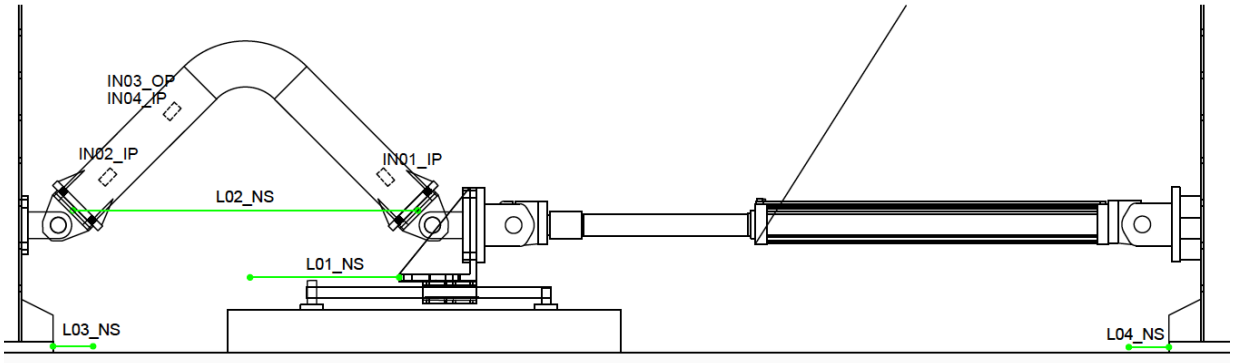

Figure 2.39 Instrumentation plan for specimen 8E-90: displacement potentiometers and inclinometers (EW=east west; NS= north south; V=vertical; IP= in plane; OP=out of plane). Note that the inclinometers are installed in the east side of the specimen

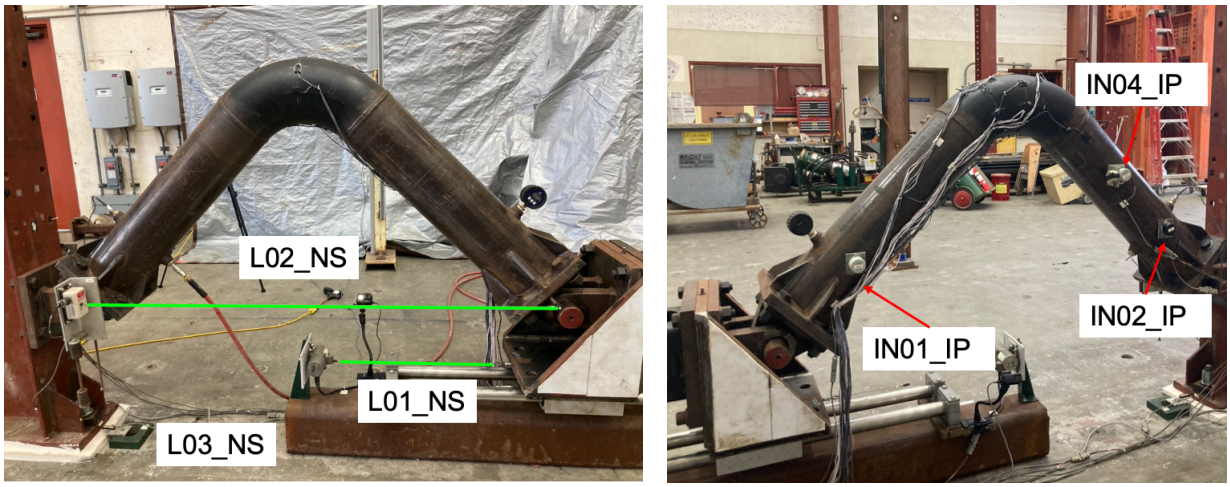

Figure 2.40 Photographs of select sensors for specimen 8E-90: (a) east side and (b) west side

2.3.8 Specimen 8E-45

Specimen 8E-45 was instrumented with eleven uniaxial strain gauges, three rosettes, four displacement potentiometers and four inclinometers. The total number of sensor channels installed on this specimen was 28. Figure 2.41 shows the location of the strain gauges, while Figure 2.42 presents the location of displacement potentiometers and inclinometers. Figure 2.43 shows photographs of select analog sensors.

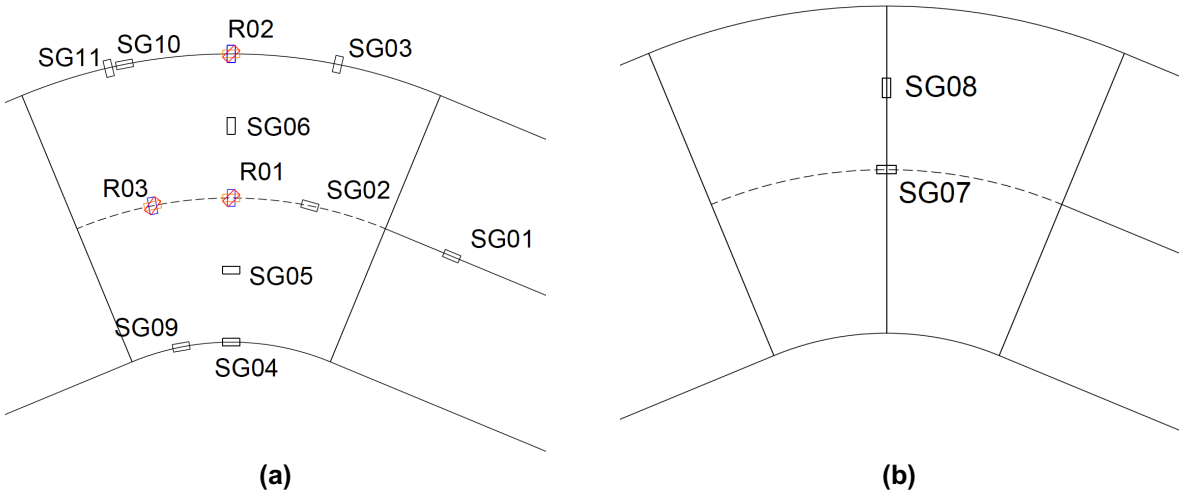

Figure 2.41 Instrumentation plan for specimen 8E-45: (a) uniaxial strain gauges and rosettes in the west and (b) east side of the specimen

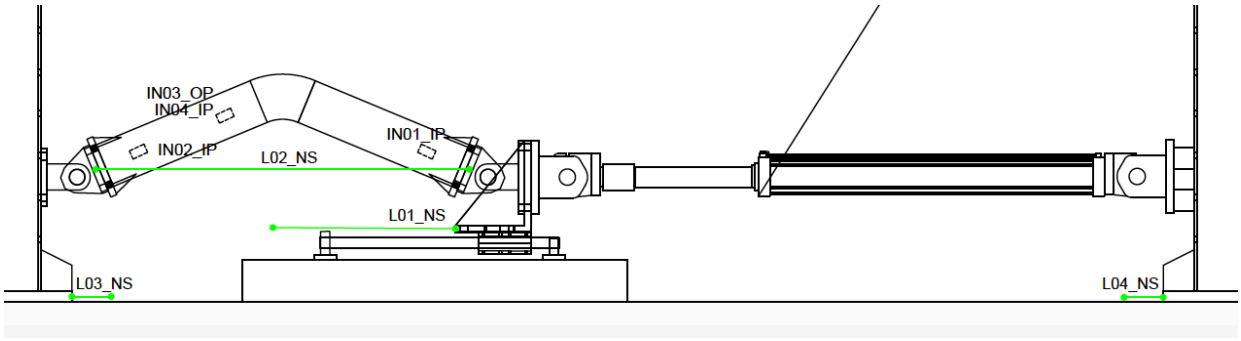

Figure 2.42 Instrumentation plan for specimen 8E-45: displacement potentiometers and inclinometers (EW=east west; NS= north south; V=vertical; IP= in plane; OP=out of plane). Note that the inclinometers are installed in the east side of the specimen

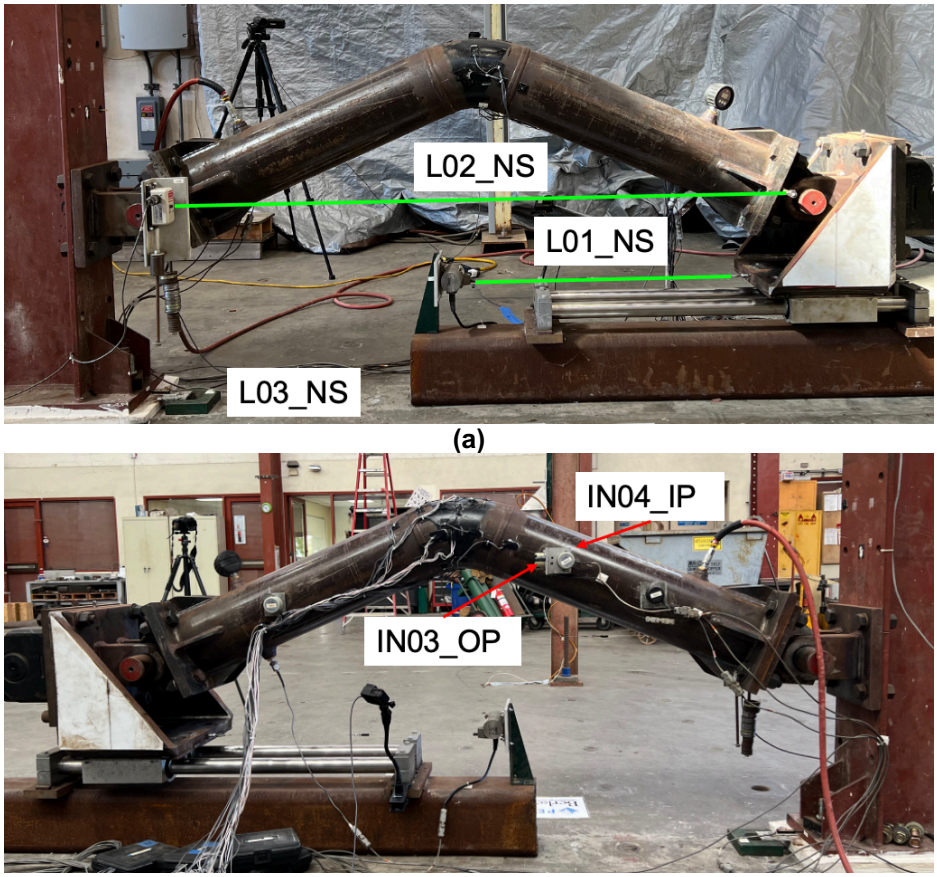

Figure 2.43 Photographs of selected sensors for specimen 8E-45: (a) east side and (b) west side

2.3.9 Camera Plan

Six cameras were installed to monitor each test, as summarized in Table 2.4. While the webcams (C5 and C6) always monitored the specimen from the same perspective, the other cameras were moved around to obtain the optimum set of views based on the type of specimen tested. The views from all cameras for the eight tests are presented in Figure 2.44 through Figure 2.51.

Table 2.4 Summary of views from cameras

Camera Name	View	Camera Type
C1	Overview from south	Canon HD
C2	Overview from north	Panasonic Lumix DMC FZ1000
C3	4T-IP, 8T-IP: South/Bottom view 4T-OP, 8T-IP: South/Side view Elbows: North/Bottom	GoPro
C4	4T-IP, 8T-IP: North/Bottom view 4T-OP, 8T-IP: North/Side view Elbows: West side view	GoPro
C5	Top view for all except 4T-OP and 8T-OP for which it shows a side view	WebCam
C6	Front view	WebCam

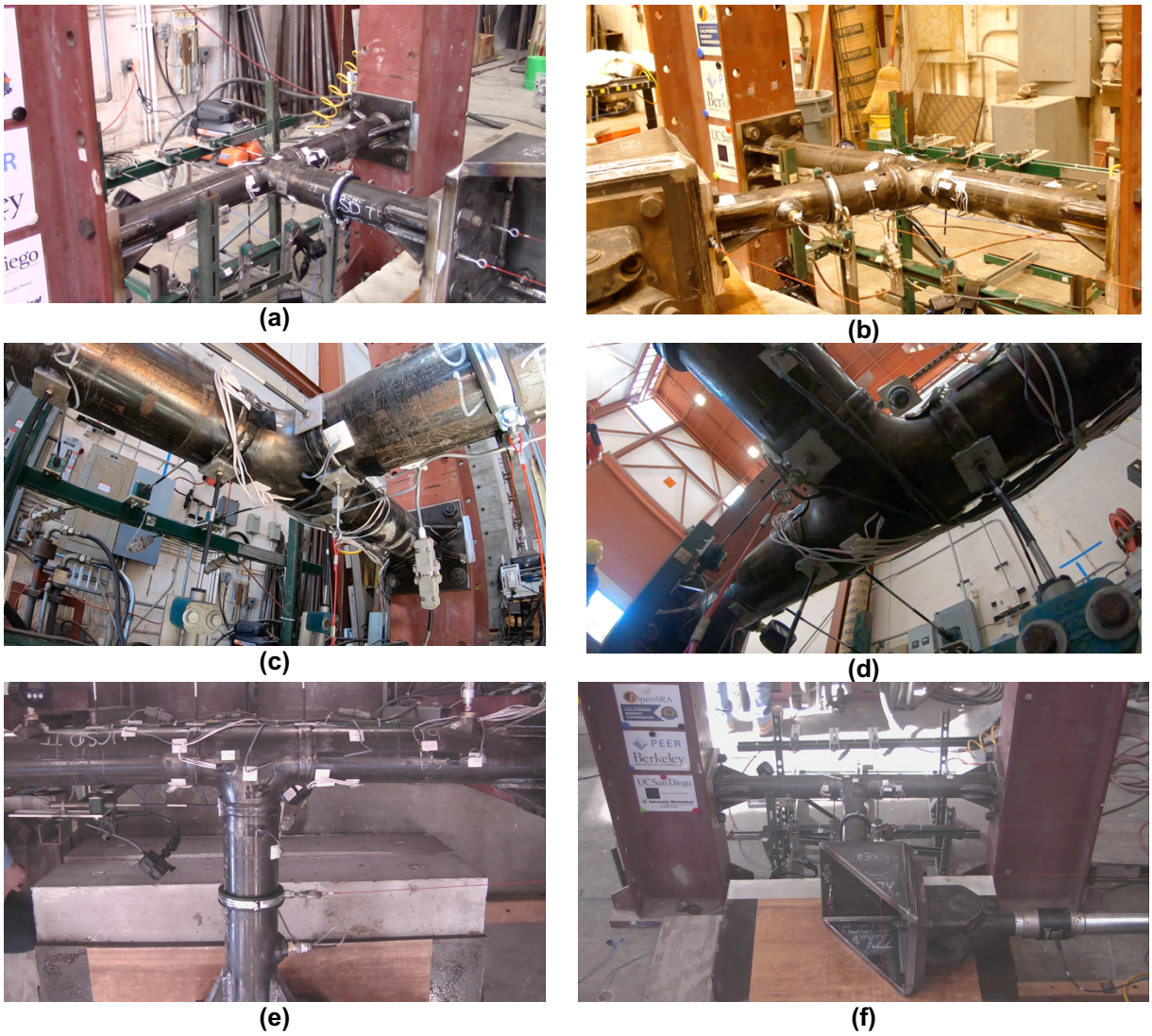

Figure 2.44 Views from the six cameras for specimen 4T-IP: (a) C1; (b) C2; (c) C3; (d) C4; (e) C5; (f) C6

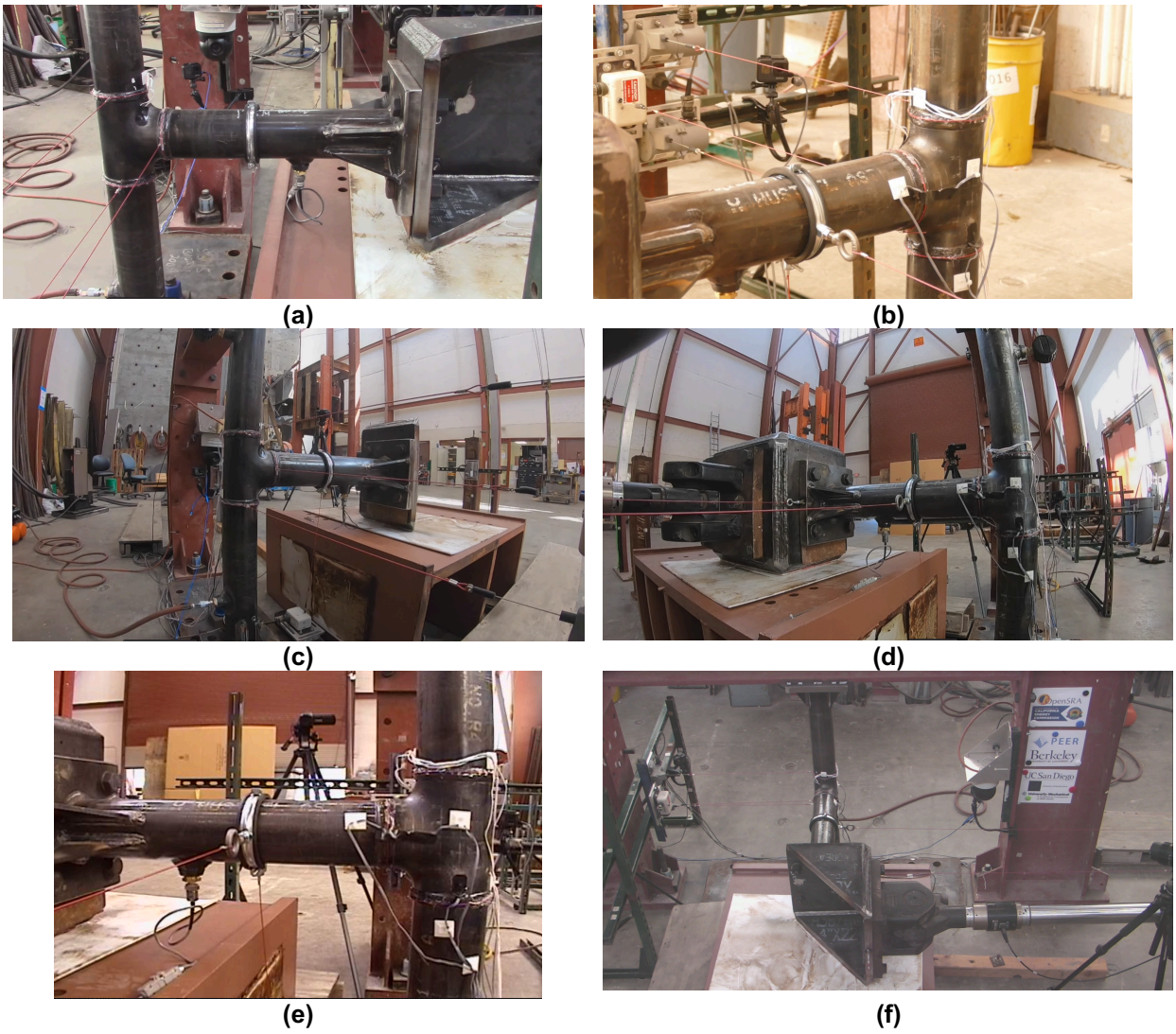

Figure 2.45 Views from the six cameras for specimen 4T-OP: (a) C1; (b) C2; (c) C3; (d) C4; (e) C5; (f) C6

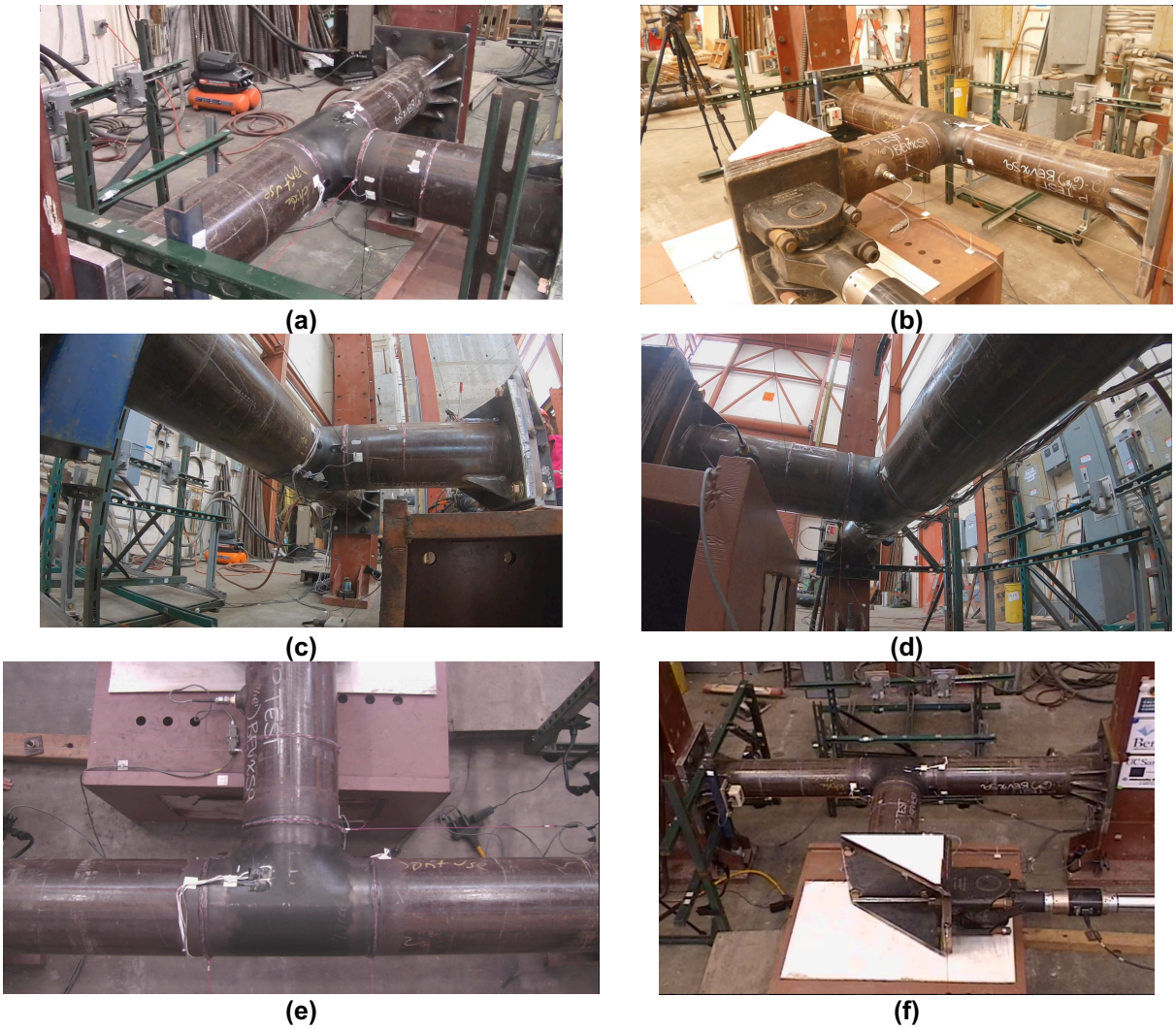

Figure 2.46 Views from the six cameras for specimen 8T-IP: (a) C1; (b) C2; (c) C3; (d) C4; (e) C5; (f) C6

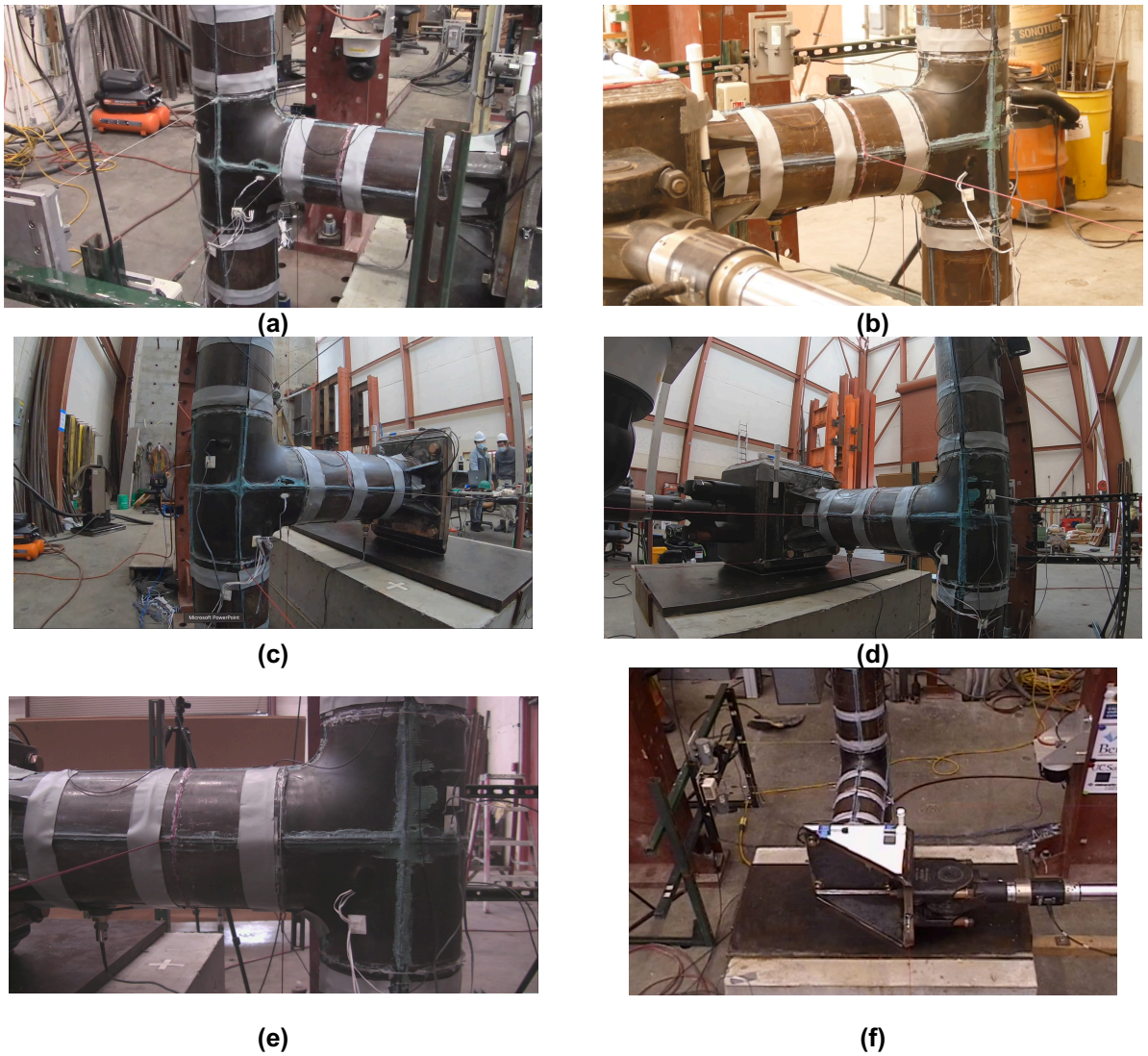

Figure 2.47 Views from the six cameras for specimen 8T-OP: (a) C1; (b) C2; (c) C3; (d) C4; (e) C5; (f) C6



Figure 2.48 Views from the six cameras for specimen 4E-90: (a) C1; (b) C2; (c) C3; (d) C4; (e) C5; (f) C6



Figure 2.49 Views from the six cameras for specimen 4E-45: (a) C1; (b) C2; (c) C3; (d) C4; (e) C5; (f) C6



Figure 2.50 Views from the six cameras for specimen 8E-90: (a) C1; (b) C2; (c) C3; (d) C4; (e) C5; (f) C6

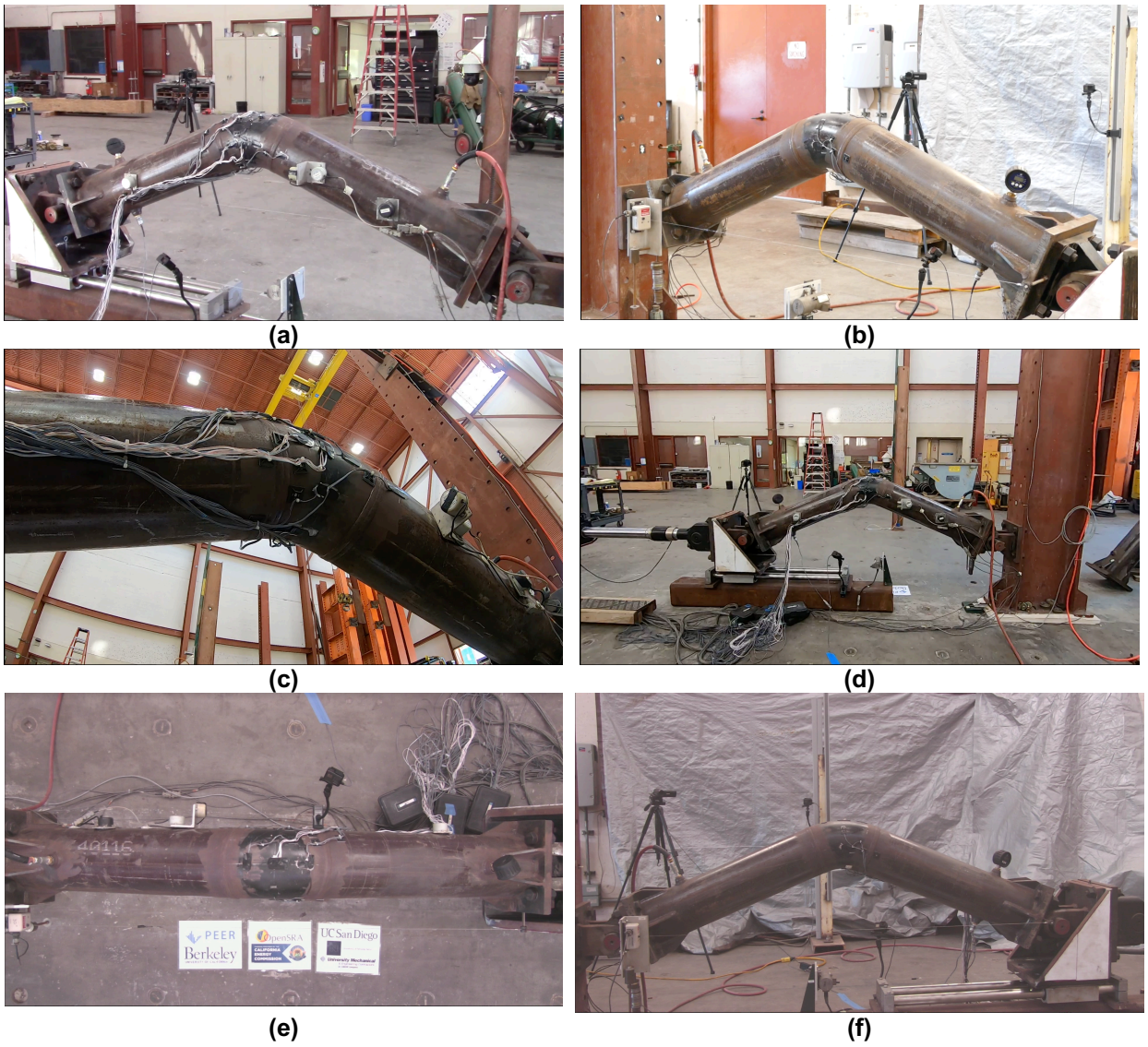

Figure 2.51 Views from the six cameras for specimen 8E-45: (a) C1; (b) C2; (c) C3; (d) C4; (e) C5; (f) C6

2.4 Description of the Test Protocol

Quasi-static, reversed cyclic, displacement-controlled loading was imposed on each specimen following the cyclic load protocol recommended by FEMA-461 (FEMA 2007). This protocol involves imposition of two full cycles (or one full "cycle set") per amplitude target, with displacement amplitudes increased by 40% of the prior cycle, in each subsequent cycle grouping. The main parameters of this protocol are the initial displacement Δ_o, the target displacement Δ_m and the number of cycle sets. The target displacement Δ_m was selected based on pre-test numerical simulations as the displacement resulting in a 20% reduction in the peak force during monotonic loading (Krawinkler et al. 2001). The selection of Δ_o was based on 0.15% of a length of interest to

the specimen, as recommended by FEMA-461. For the present purposes, this length of interest was assumed to be as one of the straight lengths of the specimen, extending from the center of rotation for both tee joints and elbows. This load protocol contained at least six cycle groups in the elastic range, as recommended by FEMA-461. A typical load protocol is shown in Figure 2.52. Note that the initial direction of load was consistently imposed in the Southward direction (i.e., the closing direction of the elbows), hence this direction is always referred to as positive.

Displacements were applied using a double-acting 50-kip hydraulic actuator with a stroke of +/- 24 in. As noted, during testing, the specimens were internally pressurized at a constant pressure between 25 and 35 psi using an air compressor. Tests were performed until a through crack developed and internal pressure reduced to zero. Table 2.5 presents the details of the load protocol for tests 4T-IP and 4T-OP. It is noted that, while sometimes failure occurred at the cycle set with a target Δ_m, in some cases failure occurred prior to attainment of Δ_m, while in others it occurred at a larger displacement. Details of the load protocol for the other specimens are presented in Appendix C. The string potentiometers LS01 was used to control the tests in all cases except when explicitly specified in these tables. Additional details regarding the numerical models of the specimens are presented in Pantoli and Hutchinson (2025).

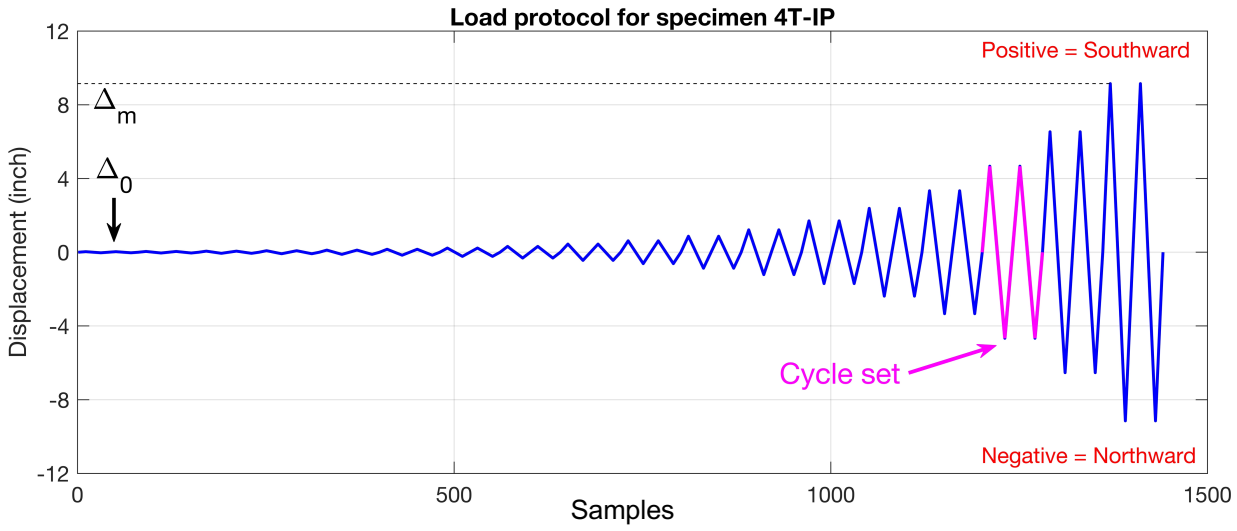

Figure 2.52 Typical load protocol (numerical values relative to the test on specimen 4T-IP)

Table 2.5 Load protocol details for specimens 4T-IP and 4T-OP

Cycle set #	Applied Displacement @L01 (in)	Time (sec/quarter cycle)	Rate (in/sec)	Notes
1	0.030	5	0.006	
2	0.042	5	0.008	
3	0.059	5	0.012	
4	0.082	5	0.016	
5	0.115	5	0.023	
6	0.161	10	0.016	
7	0.226	10	0.023	
8	0.316	10	0.032	
9	0.443	15	0.030	
10	0.620	15	0.041	
11	0.868	15	0.058	
12	1.215	30	0.040	
13	1.701	30	0.057	
14	2.381	30	0.079	
15	3.334	30	0.111	
16	4.667	30	0.156	
17	6.534	60	0.109	4T-IP: In the Northward direction the maximum displacement applied was 6.1 in because it was the limit allowed by the setup 4T-OP: the time per quarter cycles was reduced to 45 seconds, resulting in a rate of 0.145 inch/sec
18	9.147	60	0.152	Δ_m for both 4T-IP and 4T-OP

3 Project Results

This chapter presents the force-displacement and moment-rotation behavior as well as the primary identifiable limit states observed during the eight component tests performed. Inspection of each specimen during testing was performed at the first positive and negative displacement peaks in each cycle set commencing on or around material yielding. In addition, during cycle sets with larger amplitudes, the specimens were inspected at the second positive and negative peaks in each cycle set. Three limit states were consistently evident in all specimens, namely:

1. Limit state 1 (LS1): First visible ovalization. This limit state identifies the instance in which visible deformation of the component could be observed for the first time.
2. Limit state 2 (LS2): First crack. This limit state indicates the appearance of a shallow crack at locations of high strains. It is noted that most specimens were characterized by the appearance of a network of cracks, rather than a single crack.
3. Limit state 3 (LS3) Through crack. A sudden loss of internal pressure occurred when the displacement applied to the specimen resulted in one or more shallow cracks developing to through thickness cracks. This is defined as the failure of the specimen. While the first and second limit states were identified during continual physical inspections performed at peak displacement targets, this third limit state was identified instantaneously courtesy of continuous measurement of the gas pressure internal to the specimens. Because of this, the moment-rotation curves in the following sections identify LS1 and LS2 at a peak rotation amplitude, while LS3 is shown at the instantaneous rotation when it happens, which in some cases it is quite small. An example of the sudden loss of pressure created by the formation of a through crack in a specimen is shown in Figure 3.1.

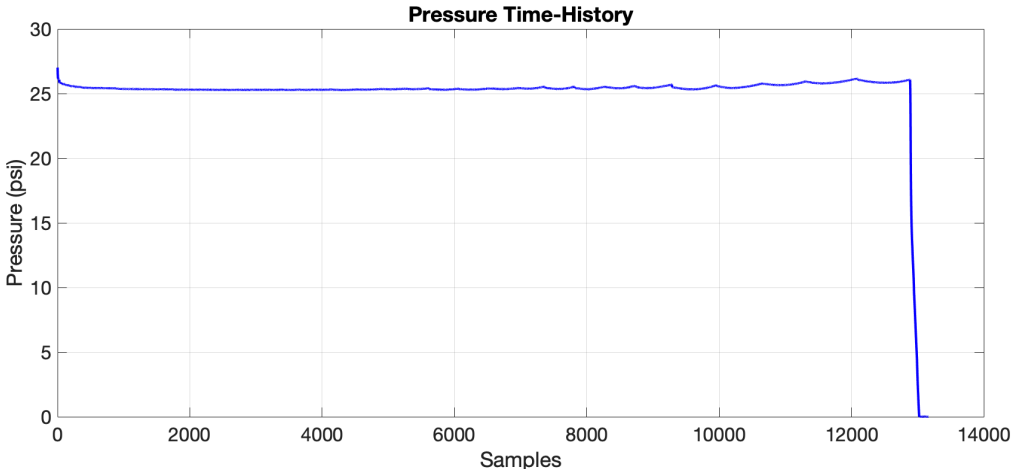

Figure 3.1 Internal pressure measured within specimen 4T-OP during testing

3.1 Force-Displacement Response

The global behavior of each specimen was recorded in terms of force and displacement. The key displacements used for the global analyses were those measured by sensor LS01 for the tee joints and LS02 for the elbows. Sensor LS02 was selected in this latter case because it was the measurement closest to the elbow itself.

Figure 3.2 presents the measured force-displacement response for each of the tee joint specimens tested. Note that for the tee joint specimens the peak force remained below the limit of the actuator (50 kip). The displacements applied were all symmetric except for a small asymmetry in displacement applied to specimen 4T-IP. In this case, it was not possible to apply displacements larger than 6.1 inch in the negative direction due to limits of the test setup. It is noted that some of the specimens, notably specimen 4T-IP, exhibited asymmetric force behavior resulting in a minor "pinching" of the global hysteresis in the negative direction. This asymmetry was not expected because the specimen is symmetric, though it may be partially explained by the rotation of the actuator head during load application, as explained in the following section.

Figure 3.3 presents the measured force-displacement response of the elbow specimens. For the 4 in. specimens, it was possible to apply symmetric displacements, as the force limit of the actuator was not achieved. The 8 in. specimens however substantially strengthen upon extension (opening) of the elbow, thus, for example for specimen 8E-90, the force limits of the actuator was achieved at approximately 9 inch displacement in the negative direction. Hence, it was possible to apply displacements larger than 9 inches only in the positive (closing) direction. For specimen 8E-45, this limit in the opening (negative) direction was attained at relatively small displacements, hence large displacements could be applied only in the positive (opening) direction.

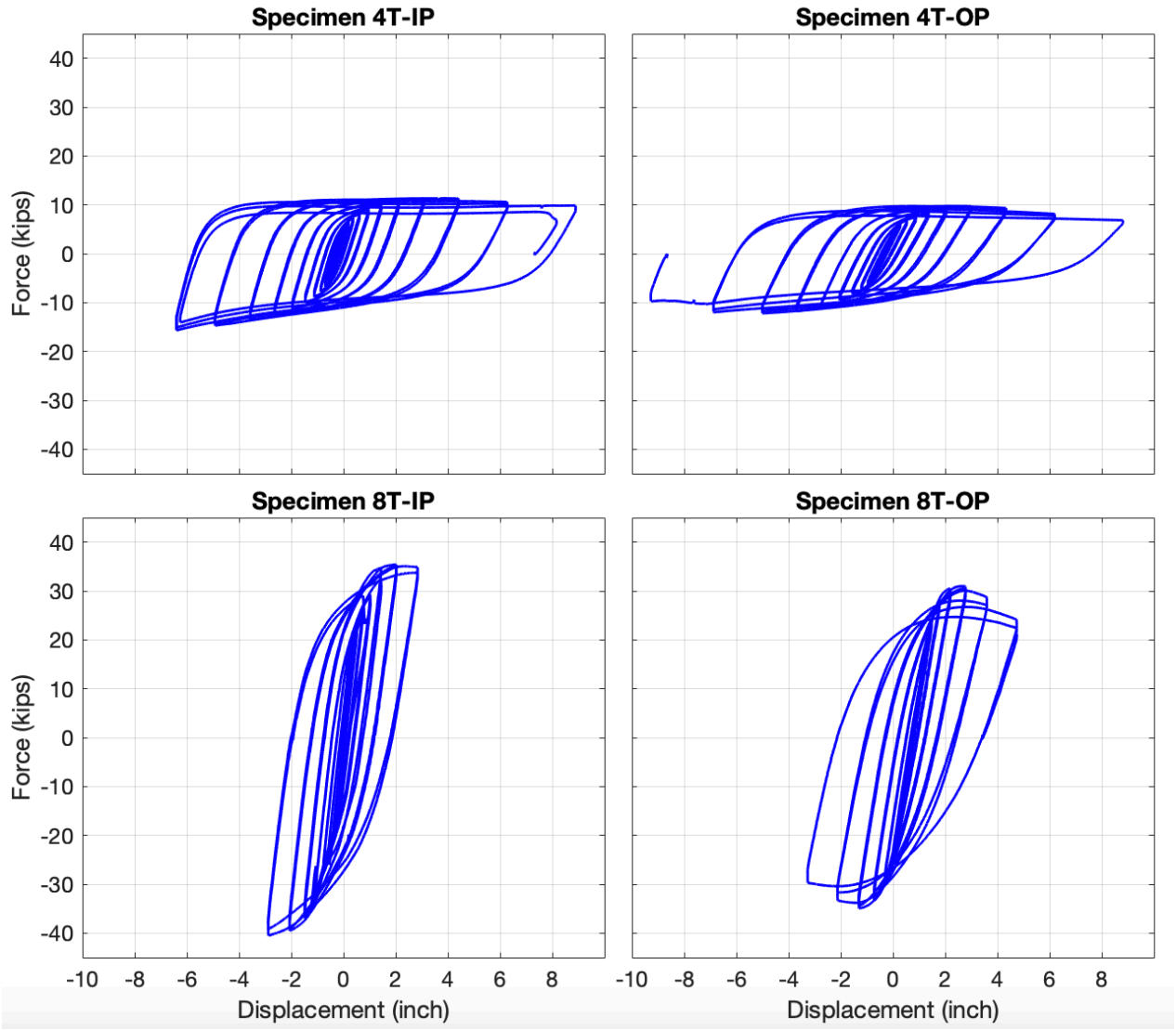

Figure 3.2 Force-displacement response of tee joint specimens

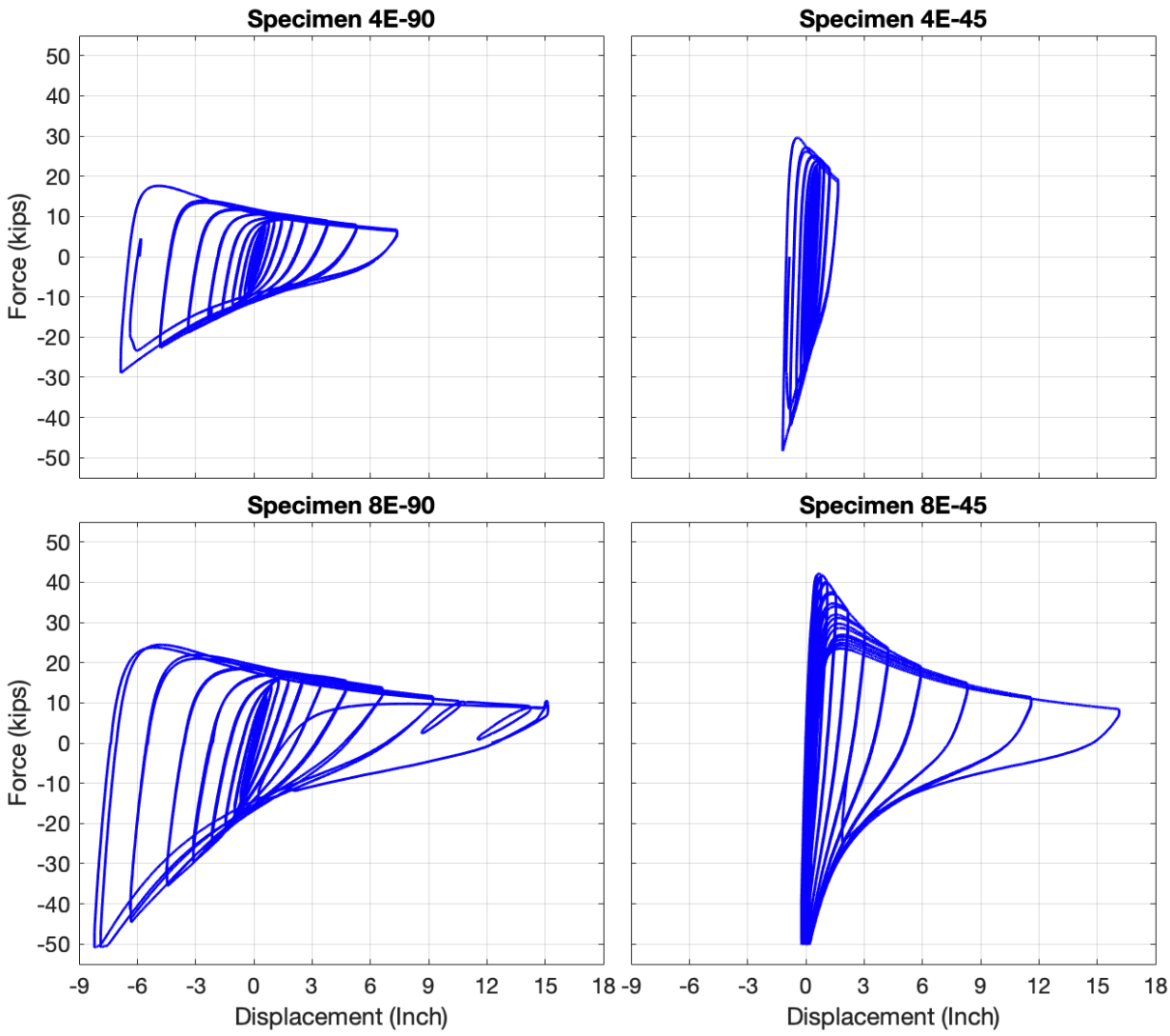

Figure 3.3 Force-displacement response of elbow specimens

3.2 Moment-Rotation Response

3.2.1 Calculation of Rotation and Moment for Tee Joints

To calculate the rotation of the tee joints α, it is assumed that the center of rotation is located where the branch pipe intersects the main pipe, see the yellow dot in Figure 3.4. This point was selected because it is centrally located within the area of highest deformation. With this assumption, the rotation of the tee joint α can be calculated as:

$$\alpha = arcsin\left(\frac{\Delta L}{L_p}\right) \tag{3.1}$$

where ΔL is the displacement measured by string potentiometer LS01 and L_p is the distance between the center of rotation and the point of attachment of the displacement sensor, see for example Figure 3.4 and Figure 2.21a for specimen 4T-IP.

The calculation of the moment is more complex due to the presence of the corbel and the rotation of the actuator around the reaction column. To perform these calculations, one may assume that the triangle show in blue in Figure 3.4 remains rigid and its dimensions are known, and that the initial length of the actuator is known, see nomenclature used in Figure 3.5. It is noted that A_0 is the initial total length of the actuator, while A_i is the total length of the actuator at a certain instant during the test. The calculation varies, depending on the direction of movement, i.e., if the actuator is extending versus compressing, Southward versus Northward directions.

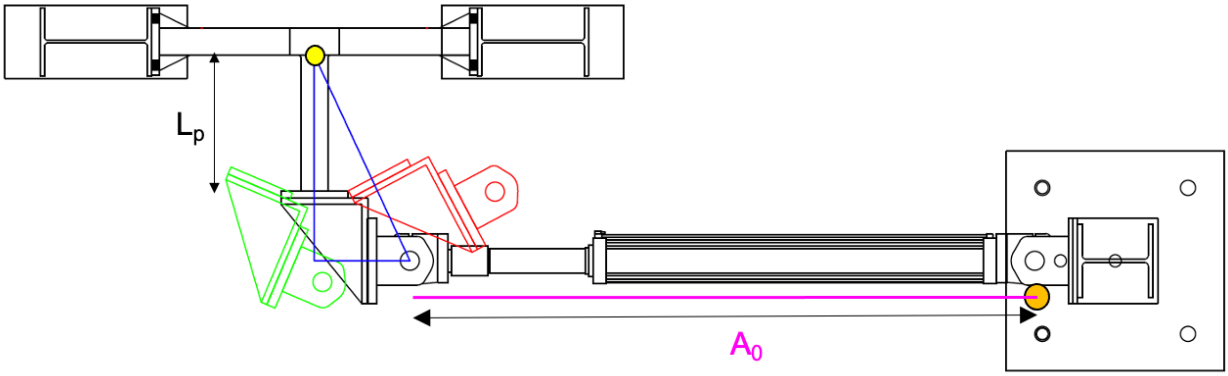

Figure 3.4 Plan view of the setup for test 4T-IP

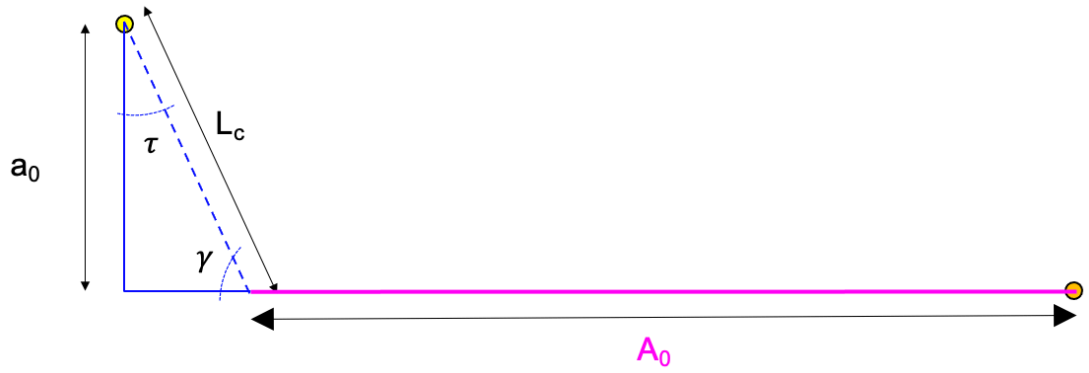

Figure 3.5 Key parameters used to calculate the moment for the tee joint specimens

Figure 3.6 shows the geometry of the specimen as the tee joint is pulled by the actuator in the northward direction (compression of actuator), see the position shown in red in Figure 3.4. As shown in this figure, the arm of the moment becomes smaller as the angle or rotation increases. The formulas used to find the arm of the moment a are presented in the equations below. Parameters required for this computation are shown in Figure 3.6.

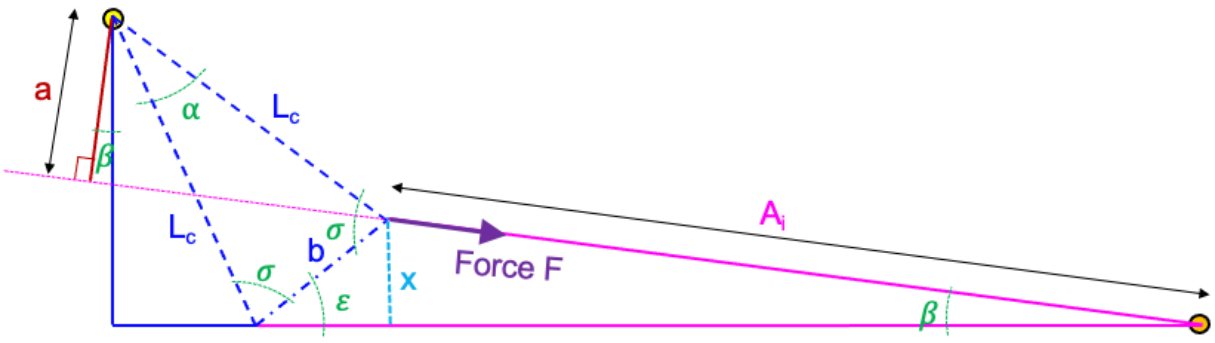

Figure 3.6 Geometry of the specimen as it moves in the northward direction

$$\sigma = \frac{180-\alpha}{2} \tag{3.2}$$

$$\varepsilon = 180 - \gamma - \sigma \tag{3.3}$$

$$b = 2L_c sin\left(\frac{\alpha}{2}\right) \tag{3.4}$$

$$x = b \cdot \sin(\varepsilon) \tag{3.5}$$

$$\beta = arcsin\frac{x}{A_i} \tag{3.6}$$

$$a = L_c \cdot \cos(\beta + \tau + \alpha) \tag{3.7}$$

Figure 3.7 shows the important geometry of the setup, in this case with the tee joint pushed in the Southward direction, i.e., green line in Figure 3.4. In this case, the equations to find the arm are those annotated within Figure 3.5. In both cases, the moment is determined by multiplying the arm by the force measured internal to the actuator.

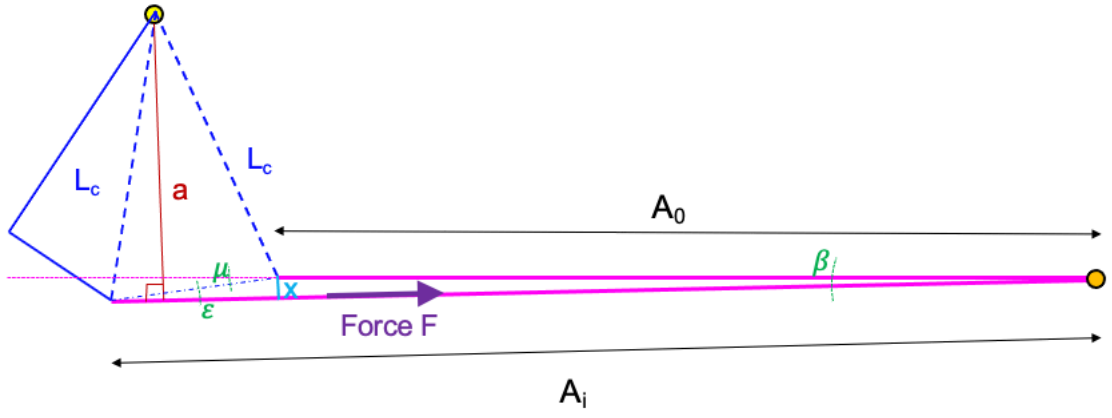

Figure 3.7 Geometry of the specimen as it moves in the southward direction

$$\mu = \sigma - \gamma \tag{3.8}$$

$$\beta = arcsin\left(\frac{bsin(\mu)}{A_0}\right) \tag{3.9}$$

$$\varepsilon = \mu - \beta \tag{3.10}$$

$$a = L_c \cdot \sin(\sigma + \varepsilon) \tag{3.11}$$

3.2.2 Calculation of Rotation and Moment for Elbows

To find the moment and rotation from the measured force and displacement, the elbow specimens were simplified as triangles, as shown in Figure 3.8 for specimen 4E-90. Figure 3.9 shows the relevant parameters used for these calculations. It is noted that ΔL is the change in length L measured by sensor LS02.

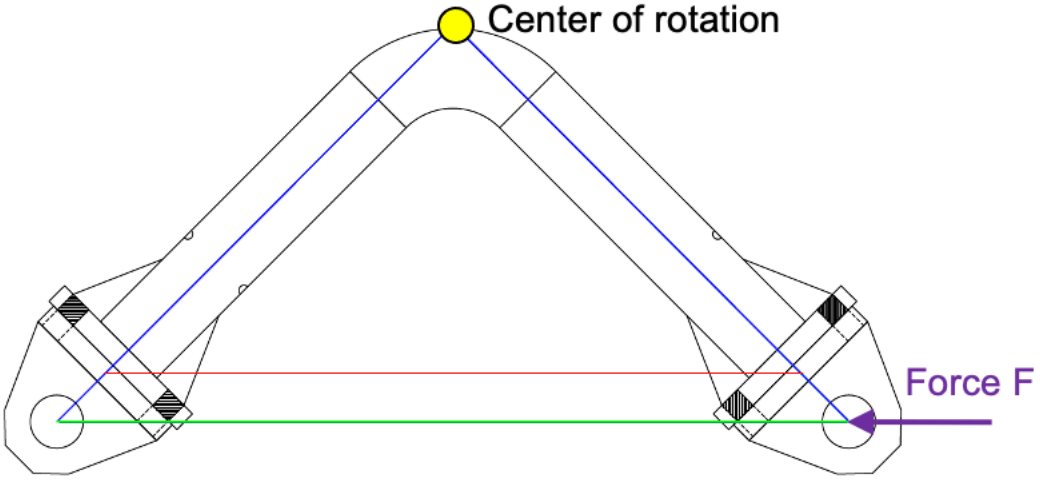

Figure 3.8 Side view of the setup for test 4E-90

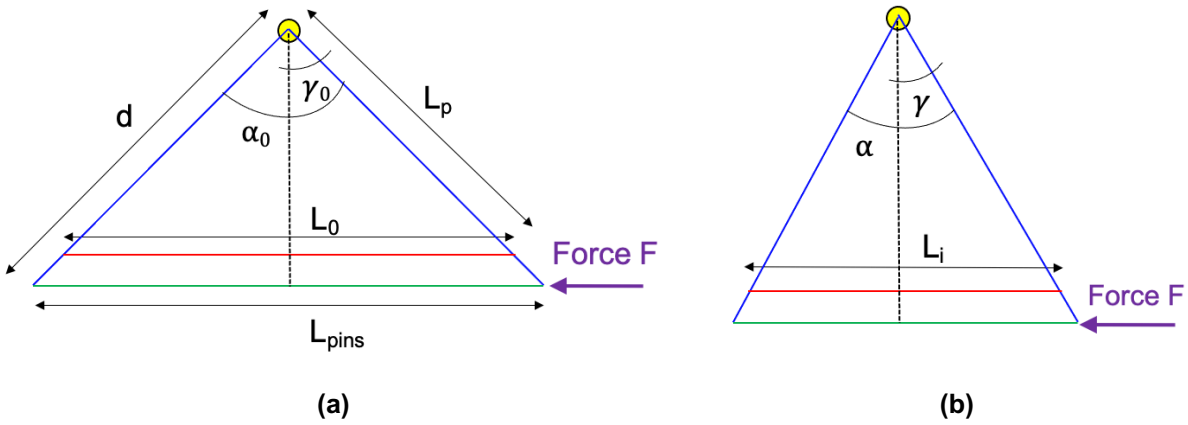

Figure 3.9 Relevant geometry for the elbow specimens: (a) undeformed and (b) deformed

$$L_i = L_0 \pm \Delta L \tag{3.12}$$

$$\gamma = arcsin\left(\frac{\frac{L_i}{2}}{L_p}\right) \tag{3.13}$$

$$Moment = F \cdot d \cdot \cos(\gamma) \tag{3.14}$$

3.2.3 Presentation of Moment-Rotation Response Results

The calculations described above are performed on each specimen's measured force-displacement response, and systematically presented for the tee joint and elbow specimens within this section. The global moment-rotation hysteresis for each tee joint specimen is presented first in Figure 3.10. These results demonstrate stable hysteresis through the loading and reloading regions of multiple cycles. Notably, each specimen, including the more brittle specimen 8T-IP, was able to sustain rotations of at least ~7 degrees. In addition, the rotation attained by the 4T specimens reached almost 24 degrees in each direction. The peak moment measured in the 4T specimens was smaller than the moment for the 8T specimens due to their smaller diameter. However, the ductility of the 4T specimens was much larger due to their lower D/t. In fact, it took several cycles of loading for shallow cracks to develop into through cracks in the 4T specimens, while in the 8T-OP specimen the shallow cracks formed and developed into through cracks within the same cycle set. As anticipated, each specimen was stronger and stiffer in the in-plane direction than in the out-of-plane. Namely, the peak moment reached in the in-plane direction was larger than that in the out-of-plane direction by 15% and 13% for 4T and 8T specimens, respectively.

Figure 3.11 presents the moment rotation hysteresis for all elbow specimens. All specimens, except 4E-45, were able to sustain deformations larger than 15 degrees in both the opening and closing directions. The relatively smaller rotation of 8 degrees attained by this specimen is attributed to the dimensions of this fitting, which not only had a small diameter and large thickness (resulting in a smaller D/t) but was also along additional dimensions. Notably, the value of "a" show in Table 2.2 was only 2.5 inches. It is also noted that the small rotational demand of specimen 8E-45 in the

opening direction was not due to premature failure, but rather limitations of the test setup. Specimen 8E-45 was so stiff in the opening direction, due to its large opening angle and diameter, that opening it further required an extensive force amplitude. Hence the limit of the actuator (50 kip) was reached in the opening direction at a very small rotation. This specimen was able to attain a very large deformation of 43.3 degrees in the closing direction prior to failure at LS3. However, this large rotation may not have been attained in full had the cyclic displacement history been applied symmetrically.

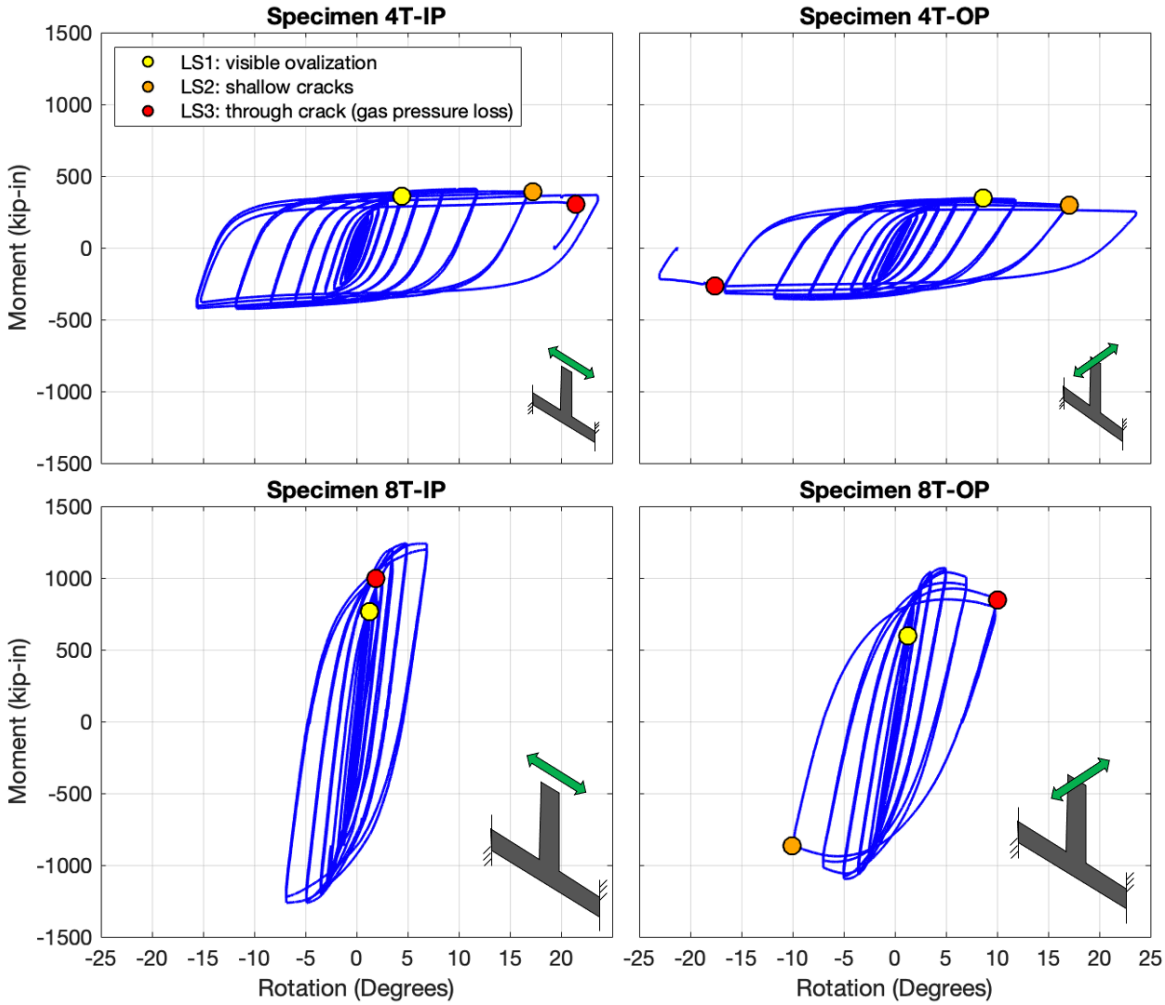

Figure 3.10 Moment-rotation hysteresis and limit states for tee joint specimens

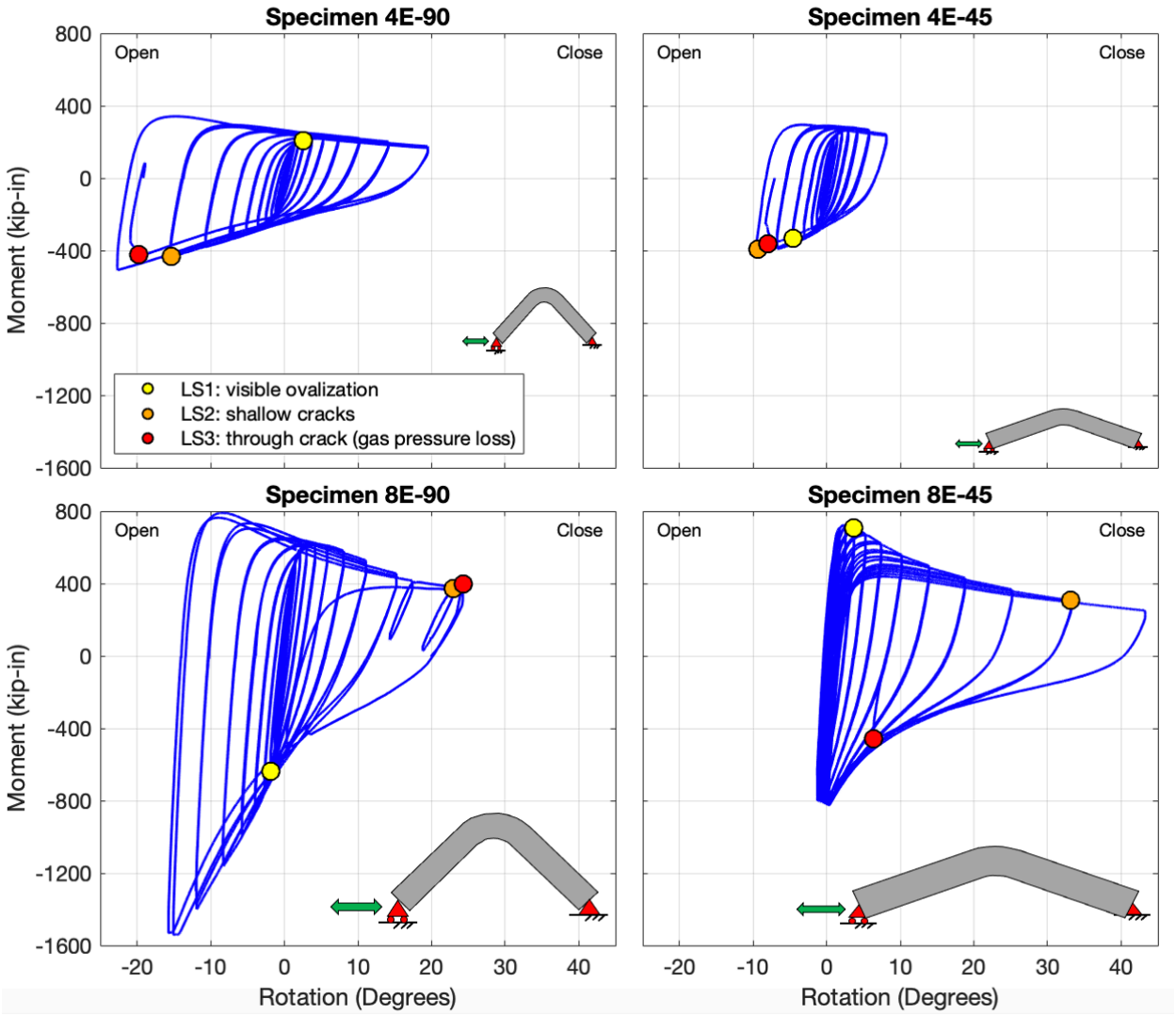

Figure 3.11 Moment-rotation hysteresis and limit states for the elbow specimens

3.3 Physical Observations

3.3.1 Tee Joints

Table 3.1 through Table 3.4 present the identified limit states for each tee joint specimen tested, while Figure 3.12 through Figure 3.15 present corresponding photographs documenting the evolution of these limit states. The applied displacements presented in these tables are positive (southward) unless specified otherwise. Since the actuator was able to apply the target displacements with reasonable accuracy, the displacement presented represents both the target and actual achieved displacement, unless specified otherwise. The first limit states achieved for all specimens was the first visible ovalization of the tee joint, while flaking was observed only in 4T-IP (Figure 3.12a).The damage to specimens 4T-IP, 4T-OP and 8T-OP was characterized by the

formation of a network of initially shallow cracks at the location of high strains (Figure 3.12b, Figure 3.13b, Figure 3.15c). These cracks became longer and extended deeper through the thickness of the fitting upon application of increased displacements (Figure 3.12e, Figure 3.13e), until the largest amplitude strain locations developed into through thickness cracks, thereby leading to failure of the specimen (Figure 3.12h, Figure 3.13f, Figure 3.15d). These cracks formed at the location of the highest strains predicted by pre-test Abaqus simulations (Pantoli and Hutchinson, 2025), namely within the shoulder of the tee for specimen 4T-IP and between the body and the neck of the tee for the OP specimens. The failure of these three specimens was ductile, and physical observations during testing revealed a gradual evolution of the crack network. In contrast, the failure of specimen 8T-IP was rather abrupt. This specimen failed at instigation of a single pronounced diagonal crack, which formed suddenly in the flat region of the body of the tee (Figure 3.14c and d). In this case, no network of shallow cracks formed prior to the appearance of this through crack and full loss of internal pressure. This failure may therefore be classified as brittle.

Table 3.1 Limit states observed for specimen 4T-IP

Cycle set #	Applied Displacement @L01 (inch)	Observation
13	1.7	First visible ovalization of the joint
14	2.4	First flaking at the top of the tee
17	+6.5 -6.1	First development of shallow cracks at the joint. Cracks during the first positive cycles and deepened during the second cycle of the cycle set
18 (first)	9.1	Major crack pattern in the north shoulder of the tee, cracks ~ 1/8 inch deep
18 (second)	8.1	At a displacement of +8.1 inch through thickness cracks developed and pressure dropped suddenly. Crack length 5 inch

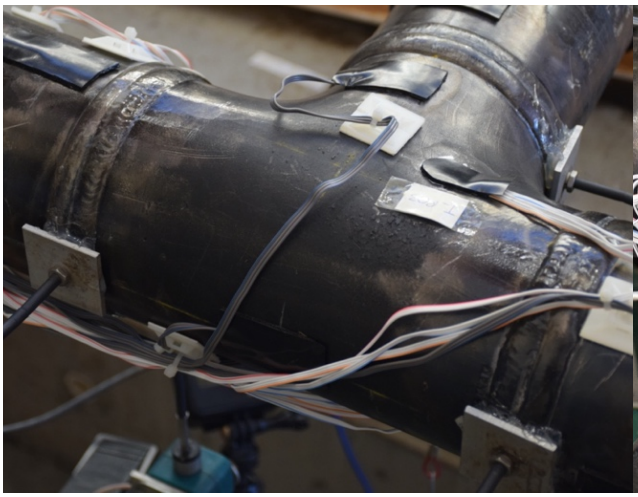

(a)



(b)

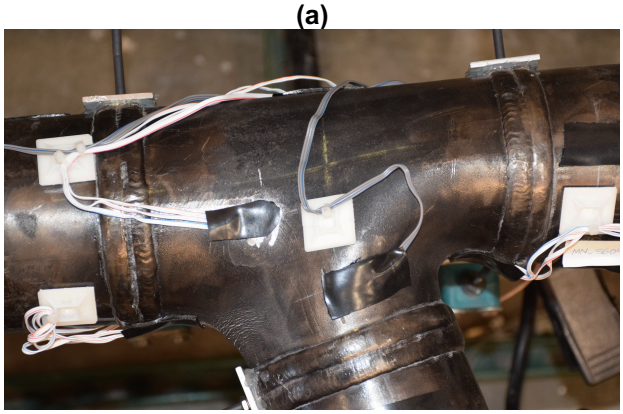

(c)

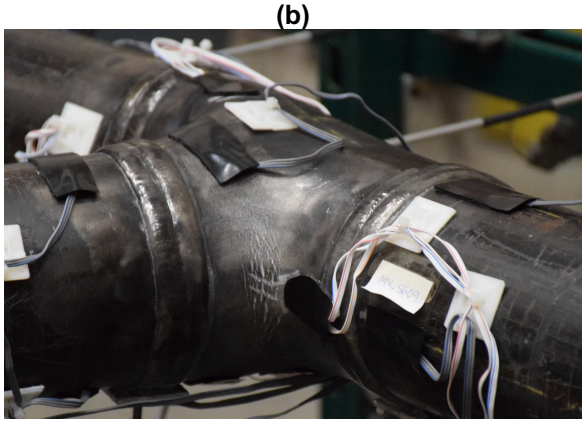

(d)

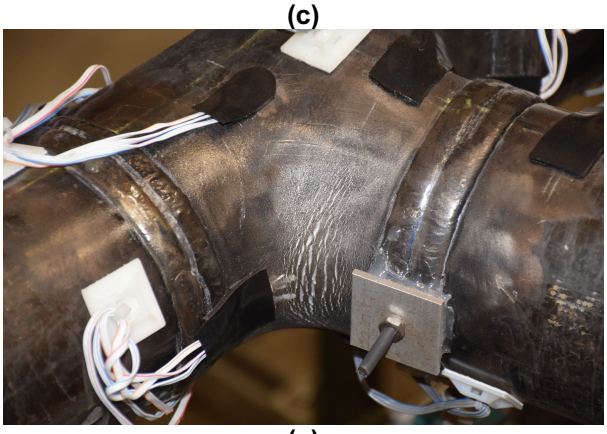

(e)

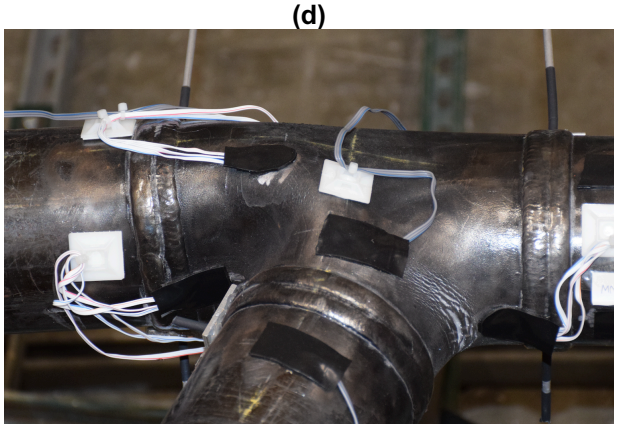

(f)

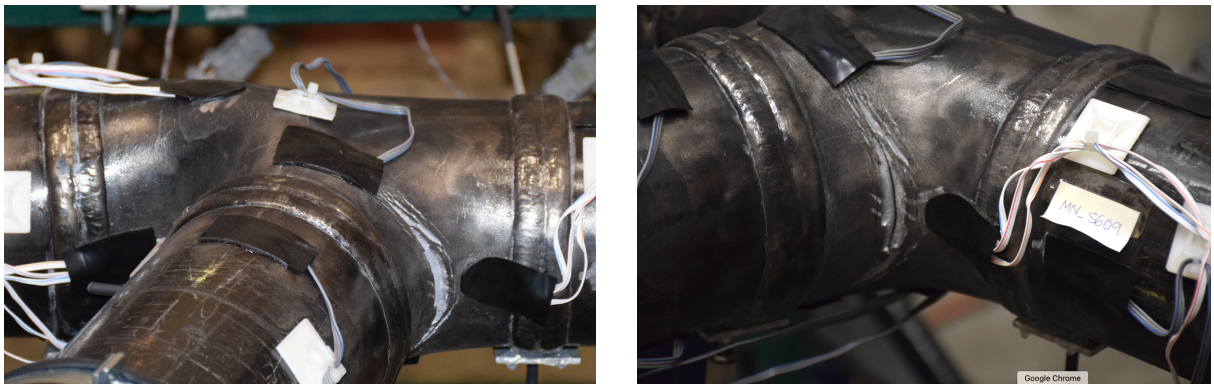

(g) (h)

Figure 3.12 Photographs of representative limit states for 4T-IP: (a) flaking of the tee joint during cycle set 14, (b) shallow cracks in the neck of the tee after the first positive peak of cycle set 17, (c) deformation of the tee joint at the first northward (negative) peak of cycle set 17, (d) cracks in the tee joint during the second southward cycle of cycle set 17 (e) cracks on the south side of the neck during the second northward cycles of cycle set 17 (f) deformed shape during the first southward cycles of cycle set 18 (g) deformed shape at the moment of failure (h) final through crack

Table 3.2 Limit states observed for specimen 4T-OP

Cycle set #	Applied Displacement @L01 (inch)	Observation
15	3.3	First major bulging of the tee
16	4.7	First flakiness at the weld from the tee joint to the branch pipe. Significant necking within the tee joint
17	6.5	First visible cracking on the north side of the tee joint. During push and pull, a symmetric pattern of cracks developed on both sides of the tee
18 (first)	+9.1	Large crack with a smiley shape on the north side
18 (first)	-8.9	Full thickness crack develops at a drift of 7.3 inch and it expanded at the end of the cycle Crack length ~6 inch



Figure 3.13 Photographs of representative limit states for 4T-OP: (a) Bulging of the tee at cycle 15, (b) cracking on the north side of the tee after the first positive peak of cycle 17, (c) necking on the south side of the tee after the first positive peak of cycle 17, (d) cracks following the second positive peak of cycle 17 (north side), (e) cracks after the first positive peak of cycle 18 (north side), and (f) through crack at cycle 18 (at the end of the cycle)

Table 3.3 Limit states observed for specimen 8T-IP

Cycle set #	Applied Displacement @L01 (inch)	Observation
10	0.7	Minor warping at the top of the tee joint
12	1.5	Visible "S" shape deformation at the top of the joint Note: when loading to the first cycle of 1.46 in the Northward direction the columns supporting the specimen slipped ~ ¼ inch Northward with also some rotation. The movement of the column was made visible by dust lines and scratches on the floor and it was documented. Data was not adjusted for this rigid motion.
13	2.0	Continue bulging of the top of the specimen
15 (first)	4.0	Through crack in the flat area of the tee and complete loss of pressure happened at a displacement of +0.73 inch Crack length: 7 inch



(a) (b)

Figure 3.14 Photographs of representative limit states for 8T-IP



(c) (d)

Figure 3.14 Photographs of representative limit states for 8T-IP…continued: (a) Deformation of the tee at cycle 12, (b) Bulging of the tee at cycle 13 (c), (d) Crack formed at cycle 15

Table 3.4 Limit states observed for specimen 8T-OP

Cycle set #	Applied Displacement @L01 (inch)	Observation
9	0.5	First ovalization of the specimen felt while touching
10	0.7	incipient ovalization on the South side
15 (first)	4.0	"necking" of the south side Incipient cracks developed on the South side of the specimen
15 (second)	4.0	Through crack and pressure loss. Data reveals that the pressure drop starts at a rotation of 8.5 degree (Δ=+3.5 inch) Crack length: 7 inch



Figure 3.15 Photographs of representative limit states for 8T-OP: (a) Incipient ovalization at Cycle 10 (b) Necking of the specimen during the first southward push of cycle 15 (c) Cracks of the specimen during the first northward push of cycle 15 (d) Through cracks in the specimen after the final cycle.

3.3.2 Elbows

Table 3.5 through Table 3.8 present the limit states observed for the elbow specimens, while corresponding photographs documenting the evolution of physical damage as observed are presented in Figure 3.16 through Figure 3.19. As predicted by the pre-test Abaqus model (Pantoli and Hutchinson, 2025) and documented by prior research (e.g., Karamanos 2016), the elbows were characterized by a behavior, which was different in the opening and closing directions. Notably, ovalization of the elbows resulted in an elbow that appeared "taller" in the opening direction (e.g., Figure 3.16d) and "squatter" in the closing direction (e.g., Figure 3.16e). Large visible deformations of the elbows were observed for each of the specimens, while flaking of the elbows and connected pipes was observed for the 8T specimens (e.g. Figure 3.18a and c).

Consistent with observations noted during the tee joint specimen tests, failure of the elbows was characterized by the formation of a network of shallow cracks (Figure 3.16c, Figure 3.17c, Figure 3.18h, Figure 3.19e), which then evolved into through cracks (Figure 3.16f, Figure 3.17f, Figure 3.18j, Figure 3.19h). The mechanism of elbow failure was not only influenced by the varying ovalization in the closing and opening directions, but also by the initial angle of the specimen and the specimens' D/t ratio. Specimens 4E-90, 4E-45 and 8E-45 each failed with transverse cracks between the flank and intrados of the elbow. However, while for the 4E specimens the cracks were thicker near the intrados, for specimen 8E-45, the cracks were thicker near the flank and thinner at the intrados. Specimen 8E-90 was the only specimen that failed with longitudinal cracks at the flanks of the specimen. The differences in behavior between the specimens with the same initial angle and different diameter (and D/t) is attributed to the fact that the 8E specimens with larger D/t could deform more freely and hence their failure mode was driven by the ovalization shape, especially in the closing direction. The 4E specimens, because of their smaller diameter and D/t, could not deform as much (were further confined), their failure was driven by the tension applied at the intrados during opening of the specimen.

Table 3.5 Limit states observed for specimen 4E-90

Cycle set #	Applied Displacement @L01 (inch)	Observation
11	1.1	Subtle flattening at the top of the specimen visible when the elbow closes
12	1.6	Vertical ovalization visible duiring opening of the elbow
16	6.1	First visible microcracks on the bottom of the elbow during opening
17 (first negative)	-8.5	Through crack and pressure loss during opening mode. Loss of pressure during the second cycle at -7.5 inch displacement Local buckling on the west face of the specimen. Width of the cracked area: 1 inch



Figure 3.16 Photographs of representative limit states for 4E-90: (a) Flattening of the top of the elbow during closing direction of cycle 11 (b) flattening of the sides during opening direction of cycle 12 (c) microcracks after the first opening cycle of set 17 first (d) ovalization of the specimen during first cycle of set 17 (e) flattening of the elbow during cycle 17 (f) Through crack developed on cycle 17

Table 3.6 Limit states observed for specimen 4E-45

Cycle set #	Applied Displacement @L01 (inch)	Observation
10	0.7	First visible ovalization in both opening and closing direction
12	1.3	First visible cracks at the bottom of the elbow during opening in the first cycle
13 (first)	1.9	0.08 inch deep crack on the west side of the elbow. Family of cracks at the bottow develop during opening
13 (second)	1.9	Failure during opening cycle Width of the cracked area: 0.75 inch

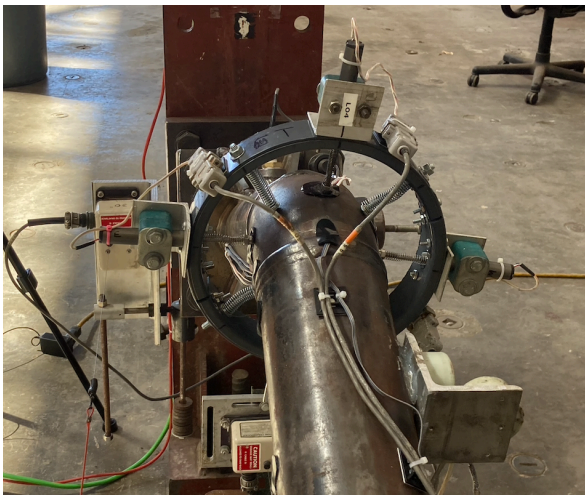

(a)



(b)

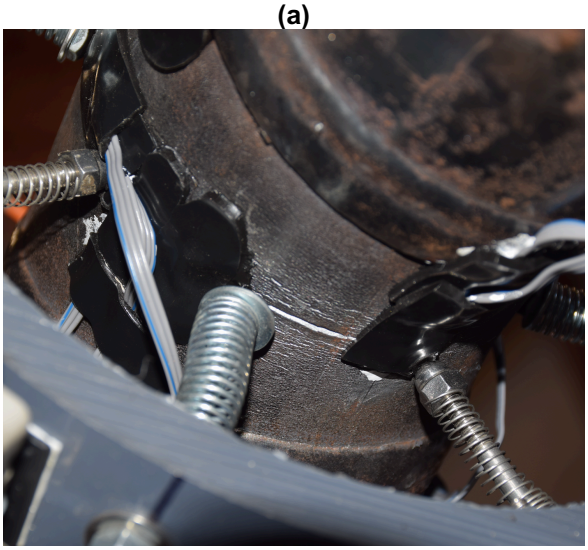

(c)

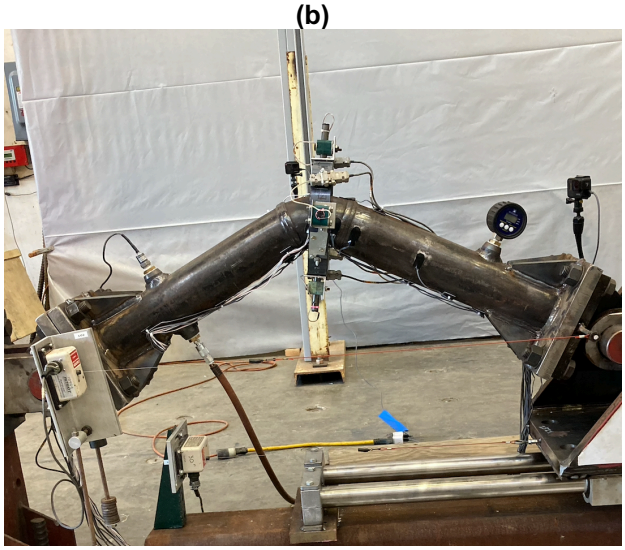

(d)

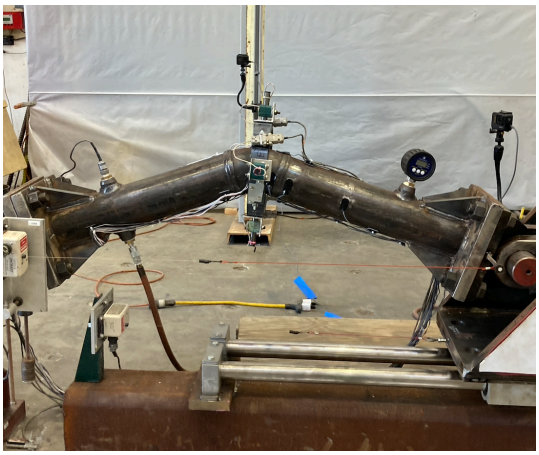

(e)



(f)

Figure 3.17 Photographs of representative limit states for 4E-45: (a) closing cycle 10 (b) open cycle 10 (c) cracks during first opening cycle of set 13 (d) overall picture during the closing of the second cycle of set 13 (e) overall picture during the second opening cycle of set 13 (f) final through crack (view from bottom)

Table 3.7 Limit states observed for specimen 8E-90

Cycle set #	Applied Displacement @L01 (inch)	Observation
10	1.4	First visible ovalization
14	5.2	First flaking observed in the push (positive) direction. Continued flaking after the second cycle. Specimen warm to touch after the second cycle
15	7.3	Flaking outside of the elbow region During the pull direction, the “bump” created during the ovalization in the positive direction remains
16	10.3	Continued flaking in the closing direction. Spacimen has a “football” shape in the clasing direction Note: cannot reach target displacement in the Northward (negative) direction because reached load capacity of the actuator In the northward direction: substantial hardening of the region in the midline of the elbow, especially after the second opening cycle. No visible damage at the bottom of the specimen
17	17.1	Monotonic push to 13.2 inch: network of cracks developed Pushed to 17.1 inch (measured by the actuator) Brought back to zero displacement Pushed back to 17 inch

		Failure upon unloading after the push at 17 inch Length of the through crack: 4 inch



Figure 3.18 Photographs of representative limit states for 8E-90

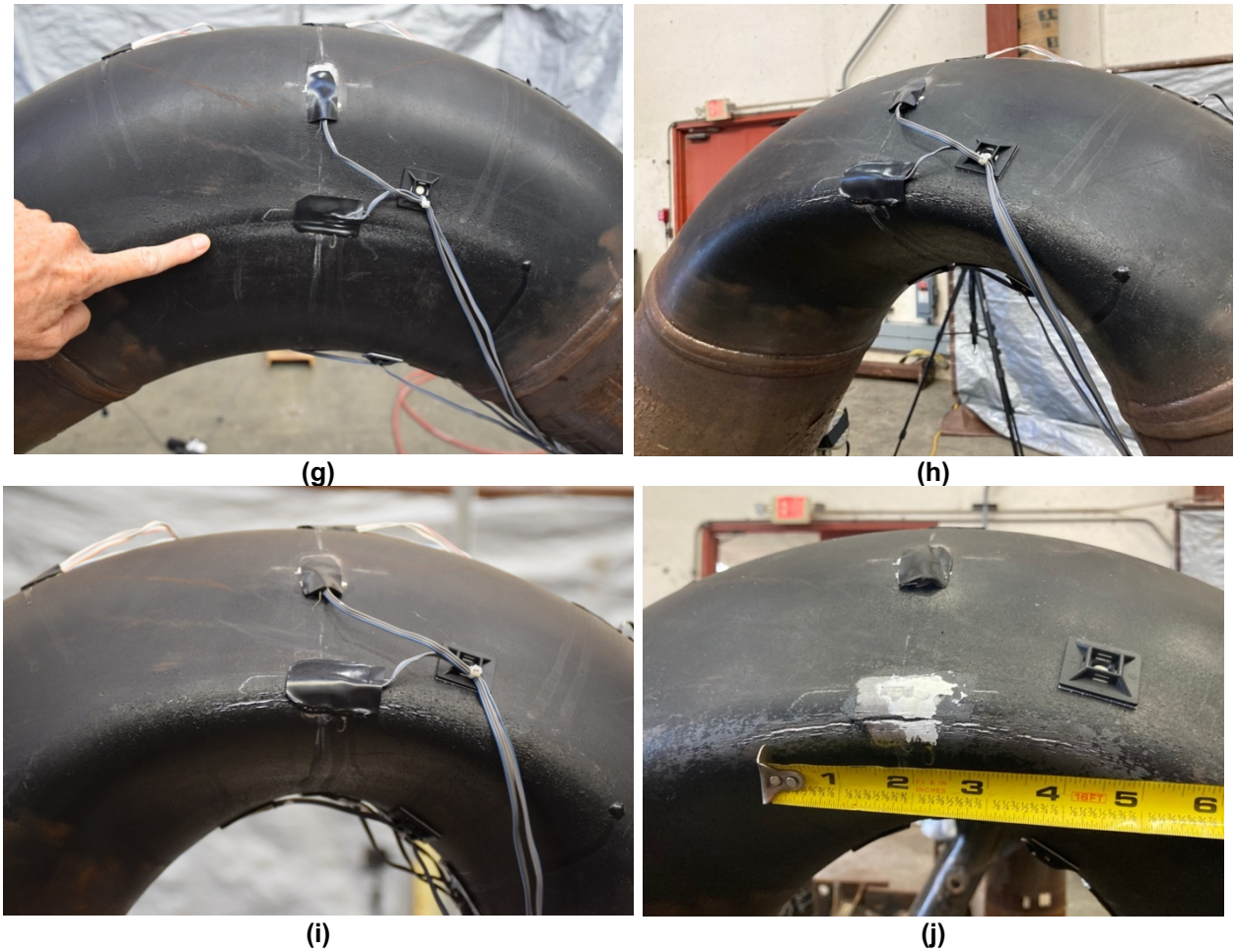

Figure 3.18 Photographs of representative limit states for 8E-90: (a) First flaking observed in the closing direction during cycle 14 (1st cycles) (b) flaking after the second closing of cycle 14 (c) flaking outside the elbow observed after the first opening cycle of cycle set 15 (d) "bump" at the midline of the elbow during the second opening cycle of cycle set 15 (e) shape of the elbow during the first closing cycle of cycle set 16 (f) deformation of the specimen during the first opening cycle of cycles set 16 (g) hardening of the side of the specimen after the second opening cycle of cycle set 16 (h) shallow crack observed during monotonic push at 13.2 inch (i) cracks during the first push at 17 inch (j) final through crack after the removal of the mastic

Table 3.8 Limit states observed for specimen 8E-45

Cycle set #	Applied Displacement @L01 (inch)	Observation
12	1.3	First visible ovalization
15	3.3	First flaking at the bottom of the specimen
19	12.8	Non-through crack observed after unloading the second cycle
20	17.9	Failure during unloading. Length of the through crack: 3 inch

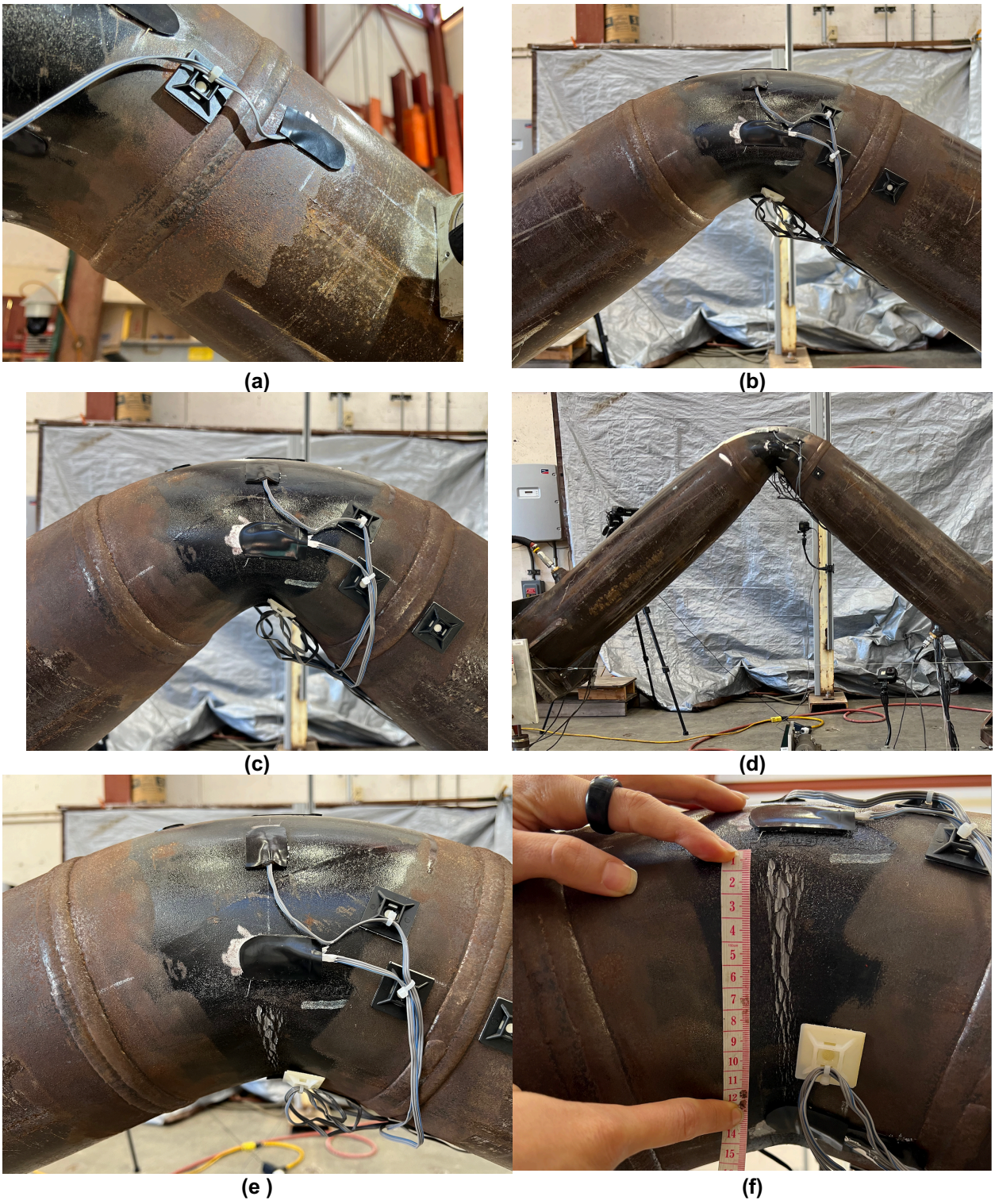

Figure 3.19 Photographs of representative limit states for 8E-45

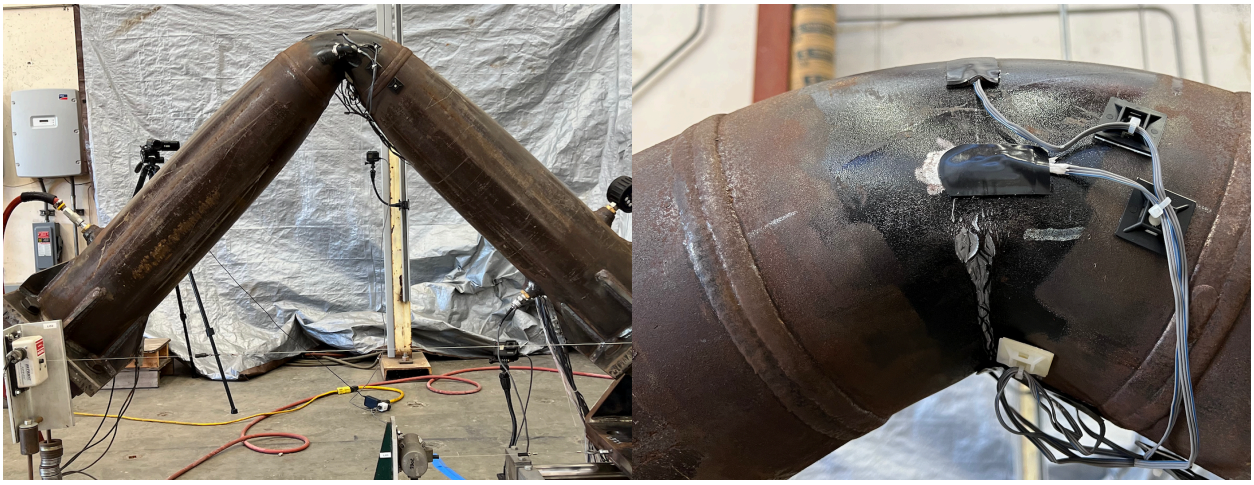

(g) (h)

Figure 3.19 Photographs of representative limit states for 8E-45…continued: (a) first flaking after the first southward cycle of cycle set 15 (b) deformed shape during the first southward cycle of cycle set 17 (c) deformed shape during the first southward cycle of cycle set 18 (d) deformed shape during the first southward cycle of cycle set 19 (e),(f) shallow crack observed upon unloading of the second cycle of cycle set 19 from the side and from below (g) deformed shape during the first southward cycle of cycle set 20 (h) through crack as when it was first observed

3.4 Strain Measurements

Strains at select locations were measured with an array of uniaxial strain gauges and rosettes, the latter of which allowed calculation of the maximum and minimum principal strains and associated direction of principal strain. A sample of the measured strains for specimen 4T-IP are presented in Figure 3.20 and **Error! Reference source not found.**. The presented histories are terminated at the instant when the sensor de-bonded.

Comparing these results with the instrumentation plans in Figure 2.22 indicates that the largest strains occurred in the neck and shoulder (SG3 and SG4), which is consistent with physical observations (Figure 3.12). Even at large rotations, the branch pipe had virtually zero strain (e.g. SG10 and SG11), while small strains were recorded in the main pipes close to the tee joint by sensors SG1, SG7, SG8, SG9. This is consistent with the deformation of the tee (see Figure 3.12c). While rosettes R1 and R4 were installed in the neck of the tee and recorded large strains, R2 and R3 were installed in the body of the tee where the Abaqus model predicted high levels of strains (Pantoli and Hutchinson, 2025). Note that the largest strains exceeded 3%. Additional histories of the recorded strains (both uniaxial strain gauges and rosettes) for other specimens are presented in Appendix D.

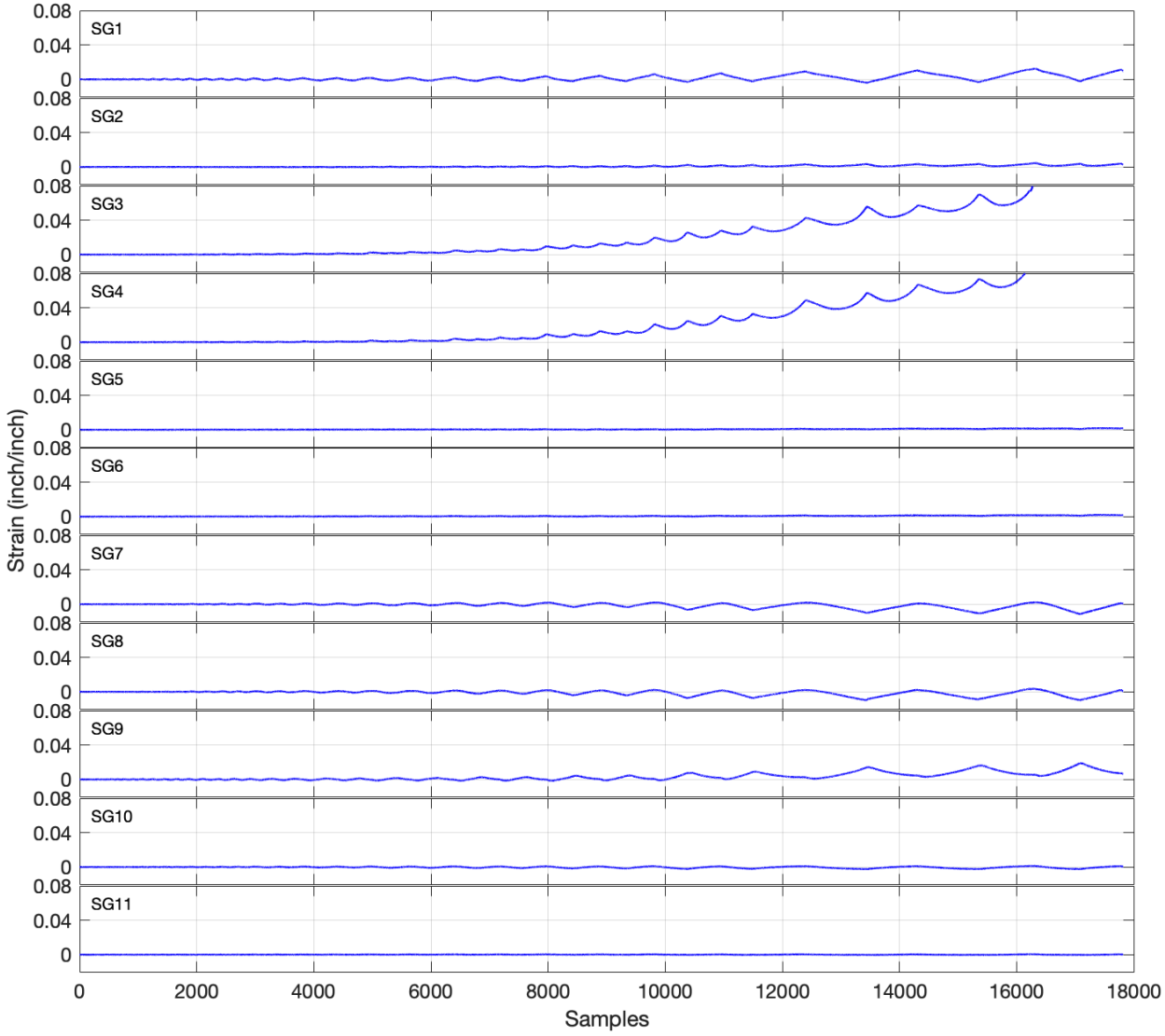

Figure 3.20 Strain measured by uniaxial strain gauges i specimen 4T-IP

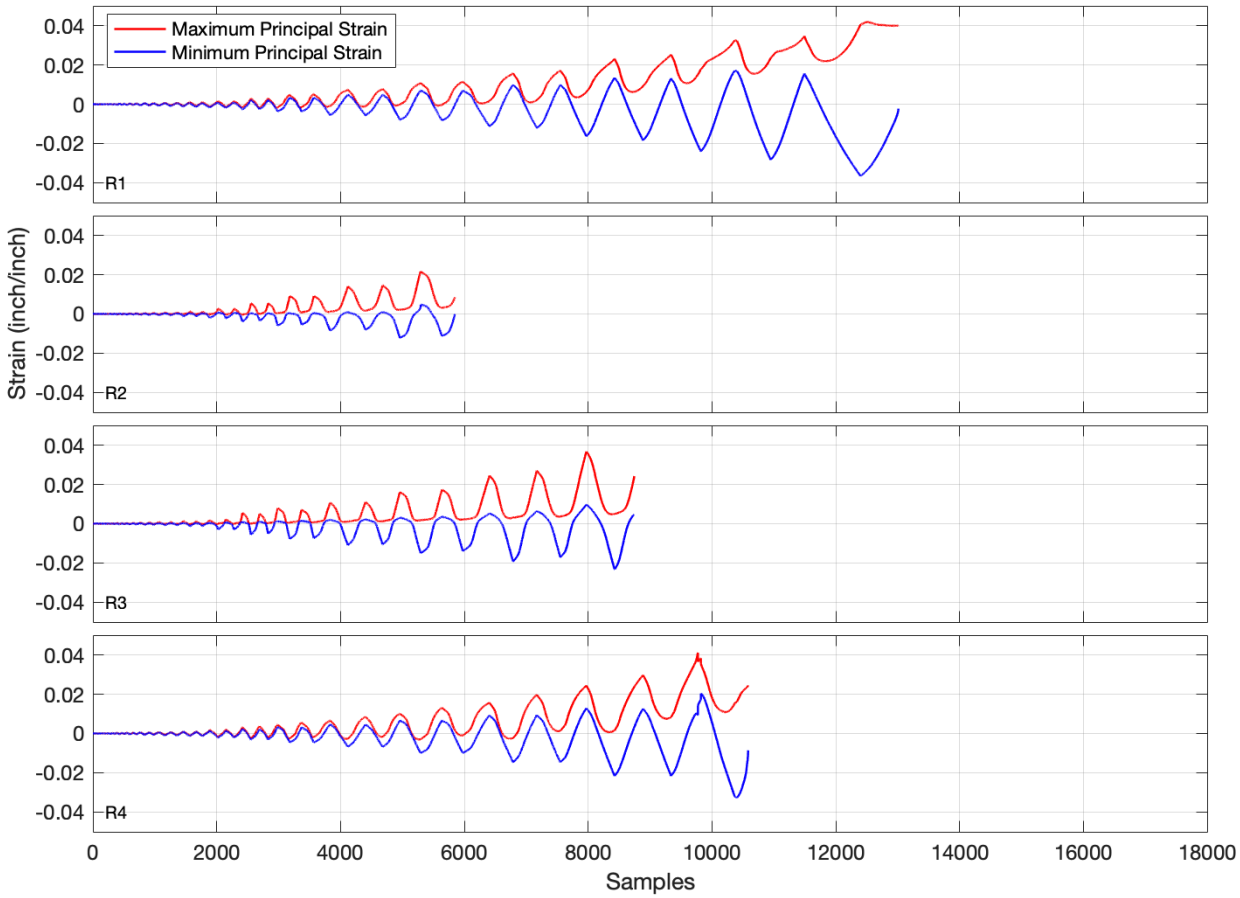
Maximum Principal Strain
Minimum Principal Strain
R1
R2
R3
R4
Strain (inch/inch)
Samples
0.04
0.02
0
-0.02
-0.04
0
2000
4000
6000
8000
10000
12000
14000
16000
18000

4 Conclusions and Recommendations

This report presents a unique experimental program conducted on the important connection components readily used throughout the natural gas surface infrastructure. Complementary to shake table experiments conducted on subsystems at the University of Nevada, Reno (Elfass et al., 2025), the present component-level quasi-static test program addressed typical fittings, namely tee joints and elbows, within low and high pressure regions of the system. Herein, the test program design, protocol, and key outcomes of a total of eight experiments, specifically four equal tee joint and four elbow specimens are documented. Half of the specimens were 4-in. diameter Schedule 80 and the remaining half were 8-in. diameter Schedule 40. The tee joint specimens were tested both in-plane and out-of-plane, while the 90 degree and 45 degree elbows were tested only in-plane. These experiments demonstrate that these fittings are generally very ductile. Notably, the development of a through crack was almost always preceded by visible deformation and a network of shallow cracks within the fitting region. In addition, the specimens displayed a large rotational capacity, from a minimum of approximately 7 degrees to more than 20 degrees. However, the tests also showed that a specific tee joint geometry can be problematic and lead to a relatively early, abrupt failure. Within this program, the 8-in. tee joint tested in-plane failed when a diagonal crack formed unexpectedly along the body of the tee, which is almost completely flat in this specific type of tee joint. Such a failure therefore may be considered brittle. Results in terms of force-displacement, moment-rotation, physical damage and associated limit state development, as well as local strain measurements are documented herein for each specimen. The authors note that such data are useful for validating high fidelity models and extending such simulation tools for the utility of additional geometries and material types, which ultimately supports advancement of seismic fragility models for subsystems with these types of fittings (Pantoli and Hutchinson, 2025).

Observations from this program render suggestions for future research, including the following:

- The abrupt failure of the large diameter 8T-IP specimen should be interrogated further; an initial experimental task may pursue even larger (e.g., 12-in. and/or 16-in. diameter) fittings of similar schedule to determine if large local compression through cracks is prevalent for these large D/t fittings.
- Studying the moment-rotation behavior and limit states for components outside of those considered herein, for example unequal tee joints (reducing tees).
- Test specimens with different types of connections, for example threaded rather than welded. The authors note that threaded elbows and tee joints are very common for very small diameter and low-pressure applications, thus their utility may be within the transmission system of the natural gas network.

GLOSSARY AND LIST OF ACRONYMS

Term	Definition
Abaqus	FEA software (Smith, 2009)
ASTM	American Society for Testing and Materials
CEC	California Energy Commission
Component	Individual parts of a subsystem. For example: a pressure vessel, straight pipes, elbows, tees, reducers, bolted flange joints.
E	Modulus of elasticity (or Young modulus)
Elbow	A pipe fitting installed between two lengths of pipe or tubing to allow a change of direction, usually a 90° or 45° angle
FEA	Finite Element Analysis
f_u	Ultimate strength
f_y	Yield strength
HSS	Hollow structural steel
IP	In-plane
LBNL	Lawrence Berkeley National Laboratory
LCI	Lettis Consultants International
M&R	Metering and pressure Regulating stations
Moment	Force multiplied by distance arm

Term	Definition
NHERI	Natural Hazards Engineering Research Infrastructure
Olet	Fitting providing an outlet from a larger to a smaller pipe
OP	Out-of-plane
PEER	Pacific Earthquake Engineering Research Center
SG	Strain Gauge
Shake table	A special equipment that can simulate ground motions similar to earthquakes
Straight tee	Tee where the three connected pipes have the same diameter (also known as equal tee, equivalent tee)
Strain	A number that describes relative deformation
Tee	A T-shaped pipe fitting with three openings used to combine or divide fluid flow (also known as T-joint/ tee joint/ tee fitting)
UC Berkeley	University of California Berkeley
UC San Diego	University of California San Diego
UMEC	University Mechanical and Engineering Contractors, a piping manufacturer
UNR	University of Nevada, Reno
Δ_0	Initial displacement
Δ_m	Target displacement
ε_u	Ultimate strain

Term	Definition
ε_y	Yield strain
α	Rotation
σ_0	initial yield stress
σ_y	yield stress

REFERENCES

ASME (2018). ASME 16.9 - Factory-made wrought buttwelding fittings. American Society of Mechanical Engineers.

Chatzopoulou, G. and Karamanos, S.A. (2020). Numerical simulation of the mechanical behaviour of steel pipe bends under strong cyclic loading. International Journal of Pressure Vessels and Piping, 188, 104239.

Cornell C.A. (1968). Eng Seis Risk Analysis, Bull. Seismo. Soc. Am., V58(5), 1583-1606, doi: 10.1785/BSSA0580051583.

Di Filippo R., Abbiati G., Sayginer O., Covi P., Bursi O.S., and Paolacci F. (2019). Numerical surrogate model of a coupled tank-piping system for seismic fragility analysis with synthetic ground motions. Pressure Vessels and Piping Conference, 59018(V008T08A029).

Elfass S., McCallen D., Wu, S. (2025). Shake Table Testing of a Surface Natural Gas Piping Subsystem. A Report for the "Performance-based Earthquake Engineering Assessment Tool for Natural Gas Storage and Pipeline Systems" Project. PEER Report 2025/17, Pacific Earthquake Engineering Research Center, University of California, Berkeley, CA. https://doi.org/10.55461/KXPG8057.

FEMA (2007). FEMA-461 - Interim Testing Protocols for Determining the Seismic Performance Characteristics of Structural and Nonstructural Components. Federal Emergency Management Agency, Washington DC. https://www.atcouncil.org/pdfs/FEMA461.pdf.

Karamanos S.A. (2016). Mechanical behavior of steel pipe bends: an overview. Journal of Pressure Vessel Technology, 138(4), doi: 10.1115/1.4031940.

Karamanos S.A., Tsouvalas D., and Gresnigt A.M. (2006). Ultimate bending capacity and buckling of pressurized 90 deg steel elbows. Journal of pressure vessel technology, 128-3(348-356), doi: 10.1115/1.2217967.

Karamanos S.A., Giakoumatos E., and Gresnigt A.M. (2003). Nonlinear response and failure of steel elbows under in-plane bending and pressure. Journal of Pressure Vessel Technology, 125-4(393-402), doi: 10.1115/1.1613949.

Karvelas C., Chatzopoulou G., Zervaki A.D., Stathas N., Strepelias E., Palios X., Bousias S. N., and Karamanos, S. A. (2021). Mechanical Response of an Industrial Piping System Under Strong Cyclic Loading. In Pressure Vessels and Piping Conference (Vol. 85352, p. V005T08A018). American Society of Mechanical Engineers.

Kim S.W., Chang S., Park D.U., and Jeon B.G. (2020). Failure criteria of a carbon steel pipe elbow for low-cycle fatigue using the damage index. Thin-Walled Structures, 153, 106800.

Kim S.W., Jeon B.G., Hahm D.G., and Kim M.K. (2020b). Ratcheting fatigue failure of a carbon steel pipe tee in a nuclear power plant using the deformation angle. Engineering Failure Analysis, 114, 104595.

Kiran A.R., Reddy G.R., Agrawal M.K., Raj M., and Sajish S.D. (2019). Ratcheting based seismic performance assessment of a pressurized piping system: Experiments and analysis. International Journal of Pressure Vessels and Piping, 177, 103995.

Kiran A.R., Reddy G.R., and Agrawal M.K. (2018). Experimental and numerical studies of inelastic behavior of thin-walled elbow and tee joint under seismic load. Thin-Walled Structures, 127, 700-709.

Krawinkler H., Parisi F., Ibarra L., Ayoub A., and Medina R. (2001). Development of a testing protocol for woodframe structures. CUREE Publication W-02.

Nakamura I. (2019). Numerical Investigation on Strength of Tee Pipes Under In-Plane/Out-of-Plane Cyclic Loading. Pressure Vessels and Piping Conference, 59018(V008T08A027), doi: 10.1115/PVP2019-93559.

Nakamura I., and Kasahara N. (2017). Excitation tests on elbow pipe specimens to investigate failure behavior under excessive seismic loads. Journal of Pressure Vessel Technology, 139(6), doi: 10.1115/1.4037952.

Pantoli E. and Hutchinson T.C. (2025). Numerical Modeling and Seismic Fragility Curve Development: Components and Subsystems of the Natural Gas Surface Infrastructure A Report for the “Performance-based Earthquake Engineering Assessment Tool for Natural Gas Storage and Pipeline Systems” Project. PEER Report 2025/15, Pacific Earthquake Engineering Research Center, University of California, Berkeley, CA. https://doi.org/10.55461/JITV8938

Papatheocharis T., Diamanti K., Varelis G.E., Perdikaris P.C., and Karamanos S.A. (2013). Experimental and numerical investigation of pipe T-junctions under strong cyclic loading. Pressure Vessels and Piping Conference, 55744 (V008T08A017), doi: 10.1115/PVP2013-97626.

Rongere F. and Eimon F. (2019). Quantification of Methane Emissions from M&R Stations. Retrieved March 10, 2022, from https://www.gti.energy/wp-content/uploads/2019/09/CH4-14-Sept18-Ford-Eimon-Presentation.pdf.

Smith, M. (2009). Abaqus/Standard User's Manual, Version 6.9. Dassault Systèmes Simulia Corp.

SoCalGas (2016). How Underground Natural Gas Storage Works. Retrieved March 17, 2022, from https://www.youtube.com/watch?v=3FSMpCazwUA.

Varelis G.E., Dib E., and Karamanos S.A. (2022). Structural Response of Subsea Pipe Elbows Under Monotonic and Cyclic Loading. International Conference on Offshore Mechanics and Arctic Engineering, 85871(V003T04A020), doi: 10.1115/OMAE2022-79151.

Varelis G.E., Karamanos S.A., and Gresnigt A.M. (2013). Pipe elbows under strong cyclic loading. Journal of Pressure Vessel Technology, 135(1), doi: 10.1115/1.4007293.

Wang, C., Sinha, S., Hubbard, P., Liang, Y., & Soga, K. (2025). Sensing and Monitoring Technologies for Natural Gas and Pipeline Systems (OpenSRA Project), PEER Report No. 2025/09. Pacific Earthquake Engineering Research Center, University of California, Berkeley, CA. https://doi.org/10.55461/YDFS8409

Watakabe T., Tsukimori K., Otani A., Moriizumi M., and Kaneko N. (2014). Study on Strength of Thin-Walled Tee Pipe for Fast Breeder Reactors Under Seismic Loading. Pressure Vessels and Piping Conference, 46070(V008T08A032), doi: 10.1115/PVP2014-28619.

Xuan F.Z., Wang C., and Li P.N. (2005). Experimental investigation of the limit load of the ANSI B16. 9 tees with and without cracks under internal pressure. Engineering Failure Analysis, 12(3), 453-464.

Yahiaoui K., Moffat D.G., and Moreton D.N. (2000). Plastic loads of cracked forged piping branch junctions: experimental results and comparison with numerical data. International journal of pressure vessels and piping, 77(5), 249-260.

Yoshizaki K., Hamada M., and O'Rourke T.D. (2000). Large deformation behavior of low-angle pipeline elbows subjected to in-plane bending. 12th World conference on earthquake engineering, paper, 1508.

APPENDIX A: WELD PROPERTIES AND PROCEDURE

Documentation provided by the manufacturers relative to the welding procedure is presented in Figures A-1 through Figure A-5.

University Mechanical
& Engineering Contractors
An EMCOR Company

QW-482 SUGGESTED FORMAT FOR WELDING PROCEDURE VERIFICATION (WPS)
(See QW-200.1, Section IX, ASME Boiler and Pressure Vessel Code)

Company Name: University Mechanical & Engineering Contractors — By: Gerald Nash
Welding Procedure Spec. No.: UM-8.0 — Date: 3/16/1988 — Support. PQR No.(s): UM-8.1
Revision No.: — Date:

Welding Process(es): GMAW-S / FCAW-G — Type(s): Semi-Automatic
(Automatic, Manual, Machine, or Semi-Auto.)

JOINTS (QW-402)
Joint Design: Sgl. V / Dbl. V / Fillet / Build-up / Repair
Backing (Yes): Opt. for GMAW-S / Req'd. for FCAW-G (No):
Backing Mat'l (Type): Weld metal or Split ring
(Refer to both backing and retainers.)

☑ Metal ☐ Nonfusing Metal
☐ Nonmetallic ☐ Other

Sketches, Production Drawings, Weld Symbols or Written Description should show the general arrangement of the parts to be welded. Where applicable, the root spacing and the details of weld groove may be specified.

(At the option of the Mfgr., sketches may be attached to illustrate joint design, weld layers and bead sequence, e.g., for notch toughness procedures for multiple process procedures, etc.)

Details

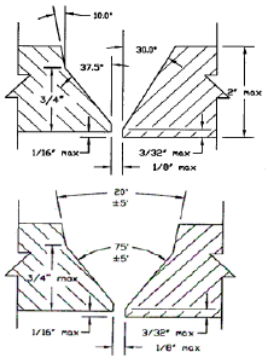

*BASE METALS (QW-403)
P-No. P-1 Group No. 1 to P-No P-1 Group No. 1
OR
Specification type and grade
to Specification type and grade
OR
Chem. Analysis and Mech. Prop.
to Chem Analysis & Mech Prop.
Thickness Range:
Base Metal: Groove .188" through 1.000" Fillet All thicknesses
Other

*FILLER METALS (QW-404)	GMAW-S	FCAW-G
Spec. No. (SFA)	SFA 5.18	SFA 5.20
AWS No. (Class)	ER70S-6	E71T-1
F-No.	F-6	F-6
A-No.	A-1	A-1
Size of Filler Metals	.035"	.035" / .045" / .063"
Weld Metal Thickness Range: Groove	0.138" Max.	.750" Max.
Fillet	All thicknesses	All thicknesses
Electrode-Flux (Class)	N/A	N/A
Flux Trade Name	N/A	N/A
Consumable Insert	N/A	N/A
Other		

*Each base metal-filler metal combination should be recorded individually.

Figure A.1 UMEC Weld Procedure (page 1)

University Mechanical
& Engineering Contractors
An EMCOR Company

QW-482 (Back)

WPS No. UM-8.0 Rev.

Positions (QW-405)
- Position(s) of Groove: All positions
- Welding Progression: Up: FCAW-G Down: GMAW-S
- Position(s) of Fillet: All positions

POSTWELD HEAT TREATMENT (QW-407): None
- Temperature Range:
- Time Range:

PREHEAT (QW-406)
- Preheat Temp. Min.: * 50 deg. F
- Interpass Temp. Max.: 500 deg. F
- Preheat Maintenance: Not required

(Continuous or special heating where applicable should be recorded)

* 175 Deg. F min. if C is >.30% and joint thickness is >1.00"

GAS (QW-408)

	Gas(es)	Percent Composition (Mixture)	Flow Rate
GMAW-S Shielding	Ar/CO2	80/20	20-40 CFH
FCAW-G Shielding	CO2	100	20-40 CFH

ELECTRICAL CHARACTERISTICS (QW-409)
- Current AC or DC: DC Polarity: EP
- Amps (Range): (see below) Volts (Range): (see below)

(Amps and volts range should be recorded for each electrode size, position, and thickness, etc. This information may be listed in a tabular form similar to that shown below.)

- Tungsten Electrode Size and Type: N/A (Pure Tungsten, 2% Thoriated, etc.)
- Mode of Metal Transfer for GMAW: Short Circuit (Spray arc, short circuiting arc, etc.)
- Electrode Wire Feed Speed Range: (see below)

TECHNIQUE (QW-410)
- String or Weave Bead: String and Weave
- Orifice or Gas Cup Size: .50" for GMAW-S / .75" to 1.00" for FCAW-G
- Initial and Interpass Cleaning (Brushing, Grinding, Etc.): Machine, grind or wire brush to remove oxides, paint and mill scale from weld area and joint surfaces. Chip, grind or brush interpasses.
- Method of Back Gouging: Grinding
- Oscillation: .25" max. for GMAW-S / 1.375" max. for FCAW-G
- Contact Tube to Work Distance: .50" max. for GMAW-S / 1.250" max. for FCAW-G
- Multiple or Single Pass (per side): Multiple or Single
- Multiple or Single Electrodes: Single
- Travel Speed (Range): (see below)
- Peening: Not allowed
- Other: All tack welds shall be ground to a "feathered" edge to blend smoothly into the root pass.

Weld Layer(s)	Process	Filler Metal Class	Filler Metal Dia.	Current Type Polar.	Current Amp. Range	Volt Range	Travel Speed Range	Other (e.g., Remarks, Comments, Hot Wire Addition, Technique, Torch Angle, Etc.)
								Wire feed speed
Root	GMAW-S	ER70S-6	.035"	DCEP	90-160	15-19	2-6 in./ min.	100-300 in./ min.
Balance	FCAW-G	E71T-1	.035"	DCEP	125-225	23-28	6-12 in./ min.	290-780 in./ min.
Balance	FCAW-G	E71T-1	.045"	DCEP	170-260	23-27	6-12 in./ min.	200-600 in./ min.
Balance	FCAW-G	E71T-1	.063"	DCEP	215-360	24-29	6-12 in./ min.	150-500 in./ min.

Figure A.2 UMEC Weld Procedure (page 2)

University Mechanical
& Engineering Contractors
An EMCOR Company

QW-483 SUGGESTED FORMAT FOR PROCEDURE QUALIFICATION RECORDS (PQR)
(See QW-200.2, Section IX, ASME Boiler and Pressure Vessel Code)
Record Actual Conditions Used to Weld Test Coupon.

Company Name	University Mechanical & Engineering Contractors		
Procedure Qualification Record #	UM-8.1	Date	3/18/88
WPS #	UM-8.0		
Welding Process(es)	GMAW-S / FCAW-G		
Types (Manual, Auto, Semi-Auto)	Semi-Automatic		

JOINTS (QW-402)

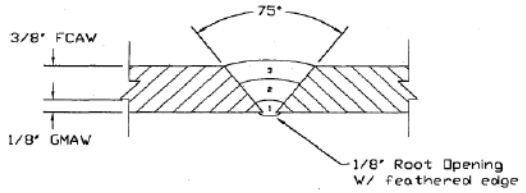

Groove Design of Test Coupon

(For combination qualifications, the deposited weld metal thickness shall be recorded for each filler metal or process used.)

BASE METALS (QW-403)			POSTWELD HEAT TREATMENT (QW-407)	None
Material Specification	SA-106		Temperature	
Type or Grade	Grade B		Time	
P-Number	P-1	to P-No. P-1	Other	
Thickness of Test Coupon	.500"			
Diameter of Test Coupon	8.625"			
Other				

GAS (QW-408)

		Percent Composition		
		Gas	Mixture	Flow Rate
Shielding	GMAW-S	Ar/CO2	80/20	30 CFH
Shielding	FCAW-G	CO2	100%	30 CFH
Backing	None			

FILLER METALS (QW-404)	GMAW-S	FCAW-G
SFA Specification	SFA-5.18	SFA5.20
AWS Classification	E70S-6	E71T-1
Filler Metal F-Number	F-6	F-6
Weld Metal Analysis A-Number	A-1	A-1
Size of Filler Metal	.035"	.045"
Other		
Weld Metal Thickness	.125"	.375"

ELECTRICAL CHARACTERISTICS (QW-409)

Current	Direct		
Polarity	Electrode Positive		
Amps.	See below	Volts	See below
Tungsten Electrode Size		N/A	
Other	GMAW-S 125A 18V		
	FCAW 240A 25.5V		

POSITION (QW-405)	
Position of Groove	6-G
Weld Progression (Uphill, Downhill)	
Other	Downhill for GMAW-S, Uphill for FCAW-G

TECHNIQUE (QW-410)

Travel Speed	GMAW-S 6 IPM, FCAW-G 10 IPM
String or Weave Bead	Weave
Oscillation	Root 1/8" Fill 1/4" Cover 1/2"
Multipass or Single Pass (per side)	Multiple
Single or Multiple Electrodes	Single
Other	

PREHEAT (QW-406)	
Preheat Temperature	Ambient >50 deg. F
Interpass Temperature	500 deg.F (max.)
Other	

Figure A.3 UMEC Weld Procedure (page 3)

University Mechanical
& Engineering Contractors
An EMCOR Company

QW-483 (Back)

PQR No. UM-8.1

Tensile Test (QW-150)

Specimen No.	Width	Thickness	Area	Ultimate Total Load (lb)	Ultimate Unit Stress (psi)	Type of Failure & Location
1	.733"	.512"	.375"	30,000	80,000	Ductile - Base Metal
2	.693"	.502"	.348"	28,400	81,609	Ductile - Base Metal

Guided-Bend Tests (QW-160)

Type and Figure No.	Result
Face bend QW-462.3 (a)	Passed
Root bend QW-462.3 (a)	Passed
Face bend QW-462.3 (a)	Passed
Root bend QW-462.3 (a)	Passed

Toughness Tests (QW-170)

Specimen No.	Notch Location	Specimen Size	Test Temp.	Impact Values ft-lb	Impact Values % Shear	Impact Values Mils	Drop Weight Break (Y/N)

Comments:

Fillet-Weld Test (QW-180)

Result--Satisfactory: Yes No Penetration into Parent Metal: Yes No

Macro--Results:

Other Tests

Test Type

Deposit Analysis

Other

Welder's Name Walter E. Mangas Clock No. N/A Stamp No. A-1

Tests Conducted By Decisive Testing, Inc. Laboratory Test No. DTW-194

We certify that the statements in this record are correct and that the test welds were prepared, welded, and tested in accordance with the requirements of Section IX of the ASME Code.

Manufacturer University Mechanical & Eng. Contr.

Date 3/18/1988 By Gerald Nash, Q.A. Manager

AWS QC 1 GERALD G. NASH 91070411 CWI

(Illustrative only and may be modified to conform to the type and number of tests required by the Code.)

Figure A.4 UMEC Weld Procedure (page 4)

DECISIVE TESTING INC.
MECHANICAL CHEMICAL METALLURGICAL
X-RAY MAG PARTICLE PENETRANTS ULTRA-SONICS EDDY CURRENT METALLOGRAPHY

Phone: 263-3135

382 FEDERAL BLVD. SAN DIEGO, CA. 92102

Date March 18, 1988

Lab No. DTW 194

Your P.O. No. 339902
Job# 1922-19-8160
Specification ASME Section IX

Ship To: University Mechanical
4464 Alvarado Road
San Diego, CA 92120

Material
8.625" dia. x .5" thk. SA106 Grade B
Pipe to same

Proc UM 8.0

Report of Mechanical Test

Ident. Number	Actual Size	Actual Area	Tensile Strength: Actual Load Pounds	Tensile Strength: Pounds per Sq. In.	Yield Strength: Actual Load Pounds	Yield Strength: Pounds per Sq. In.	Elongation: IN...In	Elongation: Percent	Reduct. of Area: Reduced Dimen.	Reduct. of Area: Percent	Bend Test: Type	Bend Test: Results
#1	.512" / .733"	.3752"	30,000	79,957					Bends			
								Root	-	Accepted		
								Face	-	Accepted		
#2	.502" / .693"	.3478"	28,400	81,656				Root	-	Accepted		
								Face	-	Accepted		
Maximum Requirements												
Minimum Requirements				60,000								

Yield Strength determined by: 0.2% Offset Hardness:

Speed of Testing: Grain Size:

Micro Hardness Survey

Depth of Hardness:	.001	.002	.003	.004	.005	.010	Core
Carburization							
Decarburization							

Report of Chemical Analysis

Sample No.		Sample No.	
Carbon		Boron	
Manganese		Vanadium	
Sulfur		Ta + Nb	
Phosphorus		Magnesium	
Silicon		Aluminum	
Nickel		Tin	
Chromium		Lead	
Molybdenum		Iron	
Copper		Cadium	
Titanium		Zinc	
Tungsten		Antimony	
		Cobalt	

Remarks: Pipe Serial No. 4/Procedure# UM8.0/Welder: Walt Mangas
Record# UM-8.1/Process: GMAW/FCAW

☒ Does Conform ☐ Sample Returned

☐ Does not Conform ☒ Sample Discarded

km

Respectfully submitted:

Received by

Figure A.5 UMEC Weld Procedure (page 5)

APPENDIX B: MILL CERTIFICATES

Figures B-1 through Figure B-6 present the mill certificates for raw material used to fabricate each specimen reported in the program described in this report.

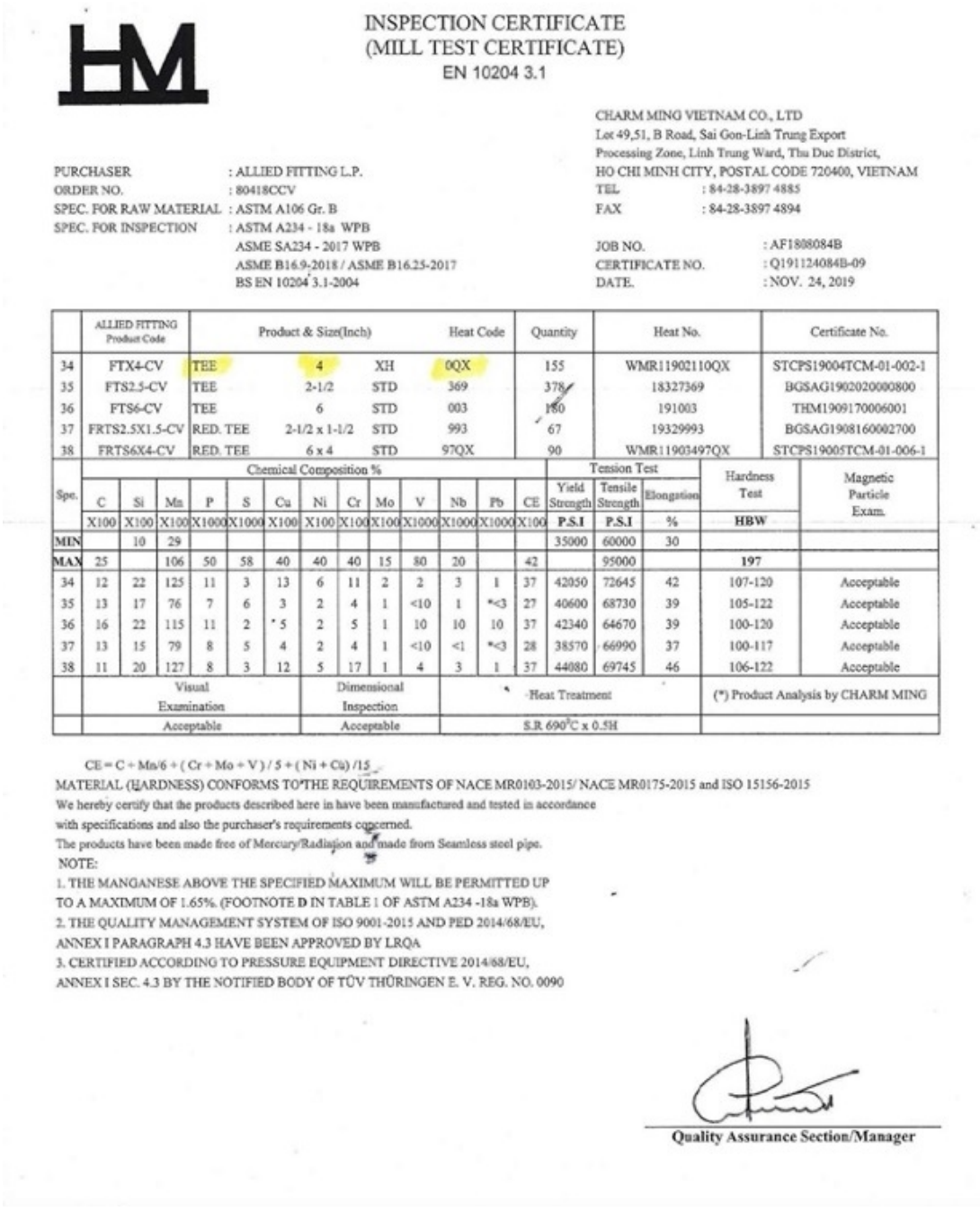

INSPECTION CERTIFICATE
(MILL TEST CERTIFICATE)
EN 10204 3.1

CHARM MING VIETNAM CO., LTD
Lot 49,51, B Road, Sai Gon-Linh Trung Export
Processing Zone, Linh Trung Ward, Thu Duc District,
HO CHI MINH CITY, POSTAL CODE 720400, VIETNAM
TEL : 84-28-3897 4885
FAX : 84-28-3897 4894

PURCHASER : ALLIED FITTING L.P.
ORDER NO. : 80418CCV
SPEC. FOR RAW MATERIAL : ASTM A106 Gr. B
SPEC. FOR INSPECTION : ASTM A234 - 18a WPB
ASME SA234 - 2017 WPB
ASME B16.9-2018 / ASME B16.25-2017
BS EN 10204 3.1-2004

JOB NO. : AF1808084B
CERTIFICATE NO. : Q191124084B-09
DATE. : NOV. 24, 2019

	ALLIED FITTING Product Code	Product & Size(Inch)			Heat Code	Quantity	Heat No.	Certificate No.
34	FTX4-CV	TEE	4	XH	0QX	155	WMR11902110QX	STCPS19004TCM-01-002-1
35	FTS2.5-CV	TEE	2-1/2	STD	369	378	18327369	BGSAG1902020000800
36	FTS6-CV	TEE	6	STD	003	180	191003	THM1909170006001
37	FRTS2.5X1.5-CV	RED. TEE	2-1/2 x 1-1/2	STD	993	67	19329993	BGSAG1908160002700
38	FRTS6X4-CV	RED. TEE	6 x 4	STD	97QX	90	WMR11903497QX	STCPS19005TCM-01-006-1

Spe.	Chemical Composition %													Tension Test			Hardness Test	Magnetic Particle Exam.
	C	Si	Mn	P	S	Cu	Ni	Cr	Mo	V	Nb	Pb	CE	Yield Strength	Tensile Strength	Elongation		
	X100	X100	X100	X1000	X1000	X100	X100	X100	X100	X1000	X1000	X1000	X100	P.S.I	P.S.I	%	HBW	
MIN		10	29											35000	60000	30		
MAX	25		106	50	58	40	40	40	15	80	20		42		95000		197	
34	12	22	125	11	3	13	6	11	2	2	3	1	37	42050	72645	42	107-120	Acceptable
35	13	17	76	7	6	3	2	4	1	<10	1	*<3	27	40600	68730	39	105-122	Acceptable
36	16	22	115	11	2	* 5	2	5	1	10	10	10	37	42340	64670	39	100-120	Acceptable
37	13	15	79	8	5	4	2	4	1	<10	<1	*<3	28	38570	66990	37	100-117	Acceptable
38	11	20	127	8	3	12	5	17	1	4	3	1	37	44080	69745	46	106-122	Acceptable

Visual Examination	Dimensional Inspection	Heat Treatment	(*) Product Analysis by CHARM MING
Acceptable	Acceptable	S.R 690°C x 0.5H	

CE = C + Mn/6 + (Cr + Mo + V) / 5 + (Ni + Cu) /15

MATERIAL (HARDNESS) CONFORMS TO THE REQUIREMENTS OF NACE MR0103-2015/ NACE MR0175-2015 and ISO 15156-2015

We hereby certify that the products described here in have been manufactured and tested in accordance with specifications and also the purchaser's requirements concerned.

The products have been made free of Mercury/Radiation and made from Seamless steel pipe.

NOTE:

1. THE MANGANESE ABOVE THE SPECIFIED MAXIMUM WILL BE PERMITTED UP TO A MAXIMUM OF 1.65%. (FOOTNOTE D IN TABLE 1 OF ASTM A234 -18a WPB).
2. THE QUALITY MANAGEMENT SYSTEM OF ISO 9001-2015 AND PED 2014/68/EU, ANNEX I PARAGRAPH 4.3 HAVE BEEN APPROVED BY LRQA
3. CERTIFIED ACCORDING TO PRESSURE EQUIPMENT DIRECTIVE 2014/68/EU, ANNEX I SEC. 4.3 BY THE NOTIFIED BODY OF TÜV THÜRINGEN E. V. REG. NO. 0090

Quality Assurance Section/Manager

Figure B.1 Mill certificate for the 4 in. Schedule 80 tee

INSPECTION CERTIFICATE
(MILL TEST CERTIFICATE)
EN 10204 3.1

CHARM MING VIETNAM CO., LTD
Lot 49,51, B Road, Sai Gon-Linh Trung Export
Processing Zone, Linh Trung Ward, Thu Duc District,
HO CHI MINH CITY, POSTAL CODE 720400, VIETNAM
TEL : 84-28-3897 4885
FAX : 84-28-3897 4894

PURCHASER : ALLIED FITTING L.P.
ORDER NO. : PO11062
SPEC. FOR RAW MATERIAL : ASTM A106 Gr. B
SPEC. FOR INSPECTION : ASTM A234 - 19 WPB
ASME SA234 - 2019 WPB
ASME B16.9-2018 / ASME B16.25-2017
BS EN 10204 3.1-2004

JOB NO. : AF2003023A
CERTIFICATE NO. : Q200926023A-01
DATE. : SEP. 26, 2020

	ALLIED FITTING Product Code	Product & Size(Inch)			Heat Code	Quantity	Heat No.	Certificate No.
1	F4LS.75	45 ELBOW LR	3/4	STD	456	50	20-102456	0001200506-001
2	F4LS1.25	45 ELBOW LR	1-1/4	STD	456	250	20-102456	0001200506-007
3	F9LX1.5	90 ELBOW LR	1-1/2	XH	363	150	10305363	BGSAG2007090007200
4	F9LX3	90 ELBOW LR	3	XH	503	300	10303503	BGSAG2003100002500
5	F9LX4	90 ELBOW LR	4	XH	334	300	19301334	BGSAG1909200003700

Spe.	Chemical Composition %													Tension Test			Hardness Test	Magnetic Particle Exam.
	C	Si	Mn	P	S	Cu	Ni	Cr	Mo	V	Nb	Pb	CE	Yield Strength	Tensile Strength	Elongation		
	X100	X100	X100	X1000	X1000	X100	X100	X100	X100	X1000	X1000	X1000	X100	P.S.I	P.S.I	%	HBW	
MIN		10	29											35000	60000	30		
MAX	25		106	50	58	40	40	40	15	80	20		42		95000		197	
1	23	23	93	13	4	1	1	2	<1	1	3	*<3	39	38860	71050	40	131	N/A
2	23	23	93	13	4	1	1	2	<1	1	3	*<3	39	40455	65540	42	138	N/A
3	12	16	78	5	2	4	4	6	2	<1	2	*<3	27	38425	69020	41	137	N/A
4	13	14	76	8	3	3	2	8	3	<10	1	*<3	28	39440	71195	45	139	N/A
5	14	17	76	9	2	2	1	5	1	<10	1	*<3	28	37845	61625	44	139	N/A

Visual Examination	Dimensional Inspection	Heat Treatment	(*) Product Analysis by CHARM MING
Acceptable	Acceptable	N/A	

CE = C + Mn/6 + (Cr + Mo + V) / 5 + (Ni + Cu)/15

MATERIAL (HARDNESS) CONFORMS TO THE REQUIREMENTS OF NACE MR0103-2015/ NACE MR0175-2015 and ISO 15156-2015

We hereby certify that the products described here in have been manufactured and tested in accordance with specifications and also the purchaser's requirements concerned.

The products have been made free of Mercury/Radiation and made from Seamless steel pipe.

NOTE:

1. ABOVE - LISTED ELBOWS HAVE BEEN HOT - FORMED AT A TEMPERATURE ABOVE 1150° F (620°C) AND BELOW 1800°F (980°C) AND SUBSEQUENTLY COOLED IN STILL AIR.
2. THE MANGANESE ABOVE THE SPECIFIED MAXIMUM WILL BE PERMITTED UP TO A MAXIMUM OF 1.65%. (FOOTNOTE **D** IN TABLE 1 OF ASTM A234 -19 WPB).
3. THE QUALITY MANAGEMENT SYSTEM OF ISO 9001-2015 AND PED 2014/68/EU, ANNEX I PARAGRAPH 4.3 HAVE BEEN APPROVED BY LRQA
4. CERTIFIED ACCORDING TO PRESSURE EQUIPMENT DIRECTIVE 2014/68/EU, ANNEX I SEC. 4.3 BY THE NOTIFIED BODY OF TÜV THÜRINGEN E. V. REG. NO. 0090

Quality Assurance Section/Manager

Figure B.2 Mill certificate for the 4 in. Schedule 80 90-degrees elbow

INSPECTION CERTIFICATE
(MILL TEST CERTIFICATE)
EN 10204 3.1

CHARM MING VIETNAM CO., LTD
Lot 49,51, B Road, Sai Gon-Linh Trung Export
Processing Zone, Linh Trung Ward, Thu Duc District,
HO CHI MINH CITY, POSTAL CODE 720400, VIETNAM
TEL : 84-28-3897 4885
FAX : 84-28-3897 4894

PURCHASER : ALLIED FITTING L.P.
ORDER NO. : 32118CCV
SPEC. FOR RAW MATERIAL : ASTM A106 Gr. B
SPEC. FOR INSPECTION : ASTM A234 - 18a WPB
ASME SA234 - 2017 WPB
ASME B16.9-2018 / ASME B16.25-2017
BS EN 10204 3.1-2004

JOB NO. : AF1803038C
CERTIFICATE NO. : Q191124038C-01
DATE. : NOV. 24, 2019

	ALLIED FITTING Product Code	Product & Size(Inch)			Heat Code	Quantity	Heat No.	Certificate No.
1	F4LX4-CV	45 ELBOW LR	4	XH	334	144	19301334	BGSAG1909200003700

Spe.	Chemical Composition %													Tension Test			Hardness Test	Magnetic Particle Exam.
	C	Si	Mn	P	S	Cu	Ni	Cr	Mo	V	Nb	Pb	CE	Yield Strength	Tensile Strength	Elongation		
	X100	X100	X100	X1000	X1000	X100	X100	X100	X100	X1000	X1000	X1000	X100	P.S.I	P.S.I	%	HBW	
MIN		10	29											35000	60000	30		
MAX	25		106	50	58	40	40	40	15	80	20		42		95000		197	
1	14	17	76	9	2	2	1	5	1	<10	1	*<3	28	38570	61915	44	125-136	N/A

Visual Examination	Dimensional Inspection	Heat Treatment	(*) Product Analysis by CHARM MING
Acceptable	Acceptable	N/A	

CE = C + Mn/6 + (Cr + Mo + V) / 5 + (Ni + Cu) /15

MATERIAL (HARDNESS) CONFORMS TO THE REQUIREMENTS OF NACE MR0103-2015/ NACE MR0175-2015 and ISO 15156-2015

We hereby certify that the products described here in have been manufactured and tested in accordance with specifications and also the purchaser's requirements concerned.

The products have been made free of Mercury/Radiation and made from Seamless steel pipe.

NOTE:

1. ABOVE - LISTED ELBOWS HAVE BEEN HOT - FORMED AT A TEMPERATURE ABOVE 1150° F (620°C) AND BELOW 1800°F (980°C) AND SUBSEQUENTLY COOLED IN STILL AIR.
2. THE MANGANESE ABOVE THE SPECIFIED MAXIMUM WILL BE PERMITTED UP TO A MAXIMUM OF 1.65%. (FOOTNOTE **D** IN TABLE 1 OF ASTM A234 -18a WPB).
3. THE QUALITY MANAGEMENT SYSTEM OF ISO 9001-2015 AND PED 2014/68/EU, ANNEX I PARAGRAPH 4.3 HAVE BEEN APPROVED BY LRQA
4. CERTIFIED ACCORDING TO PRESSURE EQUIPMENT DIRECTIVE 2014/68/EU, ANNEX I SEC. 4.3 BY THE NOTIFIED BODY OF TÜV THÜRINGEN E. V. REG. NO. 0090

Quality Assurance Section/Manager

Figure B.3 Mill certificate for the 4 in. Schedule 80 90-degrees elbow

INSPECTION CERTIFICATE

PANTECH STEEL INDUSTRIES SDN. BHD. (508721-A)
LOT 13258 & 13259, Jalan Haji Abd. Manan,
Off Jalan Meru, 42200 Kapar, Selangor, Malaysia.
Tel: 603-3393 1633 Fax: 603-3393 1733 E-mail: info@pantechsteel.com

CERTIFIED ISO 9001

Quality Management System is certified under ISO 9001. Approval. No.: 0047956
PED 2014/68/EU Annex 1 Clause 4.3
Cert. No.: 0038/PED/MVM/0810070/1

WROUGHT CARBON STEEL BUTTWELDING FITTINGS

INSPECTION DOCUMENT: EN10204:2004 Type 3.1

Certificate No : PSI 134718-09
Date : 23-Apr-2020

Purchaser: ALLIED FITTING CORP.

Order No.	Invoice No.	Starting Material	Specification for Fittings- Seamless	Specification for Inspection
P09835-2	E000015182	Seamless Pipe	ASTM A234-18a WPB/ASME SA234-17 WPB/ CSA Z245.11-05 Cat.I Gr.241/ NACE MR 0175/NACE MR 0103/ISO15156-15*	ASME B16.9-18/ASTM A960-19

Batch No.	Part Code	Product & Size	Quantity (pcs)	Dimensional & Visual Inspection	Heat Treatment	Magnetic Particle Testing
WE214MT	FTS8-PS	8" STD TEE	57	GOOD	C&S	GOOD

Specification	Chemical Composition (%)												Tensile Test *1			Hardness (HB)	
	C	Si	Mn	P	S	Ni	Cr	Mo	Cu	V	Pb	CE	YS	TS	E*2		
Min	x100	x100	x100	x1000	x1000	x100	x100	x100	x100	x1000		x100	(KSI / MPa)		(%)	1	2
Max	-	10	29	-	-	-	-	-	-	-	-	-	240	415	-	-	
Batch No.	22	-	106	50	58	40	40	15	40	80	-	42	-	-	-	197	
WE214MT	15	15	37	20	7	2	8	4	6	4	<0.10	24	325	461	30.7	137	139

WE CERTIFY THAT ALL PRODUCTS WERE MANUFACTURED,SAMPLED,TESTED, AND INSPECTED SOLELY BY THE MANUFACTURER LISTED AT THE ADDRESS ABOVE IN ACCORDANCE WITH INDICATED SPECIFICATION AND FOUND TO MEET REQUIREMENTS. MATERIAL IS FREE FROM MERCURY AND RADIOACTIVE CONTAMINATION.
TENSILE REQUIREMENT: CONFORMS TO ASTM A370 STANDARD, LONGITUDINAL DIRECTION, GAUGE LENGTH 2" (50mm)
*FULLY KILLED
*HARDNESS ACCORDING TO NACE MR0103/ NACE MR0175/ISO15156-15

NOTE:
C: Cold formed at temperature below 620°C
S: Stress relieved in temperature between 595°C - 690°C and cooled in still air.
H : Hot formed in temperature between 620°C - 980°C and cooled in still air.
N: Normalised at 910°C
Q: Heated to 910°C and quench in water.
T: Temper between 590°C - 690°C.

*1: YS = Yield strength TS=Tensile strength E = Elongation
*2: For thickness above 7.94 mm, the minimum elongation value, E is 30. Else, E = 48t + 15, where t = specimen thickness, in

Quality Assurance Manager

Made in Malaysia

Page 9 of

Figure B.4 Mill certificate for the 8 in. Schedule 40 tee

INSPECTION CERTIFICATE
(MILL TEST CERTIFICATE)
EN 10204 3.1

CHARM MING VIETNAM CO., LTD
Lot 49,51, B Road, Sai Gon-Linh Trung Export
Processing Zone, Linh Trung Ward, Thu Duc District,
HO CHI MINH CITY, POSTAL CODE 720400, VIETNAM
TEL : 84-28-3897 4885
FAX : 84-28-3897 4894

PURCHASER : ALLIED FITTING L.P.
ORDER NO. : PO11062
SPEC. FOR RAW MATERIAL : ASTM A106 Gr. B
SPEC. FOR INSPECTION : ASTM A234 - 19 WPB
ASME SA234 - 2019 WPB
ASME B16.9-2018 / ASME B16.25-2017
BS EN 10204 3.1-2004

JOB NO. : AF2003023A
CERTIFICATE NO. : Q200926023A-03
DATE. : SEP. 26, 2020

	ALLIED FITTING Product Code	Product & Size(Inch)			Heat Code	Quantity	Heat No.	Certificate No.
11	F9LS6	90 ELBOW LR	6	STD	69Z	480	WF0082769Z	20GC015796-1
12	F9LS8	90 ELBOW LR	8	STD	974QX	336	WMR32001974QX	20GC015721-1
13	F9LS10	90 ELBOW LR	10	STD	02Z	170	WF0072102Z	20GC019331-1
14	F9LS12	90 ELBOW LR	12	STD	774H	73	50774H	BGSQG2007160000900
15	F9LS12	90 ELBOW LR	12	STD	212	15	J9K1212	WYYK1676

Spe.	Chemical Composition %													Tension Test			Hardness Test	Magnetic Particle Exam.
	C	Si	Mn	P	S	Cu	Ni	Cr	Mo	V	Nb	Pb	CE	Yield Strength	Tensile Strength	Elongation		
	X100	X100	X100	X1000	X1000	X100	X100	X100	X100	X1000	X1000	X1000	X100	P.S.I	P.S.I	%	HBW	
MIN		10	29											35000	60000	30		
MAX	25		106	50	58	40	40	40	15	80	20		42		95000		197	
11	12	23	122	8	3	11	10	12	4	2	1	5	37	53360	77575	45	136	N/A
12	11	22	124	6	3	11	4	7	1	1	1	1	34	47850	68295	40	136	N/A
13	12	25	128	6	4	5	3	10	3	2	1	5	37	42050	63365	46	138	N/A
14	17	18	90	17	8	1	<1	1	<1	<1	1	*<3	33	36105	68150	35	141	N/A
15	11	27	131	19	3	2	3	13	1	0	0	*<3	36	39440	60610	37	139	N/A

Visual Examination	Dimensional Inspection	Heat Treatment	(*) Product Analysis by CHARM MING
Acceptable	Acceptable	N/A	

CE = C + Mn/6 + (Cr + Mo + V) / 5 + (Ni + Cu)./15

MATERIAL (HARDNESS) CONFORMS TO THE REQUIREMENTS OF NACE MR0103-2015/ NACE MR0175-2015 and ISO 15156-2015

We hereby certify that the products described here in have been manufactured and tested in accordance with specifications and also the purchaser's requirements concerned.

The products have been made free of Mercury/Radiation and made from Seamless steel pipe.

NOTE:

1. ABOVE - LISTED ELBOWS HAVE BEEN HOT - FORMED AT A TEMPERATURE ABOVE 1150° F (620°C) AND BELOW 1800°F (980°C) AND SUBSEQUENTLY COOLED IN STILL AIR.
2. THE MANGANESE ABOVE THE SPECIFIED MAXIMUM WILL BE PERMITTED UP TO A MAXIMUM OF 1.65%. (FOOTNOTE D IN TABLE 1 OF ASTM A234 -19 WPB).
3. THE QUALITY MANAGEMENT SYSTEM OF ISO 9001-2015 AND PED 2014/68/EU, ANNEX I PARAGRAPH 4.3 HAVE BEEN APPROVED BY LRQA
4. CERTIFIED ACCORDING TO PRESSURE EQUIPMENT DIRECTIVE 2014/68/EU, ANNEX I SEC. 4.3 BY THE NOTIFIED BODY OF TÜV THÜRINGEN E. V. REG. NO. 0090

Quality Assurance Section/Manager

Figure B.5 Mill certificate for the 8 in. Schedule 40 90-degrees elbow

Awaji ASK

AWAJI MATERIA (THAILAND) CO.,LTD.

INSPECTION CERTIFICATE

EN 10204 3.1 : 2004

Head Office : 4-2, KAMIGAMO, SUMOTO CITY, HYOGO, 656-0015, JAPAN
Tel : (81) 799-22-1731 : FAX (81) 799-22-1730

Factory : 81, MOO 4, PRAKASA ROAD, TAMBOL BANGMUANG, AMPHUR MUANG SAMUTPRAKARN, THAILAND 10270, Tel : (662) 701-5226

ISO 9001:2015 Manufacturing Company
Certified by BVI. Certificate No. TH013595

Material manufacturer QMS acc.
PED 2014/68/EU. Annex1, Part 4.3 / AD2000-MerkBlatt W0
Certified by Lloyd's Register
Certificate No. 50207/1

Purchaser : ALLIED FITTING LP. (HOUSTON)

Date : DECEMBER 17, 2019

Certificate No. : T19-Z1854/4

Order No.	Job No.	Product	
607190AW	-	CARBON STEEL BUTT WELDING FITTINGS	MADE FROM SEAMLESS STEEL PIPE

Inspection Standard	Material Standard	Visual	Dimension	#4 UT Inspection	Magnetic Particle Test
ASME B16.9-18, ASME B16.25-17 ASTM A960-18 NACE MR-0175/ISO 15156-2-15, SS Region3 MR-0103-15	ASTM A234-GrWPB ASME SA234-17 Sec. II Part A except nuclear usage CSA Z245.11-17, GR.241 CAT. I -SS	GOOD	GOOD	W.T. INSPECTED	-

Manufacturing No. (Heat code)	Product Code	Material	Article & Size			Quantity	Note.
968M5EX	F4L58-AW	WPB	STD 45° LONG	RADIUS	ELBOW 8"	196 Pcs.	

Specification		C	Si	*3 Mn	P	S	Cu	Ni	Cr	Mo	V^	Nb	Ti	B	Ca	N	Al	C.E.	*2 Mechanical Test Y.S.	T.S.	E	T Hardness
								*1 Chemical Composition (%)											MPa		%	HB
Min.		X100	X100	X100	X1000	X1000	X100	X100	X100	X100	X100	X100	X100	X10000	X10000	X1000	X1000	X100				
		-	10	29	-	-	-	-	-	-	-	-	-	-	-	-	-		240	415	30	-
Max.		22	-	135	50	58	40	40	40	15	8	2	-	5	-	-	-	42	-	-	-	197
Heat No.																						
190501	L	10	24	121	7	2	5	2	12	1	1	1	0	4	5	4	44	33	311	474	43	143
	P	11	22	120	5	1	5	2	10	3	1	1	0	5	7	2	40	34				146

$$C.E. = C + \frac{Mn}{6} + \frac{Cr+Mo+V}{5} + \frac{Ni+Cu}{15}$$

*1 Equivalent for A234 WPB
*2 Y.S.= Yield Strength (0.2% offset). T.S. = Tensile Strength. E = Elongation (in 50mm), L = Longitudinal, T = Transverse
*3 As per foot note D of ASME SA234 Table 1.
L = Ladle Analysis, P = Product Analysis
No weld repair was performed
Steel Making by Vacuum degassed, fully silicon aluminium killed & fine grain.
All material supplied is certified to be free of mercury contamination & no mercury bearing equipment was used during manufacturing.
*4 UT = Ultrasonic thickness inspection

ELBOW / Forming temperature 850°C – 945°C and cooled in still air
TEE, REDUCER & CAP / Normalizing (cold Forming) : 910°C (Holding Time : (Nominal Wall Thickness/1mm) x 1.5 min.))

"We certify that the fitting was manufactured, sampled, tested and inspected in accordance with the specification and was found to meet the requirements."

Surveyor to

AT-242339

QA. GM. /Work Inspector S. PORNTIP
QC-AMT@awaji.co.th

Figure B.6 Mill certificate for the 8 in. Schedule 40 45-degrees elbow

APPENDIX C: LOADING PROTOCOL DETAILS

Tables C-1 through Table C-6 present the details relative to the loading protocol for all specimens except 4T-IP and 4T-OP, which are presented in Chapter 2.

Table C.1 Load protocol details for specimens 8T-IP

Cycle set #	Applied Displacement @L01 (inch)	Time (sec/quarter cycle)	Rate (inch/sec)	Notes
1	0.036	5	0.007	
2	0.050	5	0.010	
3	0.071	5	0.014	
4	0.099	5	0.020	
5	0.138	5	0.028	
6	0.194	10	0.019	
7	0.271	10	0.027	
8	0.379	10	0.038	
9	0.531	15	0.035	
10	0.744	15	0.050	
11	1.041	15	0.069	
12	1.458	15	0.097	
13	2.041	30	0.068	
14	2.857	30	0.095	Failure cycle
15	4.000	30	0.133	Not applied
16	5.600	30	0.187	Not applied
17	7.841	60	0.131	Not applied
18	10.977	60	0.183	Δ_m, Not applied

Table C.2 Load protocol details for specimens 8T-IP and 8T-OP

Cycle set #	Applied Displacement @L01 (inch)	Time (sec/quarter cycle)	Rate (inch/sec)	Notes
1	0.036	5	0.007	
2	0.050	5	0.010	
3	0.071	5	0.014	
4	0.099	5	0.020	
5	0.138	5	0.028	
6	0.194	10	0.019	
7	0.271	10	0.027	
8	0.379	10	0.038	
9	0.531	15	0.035	
10	0.744	15	0.050	
11	1.041	15	0.069	
12	1.458	15	0.097	
13	2.041	30	0.068	
14	2.857	30	0.095	8T-IP: Cycle set at failure
15	4.000	30	0.133	8T-IP: Not applied; 8T-OP: Cycle set at failure
16	5.600	30	0.187	8T-IP and 8T-OP: Not applied; 8T-OP: Δ_m
17	7.841	60	0.131	8T-IP and 8T-OP: Not applied
18	10.977	60	0.183	8T-IP: Δ_m . 8T-IP and 8T-OP: not applied

Table C.3 Load protocol details for specimen 4E-90

Cycle set #	Applied Displacement @L01 (inch)	Time (sec/quarter cycle)	Rate (inch/sec)	Notes
1	0.039	5	0.008	
2	0.055	5	0.011	
3	0.076	5	0.015	
4	0.107	5	0.021	
5	0.150	5	0.030	
6	0.210	5	0.042	
7	0.294	5	0.059	
8	0.411	15	0.027	
9	0.576	15	0.038	
10	0.806	15	0.054	
11	1.128	15	0.075	
12	1.579	15	0.105	
13	2.211	30	0.074	
14	3.095	30	0.103	
15	4.334	30	0.144	
16	6.067	45	0.135	
17	8.494	60	0.142	Cycle set at failure
18	11.892	90	0.132	Δ_m ; Cycle set not applied

Table C.4 Load protocol details for specimen 4E-45

Cycle set #	Applied Displacement @L01 (inch)	Time (sec/quarter cycle)	Rate (inch/sec)	Notes
1	0.033	5	0.007	
2	0.046	5	0.009	
3	0.065	5	0.013	
4	0.091	5	0.018	
5	0.127	5	0.025	
6	0.177	5	0.035	
7	0.248	5	0.050	
8	0.348	15	0.023	
9	0.487	15	0.032	
10	0.682	15	0.045	
11	0.955	15	0.064	
12	1.336	15	0.089	
13	1.871	30	0.062	Cycle set at failure
14	2.619	30	0.087	Δ_m ; Cycle set not applied

Table C.5 Load protocol details for specimen 8E-90

Cycle set #	Applied Displacement @L01 (inch)	Time (sec/quarter cycle)	Rate (inch/sec)	Notes
1	0.066	5	0.013	
2	0.092	5	0.018	
3	0.129	5	0.026	
4	0.181	5	0.036	
5	0.254	5	0.051	
6	0.355	5	0.071	
7	0.497	5	0.099	
8	0.696	15	0.046	
9	0.974	15	0.065	
10	1.364	15	0.091	
11	1.909	15	0.127	
12	2.673	15	0.178	
13	3.742	30	0.125	
14	5.239	30	0.175	
15	7.334	45	0.163	Δ_m
16	10.267	60	0.171	-Cycle added because specimen did not reach failure at Δ_m -In the Northward direction the test was stopped when the actuator reach 50 kip, around 9 inch of displacement
17	17.07			-The control was switched from LS01 to the actuator displacement sensor -This cycle set followed these steps: Monotonic push in the southward direction (closing) to 17.07 inch Back to zero displacement Second Push to 17.07 inch Unload to zero force. Failure during unloading.

Table C.6 Load protocol details for specimen 8E-45

Cycle set #	Applied Displacement @L01 (inch)	Time (sec/quarter cycle)	Rate (inch/sec)	Notes
1	0.03	5	0.006	
2	0.042	5	0.008	
3	0.059	5	0.012	
4	0.082	5	0.016	
5	0.115	5	0.023	
6	0.161	5	0.032	
7	0.226	5	0.045	
8	0.316	10	0.032	
9	0.443	10	0.044	
10	0.620	10	0.062	
11	0.868	10	0.087	-Northward (-) direction: cycle applied until 50 kip are reached
12	1.215	10	0.121	-Northward (-) direction: cycle applied until 50 kip are reached
13	1.701	15	0.113	-Northward (-) direction: cycle applied until 50 kip are reached
14	2.381	15	0.159	Δ_m -Northward (-) direction: cycle applied until 50 kip are reached
15	3.334	30	0.111	-Northward (-) direction: cycle applied until 50 kip are reached
16	4.667	30	0.156	-Northward (-) direction: cycle applied until 50 kip are reached
17	6.534	45	0.145	-Northward (-) direction: cycle applied until 50 kip are reached
18	9.147	60	0.152	-Northward (-) direction: cycle applied until 50 kip are reached
19	12.806	85	0.151	-Northward (-) direction: cycle applied until 50 kip are reached

Cycle set #	Applied Displacement @L01 (inch)	Time (sec/quarter cycle)	Rate (inch/sec)	Notes
20				-Northward (-) direction: cycle applied until 50 kip are reached
	17.929	115	0.156	-Failure reached during unloading

APPENDIX D: MEASUREMENTS OBTAINED BY STRAIN GAUGES

Figures D-1 through Figure D-14 presents the history of strains measured by strain gauges and rosettes for all specimens except for 4T-IP, which is presented in Chapter 3.

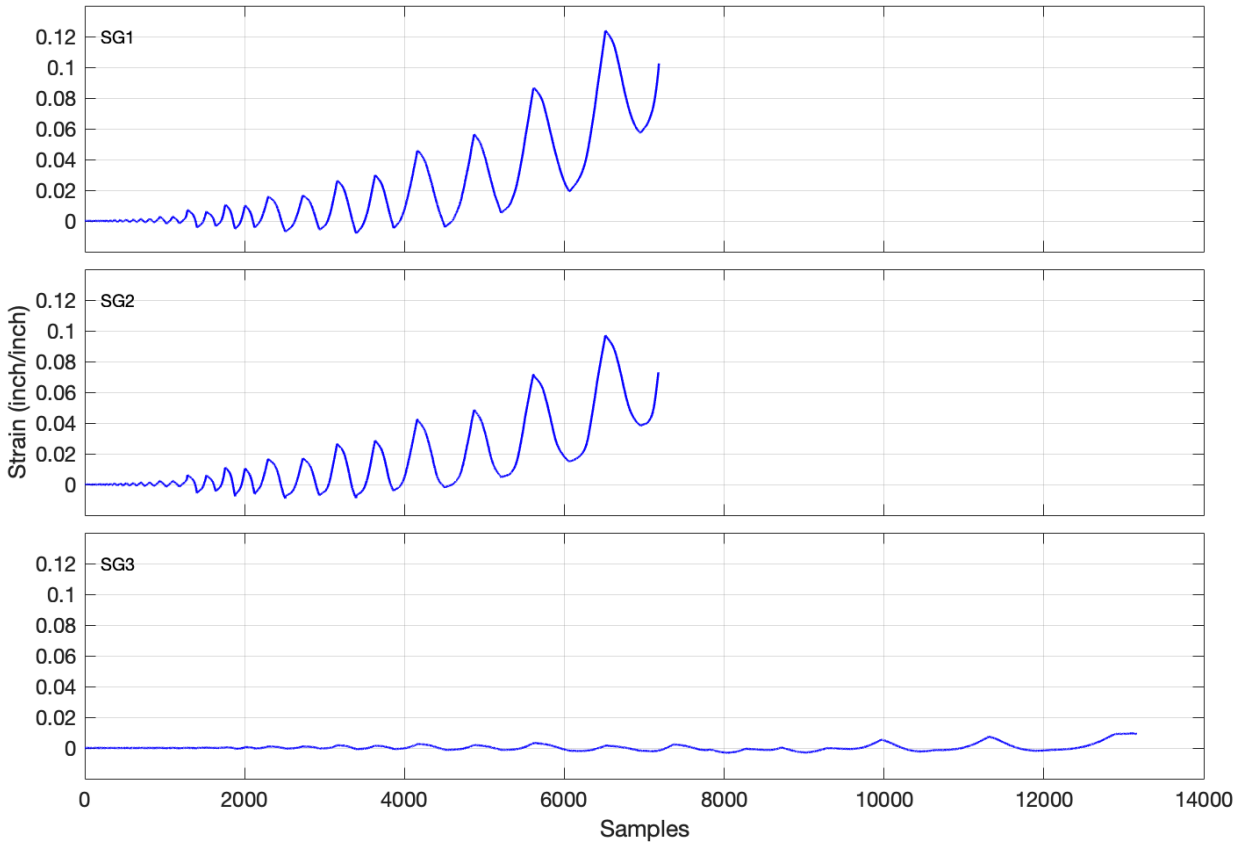

Figure D.1 Strain measured by strain gauges in specimen 4T-OP

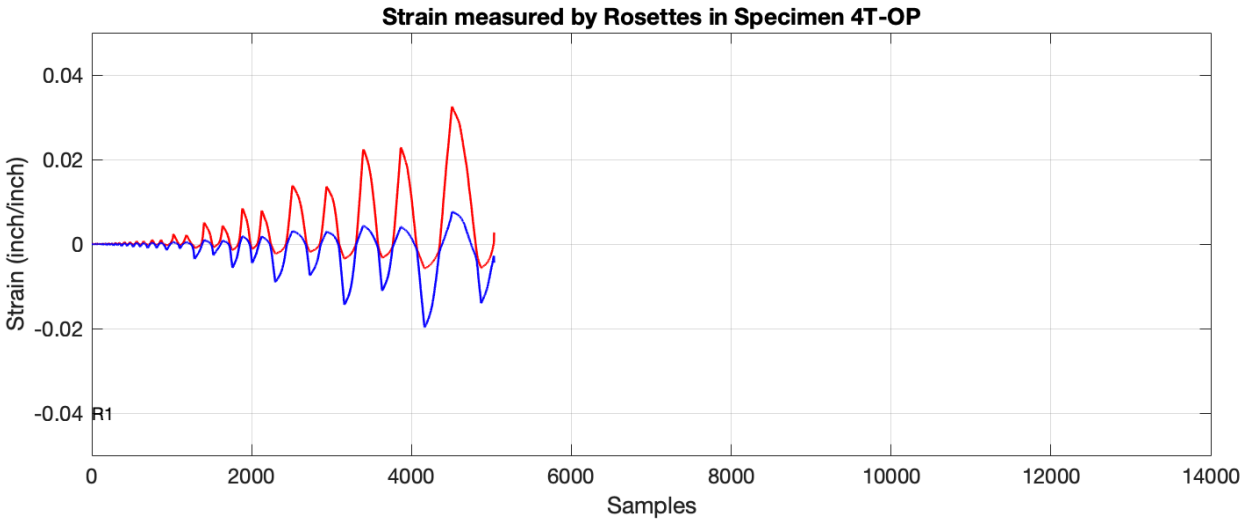

Figure D.2 Strain measured by rosettes in specimen 4T-OP

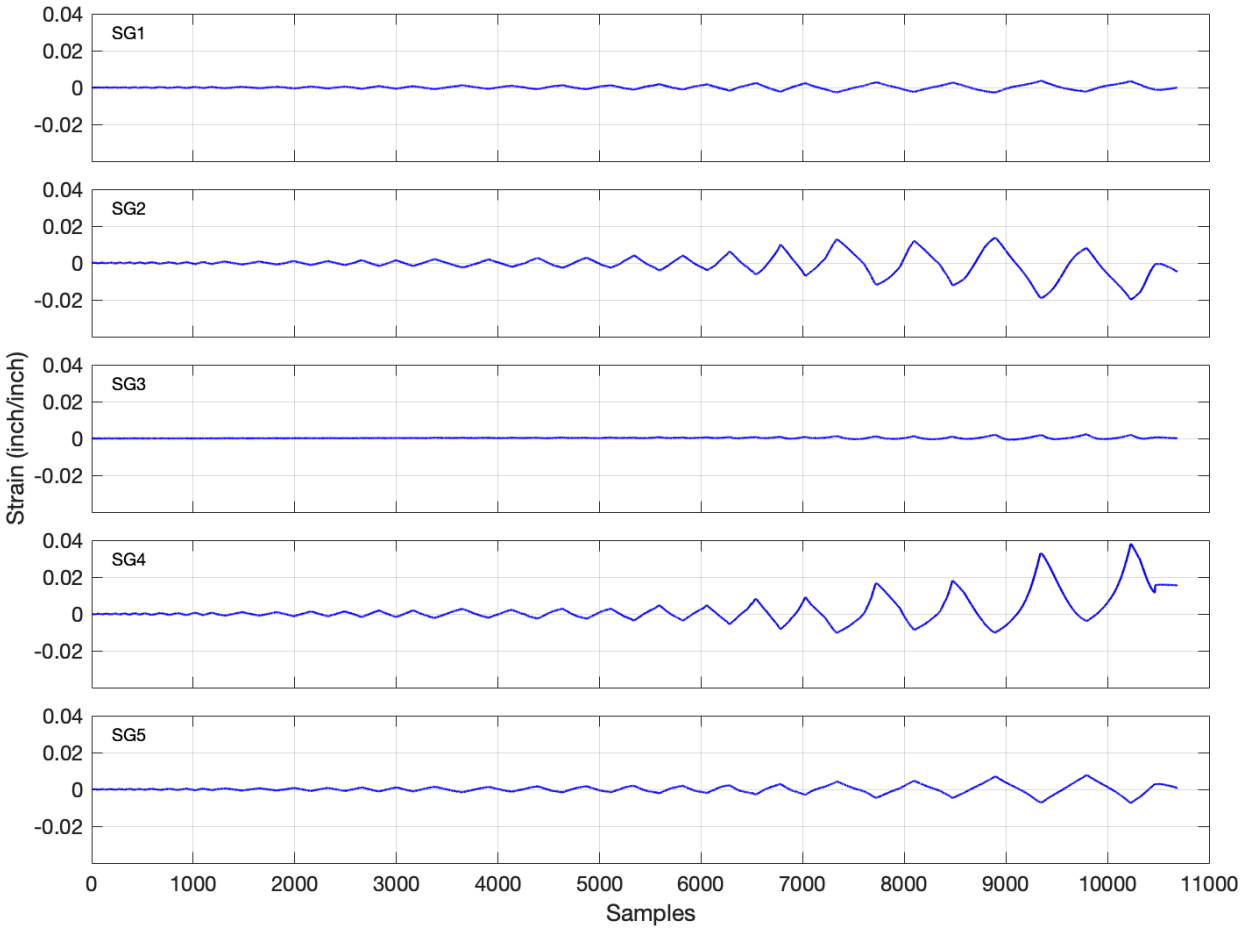

Figure D.3 Strain measured by strain gauges in specimen 8T-IP

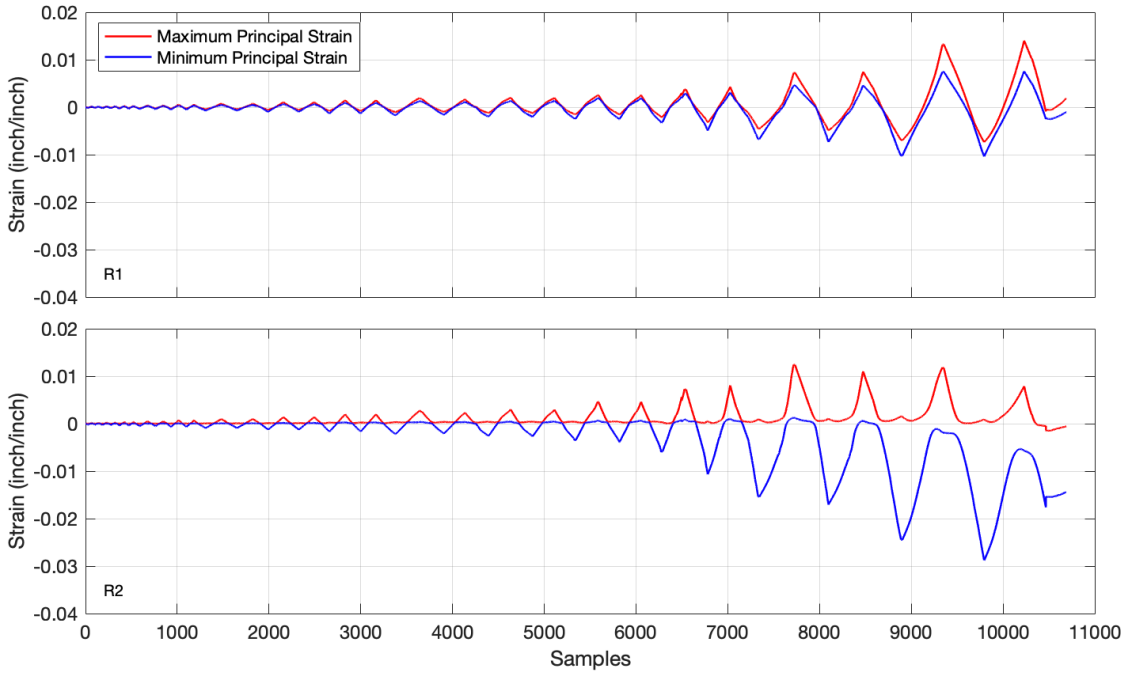

Figure D.4 Strain measured by rosettes in specimen 8T-IP

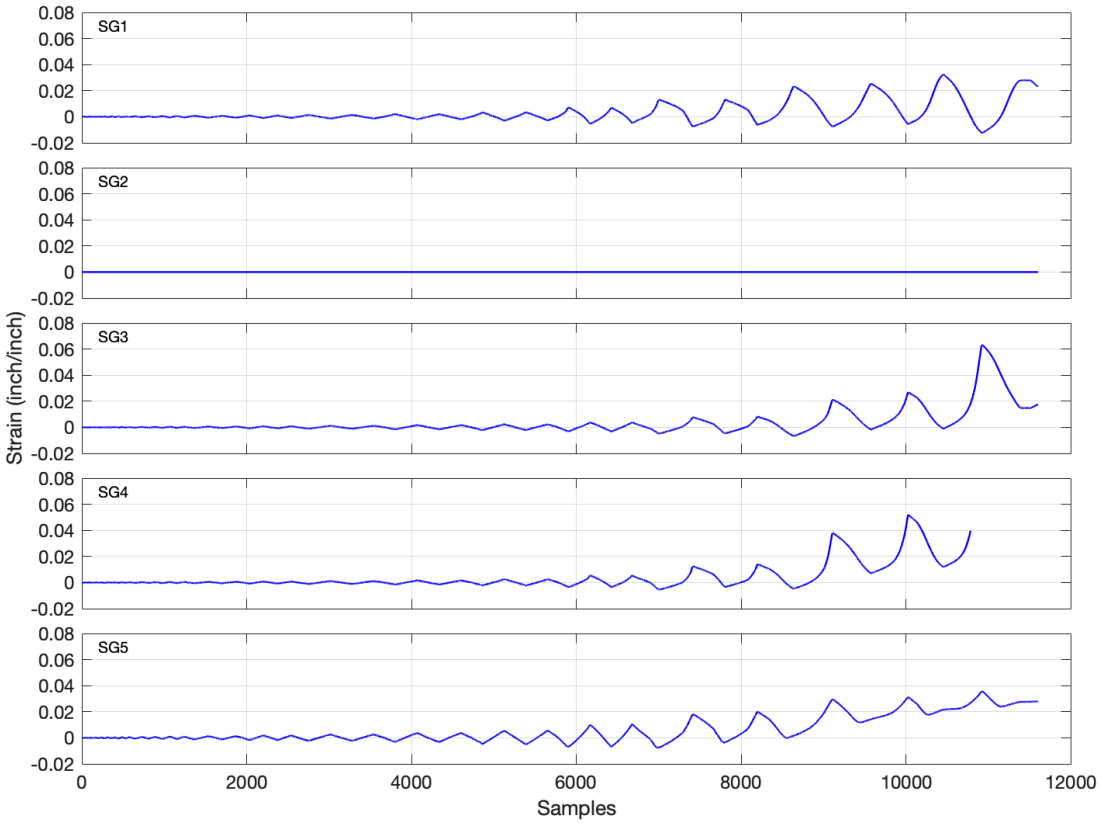

Figure D.5 Strain measured by strain gauges in specimen 8T-OP

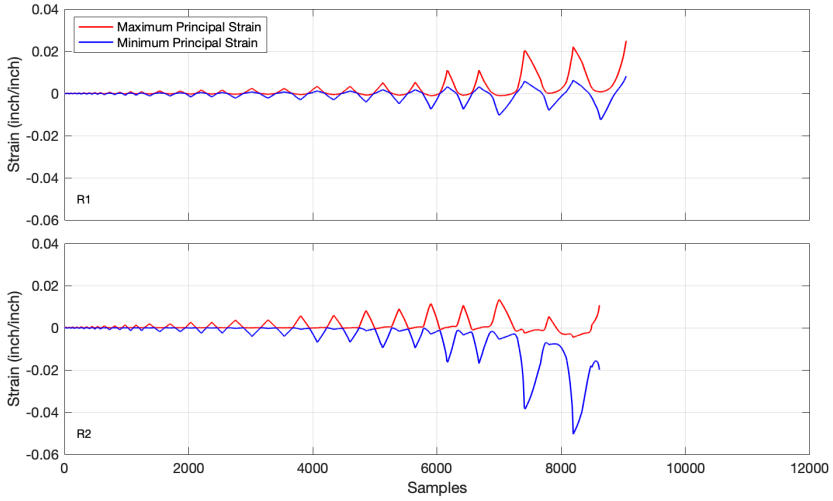

Figure D.6 Strain measured by rosettes in specimen 8T-OP

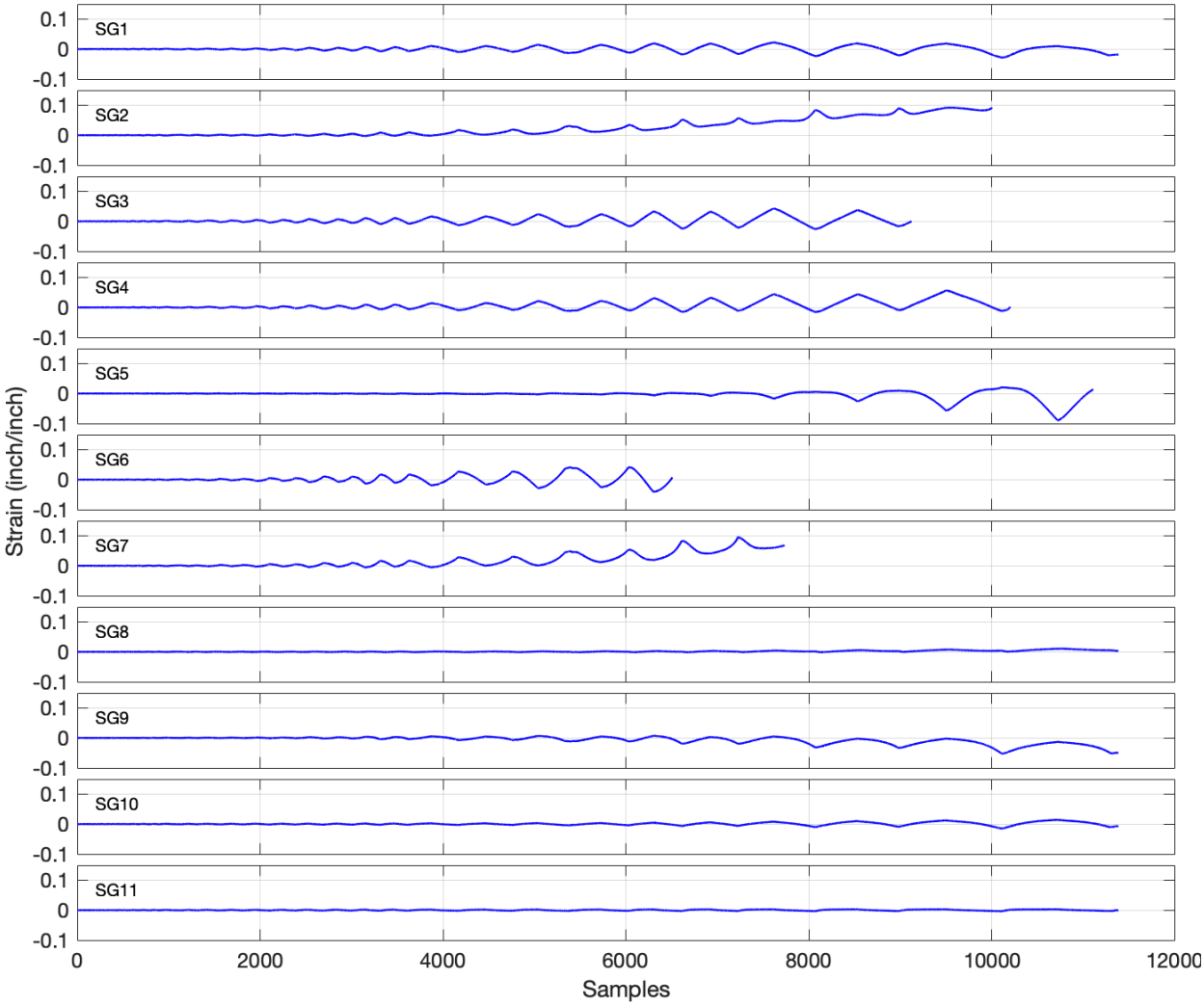

Figure D.7 Strain measured by strain gauges in specimen 4E-90

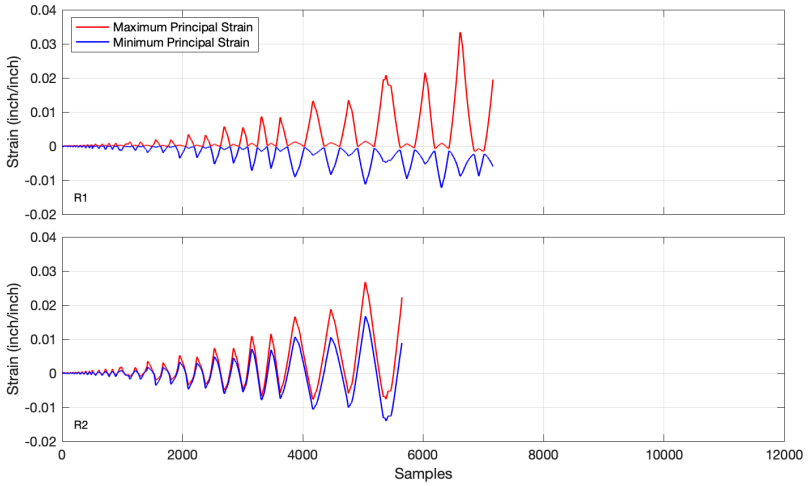

Figure D.8 Strain measured by rosettes in specimen 4E-90

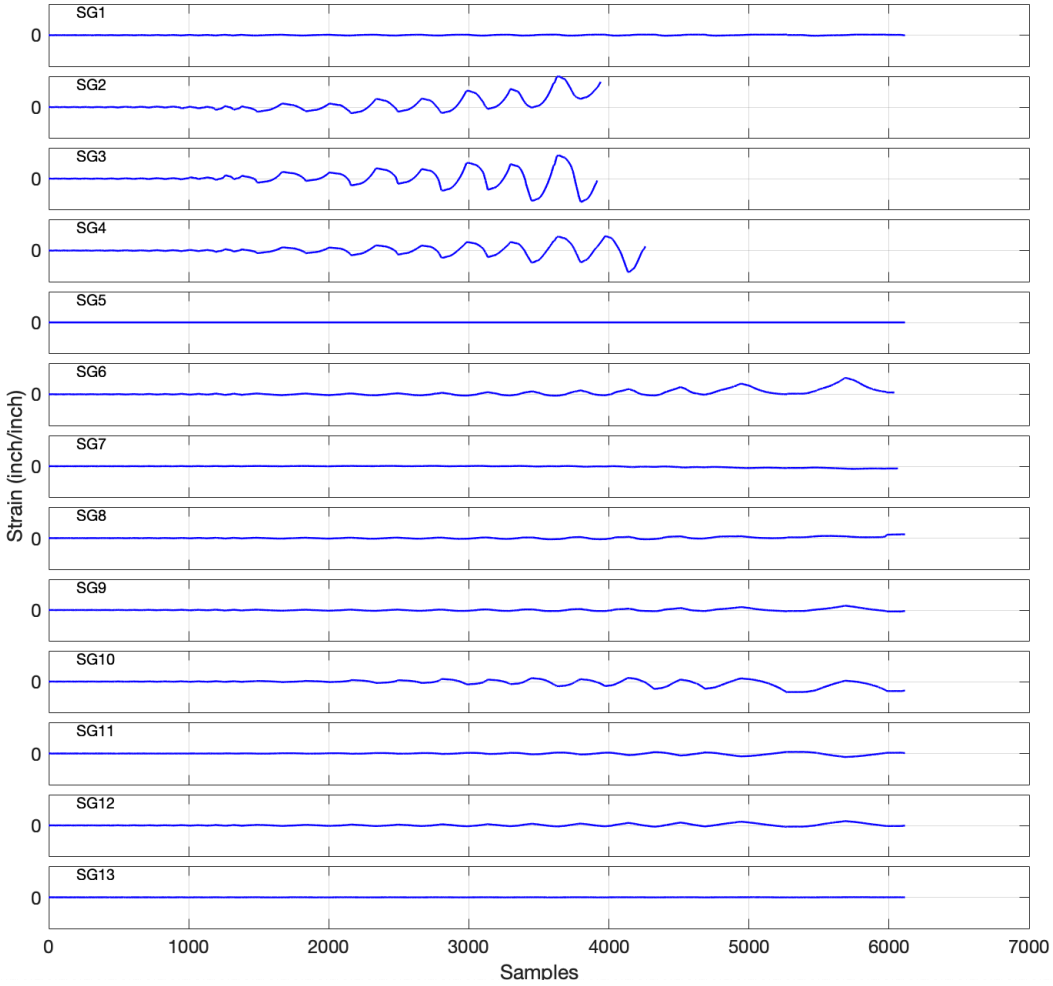

Figure D.9 Strain measured by strain gauges in specimen 4E-45

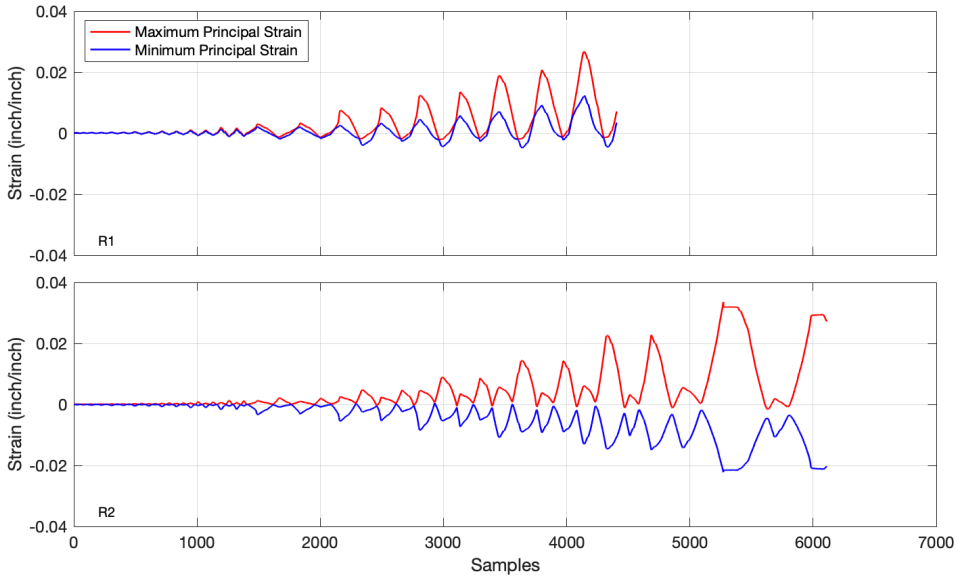

Figure D.10 Strain measured by rosettes in specimen 4E-45

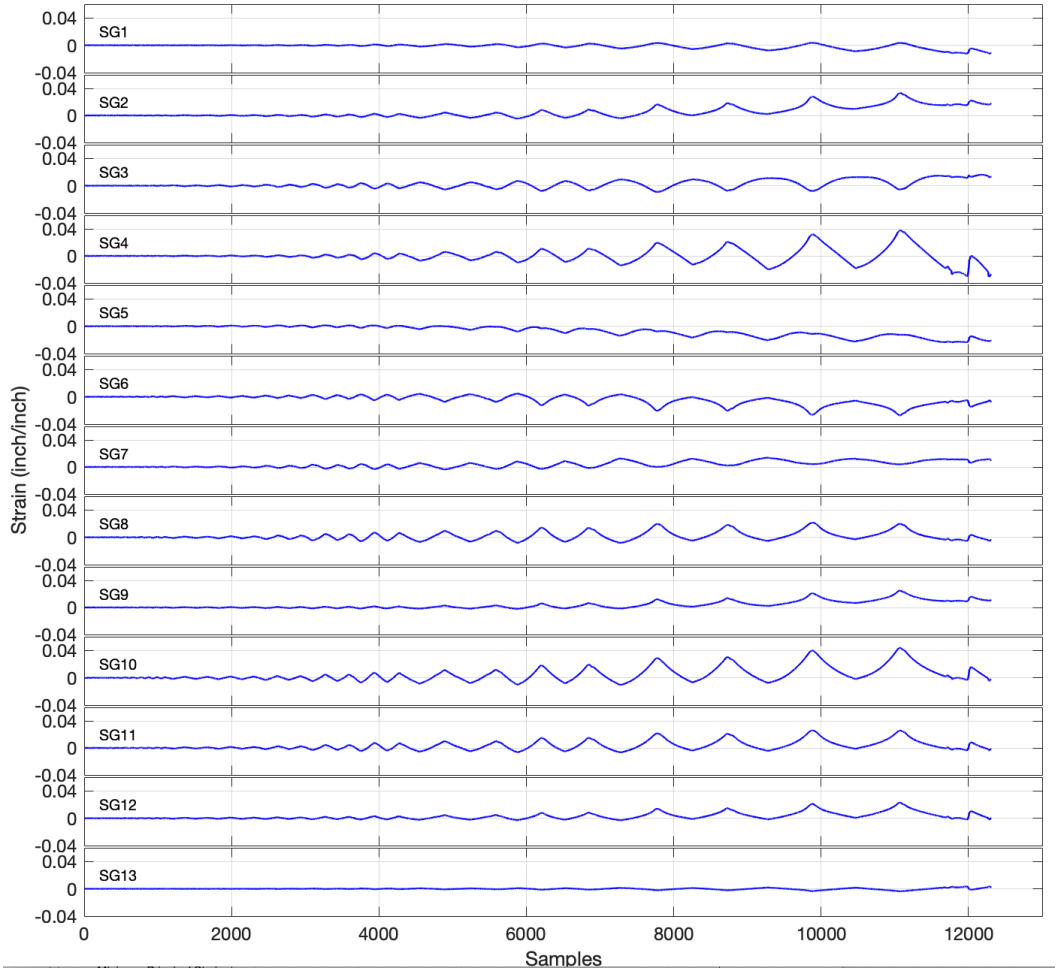

Figure D.11 Strain measured by strain gauges in specimen 8E-90

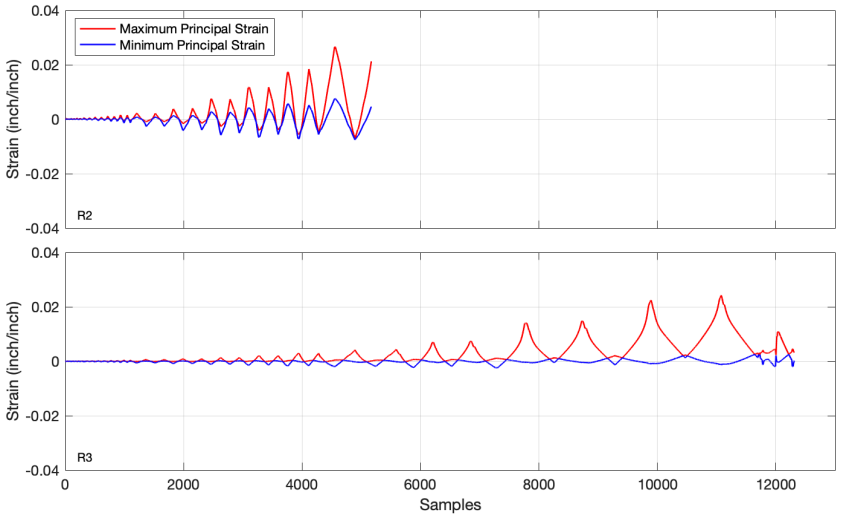

Figure D.12 Strain measured by rosettes in specimen 8E-90

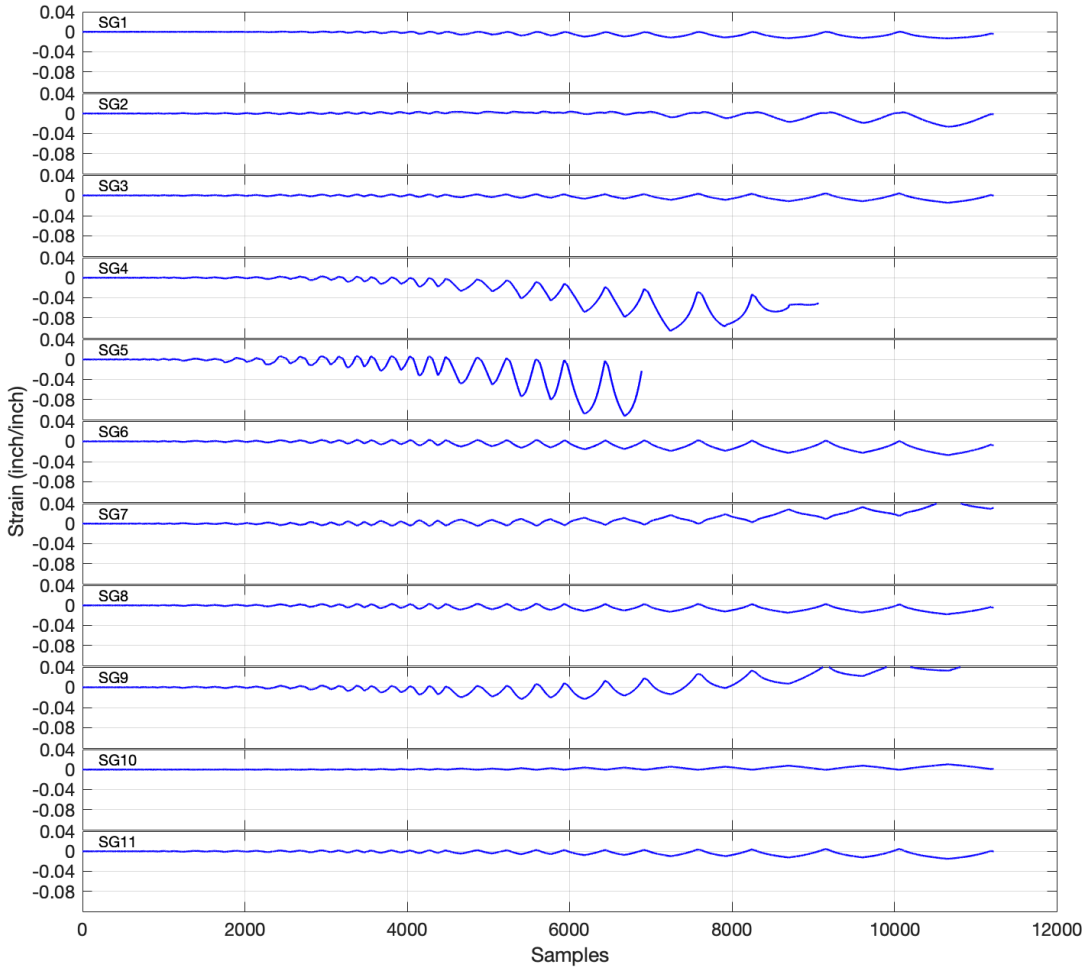

Figure D.13 Strain measured by strain gauges in specimen 8E-45

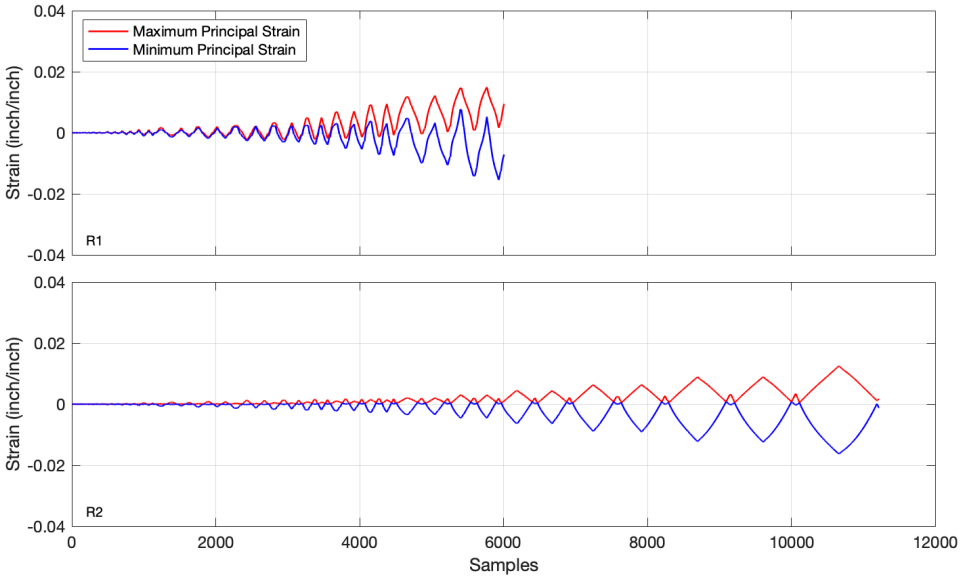

Figure D.14 Strain measured by rosettes in specimen 8E-45

The Pacific Earthquake Engineering Research Center (PEER) is a multi-institutional research and education center with headquarters at the University of California, Berkeley. Investigators from over 20 universities, several consulting companies, and researchers at various state and federal government agencies contribute to research programs focused on performance-based earthquake engineering.

These research programs aim to identify and reduce the risks from major earthquakes to life safety and to the economy by including research in a wide variety of disciplines including structural and geotechnical engineering, geology/seismology, lifelines, transportation, architecture, economics, risk management, and public policy.

PEER is supported by federal, state, local, and regional agencies, together with industry partners.

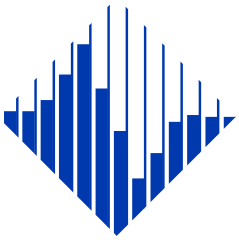

PEER Core Institutions

University of California, Berkeley (Lead Institution)
California Institute of Technology
Oregon State University
Stanford University
University of California, Davis
University of California, Irvine
University of California, Los Angeles
University of California, San Diego
University of Nevada, Reno
University of Southern California
University of Washington

Pacific Earthquake Engineering Research Center
University of California, Berkeley
325 Davis Hall, Mail Code 1792
Berkeley, CA 94720-1792
Tel: 510-642-3437
Email: peer_center@berkeley.edu

ISSN 2770-8314
https://doi.org/10.55461/PABS8360